INTERNATIONAL SCHOOL FOR ADVANCED STUDIES

DOCTORAL THESIS

Ultraviolet aspects of Peccei–Quinn Inflation

Author:
Davide DAL CIN
ddalcin@sissa.it

Referees:
Dr. Christophe Ringeval
christophe.ringeval@uclouvain.be

Supervisor:
Dr. Takeshi KOBAYASHI
takeshi.kobayashi@sissa.it

Dr. Christian Thomas Byrnes
C.Byrnes@sussex.ac.uk

A thesis submitted in fulfillment of the requirements for the degree of Doctor of Philosophy

in the

Astroparticle group
Physics department

January 4, 2024

"Not only is the Universe stranger than we think, it is stranger than we can think."

Werner Heisenberg

INTERNATIONAL SCHOOL FOR ADVANCED STUDIES

Abstract

Faculty of Physics
Physics department

Doctor of Philosophy

Ultraviolet aspects of Peccei–Quinn Inflation

by Davide DAL CIN

The possibility of observing a value of the tensor-to-scalar ratio r of the order $r \sim 10^{-3}$ would project us into a new era for the cosmology of the early Universe. Such an observation would lead to confirmation of inflation and a measurement of the energy scale at which this phase occurred, revolutionizing the idea of the early stages of the evolution of the Universe. This scale would be beyond the reach of any possible terrestrial experiment, exploring a region of energies of the order of $10^{12} - 10^{13}$GeV. Since a theory of quantum gravity is missing, this relegates inflation models to effective models that are reliable only within a certain range of energies. Hence, the question of whether the predictions of these models are reliable is crucial. In other words, is it always possible to ignore the tower of higher-dimensional operators present? This thesis aims to answer this question by focusing on the model called Peccei-Quinn inflation. This model offers the possibility of explaining inflation, dark matter and providing a solution to the strong CP problem. It also predicts a value of $r \sim 10^{-3}$ and makes this model falsifiable in the future. In addition, this thesis addresses a crucial aspect related to the production of dark matter through axions. It involves modeling the evolution after inflation, which is a crucial point. The findings significantly alter what was previously known about the Peccei-Quinn model. In the thesis we prove that Peccei–Quinn inflation is extremely sensitive to higher-dimensional operators, undermining its validity as an effective field theory. Further combined with the discussion on the axion quality required for solving the strong CP problem, we examine the validity of this scenario. We also show that after Peccei–Quinn inflation, resonant amplifications of the field fluctuations are inevitably triggered, casting serious doubts on the typical assumption of a homogeneous evolution. In conclusion, this thesis asks and tries to answer some profound questions regarding theoretical models that are in the sights of future groundbreaking observations in cosmology that will potentially provide a deeper understanding of the fundamental properties of our Universe.

Publications

The thesis is based on the following publication:

1. Davide Dal Cin and Takeshi Kobayashi.
   “Ultraviolet sensitivity of Peccei-Quinn inflation”.
   In: Phys. Rev. D 108 (6 2023), p. 063530.
   DOI: 10.1103/PhysRevD.108.063530.
   https://doi.org/10.1103/PhysRevD.108.063530

Contents

List of Figures

List of Tables

List of Abbreviations

ΛCDM	**L**ambda **C**old **D**ark **M**atter
DM	**D**ark **M**atter
DE	**D**ark **E**nergy
WIMP	**W**eakly **I**nteracting **M**assive **P**article
DOF	**D**egree **O**f **F**reedom
CMB	**C**osmic **M**icrowave **B**ackground
SDSS	**S**loan **D**igital **S**ky **S**urvey
GR	**G**eneral **R**elativity
FLRW	**F**riedmann **L**emaître **R**obertson **W**alker
3-D	**3** **D**imensional
LSS	**L**arge **S**cale **S**tructure
SEC	**S**trong **E**nergy **C**ondition
BBN	**B**ig **B**ang **N**ucleosynthesis
SVT	**S**calar **V**ector **T**ensor
PQ	**P**eccei **Q**uinn
EFT	**E**ffective **F**ield **T**heory
QG	**Q**uantum **G**ravity
IR	**I**nfra **R**ed
UV	**U**ltra **V**iolet
NI	**N**atural **I**nflation
WKB	**W**entzel **K**ramers **B**rillouin
KM	**K**inetic **M**isalignement
PR	**P**arametric **R**esonance

List of Symbols

c	Speed of light
$\hbar$	Reduced Planck constant
k_B	Boltzmann constant
G	Newton constant
$M_{\rm Pl}$	Reduce Planck mass
g	Space-time metric
γ	Metric of three space
Σ_t	Three space manifold
t_0	Present time
a_0	Scale factor today
H	Hubble constant
$\mathcal{H}$	Hubble constant in conformal time
n_s	Spectral index
$n_{\rm T}$	Tensor tilt
$\Delta_{\rm I}$	Dimensionless power spectrum
$A_{\rm S}$	Amplitude of scalar perturbations
$A_{\rm T}$	Amplitude of tensor perturbations
r	Tensor-to-scalar ratio
$\rho_{\rm crit}$	Critical density
Ω_I	Relic abundance factor
δ_{ij}	Kronecker delta
n_γ	Number density of photon today
$g(T)$	Relativistic degree of freedom
K	3-D curvature
z	Redshift
w	Equation of state
t	Cosmic time
τ	Conformal time
f	axion decay constant
T	Temperature of the Universe

Chapter 1

Introduction

The modern study of the universe is based on the ΛCDM model which provides a strong foundation to understand the large-scale structure and the expansion of the universe. This model is built on the principles of general relativity and proposes the existence of two mysterious elements: dark matter (DM) and dark energy (DE). DM constitutes around 26.8 % of the total mass-energy density of the universe and is believed to be responsible for the gravitational effects observed in very large structures such as the flat rotation curves of galaxies, the gravitational lensing of light by galaxy clusters, and the enhanced clustering of galaxies, see [65] for a review. The remaining 4.8% is made up of all the ordinary matter that we can observe, including planets, stars, and galaxies. What has been left out of the calculation is a 70 % that is constituted by dark energy and is responsible for today's acceleration [150, 140].

The standard model passed a plethora of observational tests, ranging from the cosmic microwave background (CMB) to supernovae observations and measurements from LSS [9, 4, 85, 149]. There are still open questions that the model is not able to address like the nature of DM and DE and tensions persist on the values of cosmological parameters measured by different observations [148, 179, 64].

During these decades many candidates for DM have been proposed such as weakly interacting massive particles (WIMPs)[108, 74, 151], axions, sterile neutrinos (see [36] for a review), primordial black holes [83, 81, 43], asymmetric dark matter (see [183, 141] for reviews), light dark matter (see [63] for a review), fuzzy dark matter (see [88] for a review), self-interacting dark matter (see [168] for a review), Q-balls [50], WIMPzillas [107] and Planck-scale DM [19, 69, 94]. In particular, axions exist automatically as a solution to strong CP problem [138, 177, 174] and they have received increasing attention by the community given the stronger and stronger bounds on standard WIMP dark matter and the many non-collider experimental opportunities for their detection. The behavior during and after inflation of this particle determines its relic abundance, which is still debated in the literature [72, 180, 42].

The ΛCDM model can be extended by adding cosmological inflation, which may explain the observed flatness and homogeneity of the Universe, as well as the origin of the primordial curvature perturbation [164, 162, 156, 75, 134, 114]. However, the actual mechanism of inflation is still unknown. In 40 years many models have appeared, an incomplete list includes R^2 [164], chaotic [118], extended [110, 106], power-law [2, 120], hybrid [119], natural

[65], supernatural [145], extra-natural [11], eternal [172, 76], D-term [30], F-term [130, 44], brane [59], ..., etc .... Some of these models are now ruled out, nevertheless, this varied list shows that to date a final model does not exist.

From an observational point of view, these inflationary models must fulfill the bound on the tensor power spectrum, commonly parametrized by the tensor-to-scalar ratio r, from Planck [9]. Future experiments, like [10], aim to reach $r \sim 10^{-3}$ and promise to advance the understanding of the Universe. Given this prospect, it is reasonable to explore or to understand in a deeper way models that predict r in this future ballpark. An example is Higgs inflation [29], see Section 4.11 for details, where the Higgs field with a non-minimal gravitational coupling drives inflation. Higgs inflation requires a very large gravitational coupling to be consistent with both the measurement of the Higgs self-coupling and the curvature perturbation amplitude inferred from analyses of the CMB. It has been pointed out that the large gravitational coupling lowers the cutoff scale of the effective field theory (EFT), making the predictions of the model unreliable [20, 39, 84, 40] (though a counterargument has been presented in [28]). Orthogonal to the prediction of $r \sim 10^{-3}$, Higgs inflation is extremely interesting because it is an economic and unifying model as it allows to explain the inflationary phase without introducing any additional particles to the standard model. The Higgs field, which is present due to infrared physics (unitarity of scattering amplitudes), serves as the inflaton, establishing a unique connection between high and low energy physics.

Peccei-Quinn (PQ) inflation, proposed by [61], is a well-motivated model worthy of study. The model requires the presence of a complex scalar field Φ (PQ field) in addition to the standard model. The PQ field was originally introduced to solve the strong CP problem[138], which is unrelated to the physics of the early universe. By positing that the radial component of the PQ field drives inflation, this model provides a comprehensive explanation for the strong CP problem, dark matter, and inflation, all within a single framework. Higgs inflation and PQ inflation share the qualities of being economical and unifying, making them both highly appealing. The crucial ingredient of the PQ inflation scenario is a coupling between the PQ field and the Ricci scalar. This dimension-four interaction, which is expected to exist from the point of view of an effective field theory in curved space [137], flattens the potential to realize a slow-roll [152, 90, 135, 113]. In the case of PQ inflation, its self-coupling is not constrained by experiments and thus is effectively a free parameter of the model. It can be chosen to allow for a small gravitational coupling, such that the cutoff scale is larger than the relevant energy scales during and after inflation. This has been considered as another virtue of PQ inflation.[1] Here we note that a small gravitational coupling, on the other hand, requires a large field excursion for the PQ field. This is easily understood by noting that, with a power-law potential $V \propto \phi^n$ and in the absence of a non-minimal coupling to gravity, slow-roll inflation requires

[1] It was pointed out in [77] that the gravitational coupling also helps evade the axion quality problem.

super-Planckian field ranges. The necessity of large field excursions renders the model sensitive to higher-dimensional operators, which in turn depends on the details of the ultraviolet (UV) completion of the theory, bringing us back to the situation similar to Higgs inflation.[2]

The goal of this thesis is to sharpen this message by evaluating, for the first time, the effects of higher-dimensional operators on PQ inflation. In order to constrain Planck-suppressed operators, we analyze their impact on curvature perturbations and inflation duration. (See also [89] which performed a similar study for a Higgs-like real inflaton.) The ultraviolet sensitivity of PQ inflation is reminiscent of the so-called axion quality problem [93, 87, 91], which is based on the observation that $\mathrm{U}(1)_{\mathrm{PQ}}$-breaking higher-dimensional operators can spoil the axion as a solution to the strong CP problem by displacing the axion field from the CP-conserving vacuum. This shows how the axion dynamics in the IR are influenced by unknown physics in the UV, parameterized by these operators. The figure in this thesis (Fig. 7.2) demonstrates how physics at the Planck scale can affect inflaton physics.

The UV conundrum of PQ inflation is just one face of a cube of questions. We know that the Universe has to pass from a cold empty state during inflation to the primordial thermal bath. It is crucial to understand this transition and, in light of all the above good properties of the model, how the axion (phase of the PQ field) behaves at the end of inflation. In a model similar to PQ [17], it is shown that a resonant amplification of the field fluctuation is generated when the inflaton oscillates about its origin, this amplification leads to a restoration of the PQ symmetry. Instead, in [61], it is assumed that the axion is homogeneous after inflation and the production of DM happens via the misalignment mechanism, see Section 6.4.2. One may wonder if the presence of higher-dimensional operators prevents the inflaton from oscillating around its minimum, leading to a homogeneous axion field. The objective of the thesis is to conduct a thorough investigation of the evolution of axion after inflation while considering the angular momentum of the PQ field for the first time. We demonstrate the inevitable occurrence of inhomogeneities generated from parametric resonances, which is discussed in Section 7.5.

The results presented in Section 7.5 prompt us to investigate whether we can produce sufficient initial angular momentum using higher-dimensional operators. This will help us have in-spiral trajectories in the field space and prevent parametric resonances. However, as we will see in Section 7.5, if the radial field is the inflaton, it is not possible to achieve this. But if we do not assign the radial part of Φ as the inflaton, then it becomes necessary to explore if it is possible to avoid PRs. This is because in many scenarios such as, string theory [31, 41, 59], supersymmetry [62, 58, 144, 38, 126], extra-dimensions [147, 146, 129] more than one scalar field is present during inflation and the

[2]The precise statement is that the PQ field excursion in the Jordan frame increases with a decreasing non-minimal coupling. The excursion of the canonically normalized field in the Einstein frame is larger than 10^{18} GeV, independently of the value of the non-minimal coupling.

Φ field would play the role of spectator field. Having no more constraints on g, it is possible to search for the minimum value necessary to avoid parametric resonances; guaranteeing, unless thermal restoration of the $U(1)_{\rm PQ}$, a homogeneous evolution for the field Φ. In Chapter 8, we demonstrate the existence of a region in the $l - \log_{10}|g|$ space where we can prevent parametric resonances. In this region, the abundance of dark matter is given by the kinetic misalignment mechanism discussed in Section 6.4.3. For the first time, this analysis provides bounds on the size of these operators, as shown in Fig. 8.1.

The discussion in the thesis is split into two parts. The first part aims to establish the theoretical framework of the thesis in a way that is accessible to non-experts and students. Chapter 2 presents the standard cosmological model, covering the key features of the expanding universe, Einstein's GR principles, and known matter energy components. Chapter 3 discusses the problems of the standard Big Bang cosmology and how inflation can overcome them.

In Chapter 4, we explore perturbations in the universe, starting with the perturbed metric, moving on to Einstein's field equations, and addressing the issue of gauge invariance in GR. We present the observational bounds based on the 2018 Planck results. We also review the Higgs inflation model and its issues as EFT. Finally, we derive the Lyth bound and review the δN formalism. Chapter 5 discusses reheating, including its fundamental properties and the preheating process that applies quantum field theory in a time-dependent classical background.

Chapter 6 introduces the strong CP problem and the axion as a possible solution, with a focus on the production mechanism of a relic abundance of this particle. We also examine the axion quality problem, which restricts higher-dimensional operators that break $\mathrm{U}(1)_{\rm PQ}$ and requires the axion to solve the strong CP problem.

In the second part, we present the original work that forms the core of this thesis, based on [54]. In Chapter 7, we provide a detailed review of the Peccei-Quinn inflation model and demonstrate its UV sensitivity by showing that its predictions are highly sensitive to Planck-suppressed higher-dimensional operators. We combine our new constraints with the axion quality, and cut a large parameter space of higher-dimensional operators, as shown in Fig. 7.8. We also analyze the subsequent evolution of the axion, demonstrating that the production mechanism of the DM abundance cannot be the misalignment mechanism due to parametric resonances.

In Chapter 8, we introduce a project that provides a practical application of the concepts covered in Chapter 7. This chapter aims to investigate whether a relic abundance of dark matter can be obtained through the "kinetic misalignment" mechanism by exploring a region in the parameter space where parametric resonances can be avoided. This is achieved by abandoning the assumption that the radial field is the inflaton.

We summarize the main findings of this thesis and define the roadmap for future developments in Chapter 9.

In this thesis, we use the following convention for the metric signature $(+,-,-,-)$. We will work with natural units in which $\hbar = k_B = c = 1$ and the reduced Planck mass is $M_{\rm Pl} = \sqrt{1/8\pi G}$. Moreover, x^μ represents the coordinate of spacetime and Greek indices go from 0 to 3 and Latin indices from 1 to 3. We use a dot for the cosmic time derivative $\dot{} = d/dt$ and a prime for conformal derivative $' = d/d\tau$ unless otherwise specified.

Chapter 2

Modern Cosmology

In this chapter, we will introduce the fundamental concepts for the rest of the research. We begin by reviewing the key components of the standard cosmological model in Sections 2.1 and 2.2. Then, we will derive the Hubble flow and the redshift effect resulting from an expanding Universe in Sections 2.3 and 2.4. In Section 2.5, we will analyze the possible constituents of the Universe, followed by the evolution equations in Section 2.6. Other references on these topics include [25, 52, 175, 26, 27].

2.1 The Cosmological Principle

When we have a lack of data this pushes physicists to use some guidelines, that are based on symmetries which reduce the degree of freedom (DOF) in the theory. Early cosmologists with the help of these assumptions tried to construct models that aimed to describe the Universe in a broad-brush sense. These models were based on an idea the "Cosmological Principle" which states: that on sufficiently large scales the Universe is both homogeneous and isotropic. By homogeneous we mean that the Universe looks identical everywhere in space and isotropic the same in every direction. The assumption of isotropy is sustained by the observation of the isotropy of the CMB radiation. Instead, homogeneity is sustained by the Sloan-Digital-Sky-Survey (SDSS) which provides pieces of evidence that the distribution of galaxies, on a scale larger than 300 light years, is homogeneous. The Cosmological principle, which we accept because it is in agreement with observations, embedded in GR points towards the so-called Friedmann-Lemaître-Robertson-Walker (FLRW) metric.

2.2 The FLRW metric

In GR, the geometry of the three-space (Σ_t) is encoded in a metric $\gamma_{ij}(\vec{x})$, or equivalently a line element $dl^2 = \gamma_{ij}dx^i dx^j$, where we adopt the Einstein convention for the repeated indices. The cosmological principle strongly constrains the form of the Universe, which can be described as a foliation of three spaces (Σ_t); each of which is forced to be homogeneous and isotropic.

There are three examples of this type of geometry. The simplest one is the Euclidean space with line element, in Cartesian coordinates, $dl^2 = d\vec{x}^2$,

whose symmetries are translations and 3-D rotations. A spherical surface in 4-D Euclidean space with radius a is another possibility, which is described by $dl^2 = d\vec{x}^2 + dz^2$ and respecting $z^2 + \vec{x}^2 = a^2$. The isometry of the metric is the 4-D rotations. The last possibility is a hyper-spherical surface in 4-D pseudo-Euclidean space, with line element $dl^2 = d\vec{x}^2 - dz^2$ and respecting $z^2 - \vec{x}^2 = a^2$, where, as an abuse of notation, we used the same a for these two cases. The isometry of the metric is 4-D pseudo-rotations (like Lorentz transformations).

Focusing on the last two cases, it is useful to pass to rescaled adimensional coordinates $x \to ax, z \to az$ such that the line elements are collectively described by

$$dl^2 = a^2 \left(d\vec{x}^2 \pm dz^2 \right), \quad \vec{x}^2 \pm z^2 = \pm 1. \tag{2.1}$$

The embedded metric can be derived by differentiating the conditions (2.1) leading to

$$\vec{x} \cdot d\vec{x} = z dz. \tag{2.2}$$

Inserting the previous expression in (2.1) we obtain

$$dl^2 = a^2 \left[d\vec{x}^2 \pm \frac{(\vec{x} \cdot d\vec{x})^2}{1 \mp \vec{x}^2} \right]. \tag{2.3}$$

In compact form we have

$$dl^2 = a^2 \tilde{\gamma}_{ij} dx^i dx^j = a^2 \left[d\vec{x}^2 + \mathrm{K} \frac{(\vec{x} \cdot d\vec{x})^2}{1 - \mathrm{K}\vec{x}^2} \right]. \tag{2.4}$$

where we introduced the induced metric $\tilde{\gamma}$ defined as

$$\tilde{\gamma}_{ij} = \delta_{ij} + \mathrm{K} \frac{x^i x^j}{1 - \mathrm{K}\vec{x}^2}, \tag{2.5}$$

and the 3-D curvature K defined as

$$\mathrm{K} = \begin{cases} 0 & \text{Euclidean} \\ 1 & \text{Spherical} \\ -1 & \text{Hyper-spherical.} \end{cases} \tag{2.6}$$

The positivity of dl^2 requires $a^2 > 0$.

Passing from Cartesian to polar coordinates (r, θ, ϕ) the line element (2.4) becomes

$$dl^2 = a^2 \left[\frac{dr^2}{1 - \mathrm{K}r^2} + r^2 d\theta^2 + r^2 \sin\theta^2 d\phi^2 \right]. \tag{2.7}$$

We can simplify the previous expression via the introduction of a new radial coordinate defined as $dq = dr/\sqrt{1 - \mathrm{K}r^2}$. With the new variable the line

element (2.7) becomes

$$dl^2 = a^2 \left[dq^2 + \mathrm{S}_\mathrm{K}^2(q) \left(d\theta^2 + \sin\theta^2 d\phi^2 \right) \right], \tag{2.8}$$

where we introduced

$$\mathrm{S}_\mathrm{K}(q) = \begin{cases} q & \mathrm{K} = 0 \\ \sin q & \mathrm{K} = 1 \\ \sinh q & \mathrm{K} = -1. \end{cases} \tag{2.9}$$

To pass to an expanding Universe we include (2.4) into a 4-D geometry and promote a to be a function of time, more concretely we have

$$ds^2 = g_{\mu\nu} dx^\mu dx^\nu = dt^2 - a^2(t) \tilde{\gamma}_{ij} dx^i dx^j. \tag{2.10}$$

The $g_{\mu\nu}$ metric describes the FLRW Universe and a is the scale factor. Studying the photon evolution is useful to introduce the conformal time $d\tau = dt/a(t)$ and (2.8), such that (2.10) becomes

$$ds^2 = a(t)^2 \left[d\tau^2 - dq^2 - \mathrm{S}_\mathrm{K}^2(q) \left(d\theta^2 + \sin\theta^2 d\phi^2 \right) \right], \tag{2.11}$$

that describes a metric that is conformal to the Minkowski spacetime. Photons travel along null geodesics ($ds^2 = 0$) and the light rays propagation in (2.11) is the same as in Minkowski spacetime. Along the path of the photon, from $ds^2 = 0$, we get

$$\Delta\tau = \Delta q, \tag{2.12}$$

that are the photon trajectories in the metric (2.11).

2.3 The Hubble flow

Let us consider two points P and P_0 (origin of the polar coordinates). The proper distance d_P between P and P_0 can be inferred from the FLRW metric in polar coordinates and putting $dt = 0$. From (2.7) we obtain

$$d_\mathrm{P} = a \int_0^r \frac{dr}{\sqrt{1 - \mathrm{K}r^2}} = a f(r), \tag{2.13}$$

where

$$f(r) = \begin{cases} r & \mathrm{K} = 0 \\ \sin^{-1} q & \mathrm{K} = 1 \\ \sinh^{-1} q & \mathrm{K} = -1. \end{cases} \tag{2.14}$$

This definition of distance is not useful operationally since required to measure instantaneously the distance between P and P_0. The coordinates (r, θ, ϕ) are attached to each point and follow the expanding Universe and one can

define a comoving coordinate

$$d_C = f(r)a_0, \tag{2.15}$$

such that the relation between d_C and d_P is

$$d_P = \frac{a(t)}{a_0} d_C. \tag{2.16}$$

Since $a(t)$ is changing in time then the proper distance d_P changes and the source P has a radial velocity with respect to P_0 given by

$$v_r = \dot{a} f(r) = \frac{\dot{a}}{a} d_P. \tag{2.17}$$

Equation (2.17) is the Hubble law and $\dot{a}/a = H$ is the Hubble constant. In the case in which the point P has a velocity measured by a comoving observer (i.e. comoving with the Hubble flow), then P has a peculiar velocity (v_{pec}) and equation (2.17) becomes

$$v_{tot} = v_{pec} + H d_P. \tag{2.18}$$

Finally the value of H today is $H_0 = 67.32 \pm 0.42 \text{kms}^{-1}\text{Mpc}^{-1}$ [9].

2.4 The Redshift effect

Observations are made through the motion of light that is coming to us from distant galaxies. As we saw previously, galaxies are moving away or towards us due to the Hubble flow and we expect differences between the observed wavelength, λ_0, and the emitted wavelength, λ_e. We define the redshift of a source by the quantity

$$z = \frac{\lambda_0 - \lambda_e}{\lambda_0}, \tag{2.19}$$

where the observer is located at the origin of the polar coordinates system. Instead the source is located at r and emits light at t_e with wavelength λ_e. Since light moves on $ds^2 = 0$, from (2.7), we get

$$\int_{t_e}^{t_0} \frac{dt}{a(t)} = \int_0^r \frac{dr}{\sqrt{1 - Kr^2}} = f(r). \tag{2.20}$$

The observer and source move with Hubble flow and from this, we can conclude that the distance $f(r)$ is the same at different times. We can write

$$\int_{t_e'}^{t_0'} \frac{dt}{a(t)} = f(r) = \int_{t_e}^{t_0} \frac{dt}{a(t)}, \tag{2.21}$$

where t'_e and t'_0 are different emission and observation times respectively. If we choose t'_e and t'_0 as $t'_e = t_e + \delta t_e$ and $t'_0 = t_0 + \delta t_0$, from (2.21) we get

$$\frac{\delta t_e}{a(t_e)} = \frac{\delta t_0}{a_0}, \tag{2.22}$$

that holds for small $\delta t_e, \delta t_0$. If the two previous intervals correspond to the emission and absorption times we obtain

$$\frac{a(t_e)}{\lambda_e} = \frac{a_0}{\lambda_0}. \tag{2.23}$$

From the definition of redshift (2.19) we obtain

$$1 + z = \frac{a_0}{a(t_e)}. \tag{2.24}$$

If t_e is close to t_0 we can expand

$$a(t_e) = a(t_0)\left(1 + H_0\left(t_e - t_0\right) + \dots\right), \tag{2.25}$$

Plugging the last equation in (2.24) we obtain

$$z \simeq H_0\left(t_0 - t_e\right). \tag{2.26}$$

For close-by objects, we can approximate $t_0 - t_e \simeq d$, where d is the physical distance between the two sources. Finally, we get

$$z \simeq H_0 d, \tag{2.27}$$

that show how z increases linearly with d and the slope is given by H_0 .

2.5 The Dynamics of the Universe

Up to now what we discuss does not rely on the particular behavior of the cosmological expansion. We saw that the FLRW metric contains an unknown function, the scale factor $a(t)$, whose dynamic is governed by Einstein's field equations. We need to provide information about the matter content of the Universe that is encoded in stress-energy tensor $T_{\mu\nu}$. Due to homogeneity and isotropy the form of the stress-energy tensor is constrained to be

$$T_{00} = \rho(t), \quad T_{i0} = 0, \quad T_{ij} = -P(t) g_{ij}, \tag{2.28}$$

where ρ and P are generic unknown time-dependent functions and they represent the energy and pressure densities respectively. This $T_{\nu\mu}$ is the one of a perfect fluid as seen by a coming observer, and in a covariant form reads

$$T^{\nu}_{\mu} = (\rho + P)\, U^{\mu} U_{\nu} - P \delta^{\mu}_{\nu}, \tag{2.29}$$

where $U^\mu = dx^\mu/ds$ is the relative four-velocity between the fluid and the observer, while ρ and P are the energy and pressure densities in the rest-frame of the fluid. For a comoving observer with the fluid, $U^\mu = (1,0,0,0)$, we recover (2.28).

The evolution of ρ and P are governed by the continuity equation that in GR is

$$\nabla_\mu T^{\mu\nu} = 0, \tag{2.30}$$

where ∇_μ is the covariant derivative. The $\nu = 0$ component gives the evolution of ρ that is

$$\dot{\rho} + 3H(\rho + P) = 0. \tag{2.31}$$

2.5.1 The budget of the Universe

The content of the Universe is varied and we can classify it as :

1. **Non-relativistic matter**: Describes the "matter" that have negligible pressure $P \ll \rho$. From (2.31) we get the following scaling for ρ, $\rho \simeq a^{-3}$. This behavior represents the dilution given by the volume expansion.

2. **Relativistic**: We define "radiation" as a form of matter such that $P = \rho/3$. Photons or in general relativistic particles fall into this category. From (2.31) we get $\rho \simeq a^{-4}$. The extra dilution for relativistic particles with respect to ordinary matter came from the redshift of the energy.

3. **Dark energy**: Recently the Universe has been observed to be accelerated. Our Universe seems to be dominated by the strange form of "matter" with negative pressure $P = -\rho$. From (2.31) we get $\rho \simeq a^0$, and the energy density remains constant.

It is customary to introduce a relation between P and ρ as

$$P = w\rho, \tag{2.32}$$

where w is the equation of the state of "matter" under consideration. If we insert (2.32) in (2.31) we get

$$\rho \sim a^{-3(1+w)}, \tag{2.33}$$

that is the general scaling of ρ with the scale factor a. From $w = 0$ or $w = 1/3$, we obtain the scaling for non-relativistic and relativistic matter respectively, as expected.

2.6 Friedmann Equations

The Einstein equations are

$$G_{\mu\nu} = R_{\mu\nu} - \frac{g_{\mu\nu}R}{2} = \frac{1}{M_{\rm Pl}^2} T_{\mu\nu}, \tag{2.34}$$

where $R_{\mu\nu}$ and R are the Ricci tensor and scalar. If we insert the ansatz (2.10) for the metric and the stress-energy tensor (2.28) in (2.34) we obtain

$$M_{\rm Pl}^2\left(\frac{\dot{a}}{a}\right)^2 = \frac{\rho}{3} - \frac{M_{\rm Pl}^2 \mathrm{K}}{a^2}, \tag{2.35}$$

$$M_{\rm Pl}^2\frac{\ddot{a}}{a} = -\frac{1}{6}\left(\rho + 3P\right). \tag{2.36}$$

From (2.35) with $\mathrm{K} = 0$ we define the critical density $\rho_{\rm crit}$ as follow

$$\rho_{\rm crit,0} = 3M_{\rm Pl}^2 H_0^2 = 1.05 \times 10^{-5} h^2 \mathrm{GeV cm}^{-3}, \tag{2.37}$$

where h is introduced from the Hubble parameter today as follows

$$H_0 = 100h\mathrm{kms}^{-1}\mathrm{Mpc}^{-1}, \tag{2.38}$$

and its value is $h \simeq 0.7$ from Planck [9]. It is common to introduce the following parameter Ω as follow

$$\Omega_{\rm I,0} = \frac{\rho_{\rm I,0}}{\rho_{\rm crit,0}}. \tag{2.39}$$

With the last definition, we can rewrite (2.35) as follows

$$H^2 = H_0^2\left[\Omega_{\rm r,0}\left(\frac{a_0}{a}\right)^4 + \Omega_{\rm m,0}\left(\frac{a_0}{a}\right)^3 + \Omega_{\rm K,0}\left(\frac{a_0}{a}\right)^2 + \Omega_{\Lambda,0}\right], \tag{2.40}$$

where $\Omega_{\rm K,0} = -\mathrm{K}/a_0^2 H_0^2$ and r, m, Λ stand for radiation, matter and cosmological constant. From type IA supernova, CMB, and LSS we know that the Universe is filled by [9, 4, 85, 149]

$$\Omega_{\rm K,0} \leq 0.01, \quad \Omega_{\rm r,0} = 9.4 \times 10^{-5}, \quad \Omega_{\rm m,0} = 0.32, \quad \Omega_{\Lambda,0} = 0.68. \tag{2.41}$$

Chapter 3

The Inflationary scenario

We will introduce the standard notion of particle horizon and Hubble sphere in Section 3.1, which are tightly linked to the discussion of puzzles of the standard Big Bang cosmology, Section 3.2. They represent a serious problem since they point towards a "high" degree of fine-tuning of the initial conditions of the Universe for explaining what we observe. In Sections 3.3 and 3.4, we analyzed inflation as a possible solution to these puzzles. Other references on these topics include [26, 27, 133, 112, 127, 29, 20].

3.1 Horizons and Hubble radius

Signals, in a casual theory, can at most travel at the speed of light. It is therefore necessary to study the dynamics of photons to understand the casual structure of the Universe. Using the suitable coordinate (2.11), we can define the comoving particle horizon $q(\tau)$ as

$$q(\tau) = \tau - \tau_{\rm i} = \int_{t_{\rm i}}^{t} \frac{dt}{a(t)}, \tag{3.1}$$

where the hypersurface $\tau_{\rm i}$ is the Big Bang singularity. Equation (3.1) represents the largest comoving distance from which an observer at time t will be able to receive signals. The particle horizon takes into account all the history of the observer and any possible causal influence has to come within this region. It is (3.1) that plays an important role in the horizon problem.

From (3.1) we can introduce another crucial ingredient, the comoving Hubble radius. Indeed, the relation (3.1) can be rewritten as

$$q(a) = \int_{\ln a_{\rm i}}^{\ln a} (aH)^{-1}\, d\ln a, \tag{3.2}$$

and the casual structure of the Universe is controlled by $(aH)^{-1}$, the so called comoving Hubble radius. In a Universe dominated by a single fluid with an equation of state (2.32), we get

$$q(a) = \frac{2H_0^{-1}}{1+3w}\left[a^{\frac{1+3w}{2}} - a_{\rm i}^{\frac{1+3w}{2}}\right] \simeq \frac{2}{1+3w}\,(aH)^{-1}, \tag{3.3}$$

where we neglect the contribution from $a_{\rm i}$. The last quantity is finite if $1+3w > 0$ (strong energy condition (SEC)), indeed $\tau_{\rm i} = 2a_{\rm i}^{\frac{1+3w}{2}}/(1+3w)H_0$ goes to zero when $a_{\rm i}$ goes to zero if $1+3w > 0$. From (3.3) we note that numerically the comoving particle horizon and Hubble radius roughly agree. Here, we want to stress that the two quantities are very different:

1. Comparing a comoving separation λ, of the two particles, with the Hubble radius determines if the two particles can communicate at a given time (within the next Hubble time).

2. Comparing λ with q determines if two particles could or could not have communicated.

For the solution of the horizon problem, as we will soon see, will be crucial to obtain $q \gg (aH)^{-1}$.

3.2 The Horizon and flatness problems

An observer can potentially observe all events that belong to the particle horizon. At the time of CMB formation, which occurred 380,000 years after the Big Bang, the CMB consisted of 10^4 disconnected patches. These patches corresponded to two points in the sky that were separated by one degree. The particle horizons of these two points did not overlap, indicating that there was not enough time for them to interact. The CMB shows isotropy on scales larger than one degree, which poses the horizon problem: how could two points that were casually disconnected have the same temperature?

Instead, the flatness problem is an issue of "fine-tuning". From (2.35) we know that Ω obeys

$$\Omega - 1 = \frac{\mathrm{K}}{a^2 H^2}. \tag{3.4}$$

During radiation H scales as $H \simeq \rho \simeq a^{-4}$ and (3.4) tells us that $\Omega - 1$ scales as $\Omega - 1 \simeq a^2$. We can evolve back in time the $\Omega - 1$ factor and obtain its value at BBN

$$\frac{|\Omega - 1|_{T=T_{\rm BBN}}}{|\Omega - 1|_{T=T_0}} \approx \left(\frac{T_0}{T_{\rm BBN}}\right)^2 \approx 10^{-16}, \tag{3.5}$$

where we used $T \sim 1/a$ and the numerical values for the temperatures today ($T_0 \sim 10^{-13}$GeV) and at Big Bang nucleosynthesis (BBN) ($T_{\rm BBN} \sim 10^{-3}$GeV). Observation is pointing towards a value for $|\Omega - 1|_{T=T_0}$ to be $|\Omega - 1|_{T=T_0} \lesssim 0.01$, and to get this value we need to fine-tune $|\Omega - 1|_{T=T_{\rm BBN}}$ close to one with a precision of 10^{16}. The flatness problem is the request for this extremely high tuning.

3.3 A possible solution of the previous puzzles

As one may imagine a solution to the previous problem is provided by inflation. Our description of q, relation (3.1), already gives us an intuition of the

way to go. We need to obtain a large q, and we achieve this with a sufficiently long period where the Hubble radius decreases

$$\frac{d}{dt}\frac{1}{aH} < 0. \tag{3.6}$$

The last relation, as we will see, requires a violation of the SEC condition, namely $1+3w<0$. Moreover, relation (3.6) will be our definition of inflation. With a violation of the SEC condition now the integral in (3.2) is dominated by the initial contribution

$$\tau_{\rm i} = \frac{2H_0^{-1}}{1+3w} a_{\rm i}^{\frac{1+3w}{2}}, \tag{3.7}$$

that is diverging to $-\infty$ when $a_{\rm i}$ goes to zero if $w<-1/3$. This divergence gives us more time before decoupling and possibly the particles may have a chance to interact. The space-like singularity $\tau=-\infty$ is pushed to past infinity and inflation replaces $\tau=0$ with its end. Within this scenario, at $\tau=0$ the standard Big Bang cosmology starts.

Our main goal is to obtain $N_k = \ln a_{end}/a(k)$ which represents the number of e-folds before the end of inflation at which a generic comoving scale k equals the Hubble scale aH. Then we will specialize on $N_{\rm hor}$, which evaluates N_k at the present Hubble scale $k_{\rm hor}=a_0H_0$. Hence, $N_{\rm hor}$ represents the number of e-folds needed to solve the aforementioned problem.

Our quantity of interest is k/a_0H_0, which represents a generic scale k measured in units of the present Hubble scale. We model the history of the Universe after inflation considering a possible phase of reheating governed by an equation of state $w_{\rm reh}$, the radiation phase, and matter[1]. The transition between each phase is assumed to be instantaneous. We can rewrite k/a_0H_0 as follows

$$\frac{k}{a_0H_0} = \frac{a_kH_k}{a_0H_0} = e^{-N_k}\frac{a_{\rm end}}{a_{\rm reh}}\frac{a_{\rm reh}}{a_{\rm eq}}\frac{H_k}{H_0}\frac{a_{\rm eq}}{a_0}, \tag{3.8}$$

where in going from left to right we used $k=a_kH_k$, $N_k=\ln a_{end}/a(k)$, and we inserted the phases of the expansion of the Universe.

The history assumed, relations (2.33) and (2.24) tell us that $a_{\rm end}/a_{\rm reh} = (\rho_{\rm reh}/\rho_{\rm end})^{1/3(1+w_{\rm reh})}$, $a_{\rm reh}/a_{\rm eq} = \left(\rho_{\rm eq}/\rho_{\rm reh}\right)^{1/4}$, and $a_0/a_{\rm eq} = 1+z_{\rm eq}$. With these relations, expression (3.8) becomes

$$N_k = -\ln\frac{k}{a_0H_0} + \frac{1}{3(1+w_{\rm reh})}\ln\frac{\rho_{\rm reh}}{\rho_{\rm end}} + \frac{1}{4}\ln\frac{\rho_{\rm eq}}{\rho_{\rm reh}} + \ln\frac{H_k}{H_0} - \ln 1+z_{\rm eq}, \tag{3.9}$$

where H_k is the Hubble scale during inflation, H_0 is the Hubble scale today, $\rho_{\rm reh}$ is the energy density at reheating, $\rho_{\rm end}$ is the energy density at the end of inflation, $\rho_{\rm eq}$ is the energy density at the moment of equivalence between matter and radiation and z_{eq} the redshift of this moment.

If we set k to the horizon scale today $k_{hor}=a_0H_0$, we assume instantaneous reheating $\rho_{\rm reh}=\rho_{\rm end}$, and a constant H during inflation $H_k \simeq H_I$,

[1] We neglect the last phase of dark energy domination

relation (3.9) becomes

$$N_{\rm hor} \simeq \frac{1}{4}\ln\frac{\rho_{\rm eq}}{\rho_{\rm reh}} + \ln\frac{H_I}{H_0} - 8, \tag{3.10}$$

where we used $1+z_{\rm eq} \simeq 3000$. From (2.35) the ratio $\rho_{\rm eq}/\rho_{\rm reh}$ becomes $\rho_{\rm eq}/\rho_{\rm reh} = H_{\rm eq}^2/H_I^2$ and (3.10) becomes

$$N_{\rm hor} \simeq 68 + \frac{1}{2}\ln\frac{H_I}{M_{\rm Pl}}, \tag{3.11}$$

where we used $H_{\rm eq} = 5.25\times10^6 h^3\Omega_{m,0}^2 H_0$, $H_0 = 1.75\times10^{-61} h M_{\rm Pl}$, $\Omega_{m,0} = 0.32$ from (2.41) and $h \simeq 0.7$ from (2.38) [111] . This relation tells us that the number of e-folds needed to solve the horizon problem crucially depends on the scale of inflation. Hence, the precise value of $N_{\rm hor}$ is a model-dependent statement. For what concern this thesis H_I will be set to $H_I \sim 10^{-6}M_{\rm Pl}$, such that $N_{\rm hor}$ becomes $N_{\rm hor} \sim 61$.

The value $N_{\rm hor} \sim 61$ just derived is based on assumptions that in general are not expected to hold, and the correct $N_{\rm hor,c}$ will be different. If we allow for a non-instantaneous reheating (with for simplicity $w_{\rm reh} = 0$) and a possible drop in the energy density at the end of inflation $\rho_{\rm end} \neq 3M_{\rm Pl}^2H_I^2$ relation (3.11) becomes [111, 132]

$$N_{\rm hor,c} = N_{\rm hor} + \frac{1}{4}\ln\frac{3M_{\rm Pl}^2H_I^2}{\rho_{\rm end}} + \frac{1}{12}\ln\frac{\rho_{\rm reh}}{\rho_{\rm end}}. \tag{3.12}$$

The last two terms are the missing effects discussed above. In the scenario concerned by this thesis, the reduction in the energy density at the end of inflation is one or two orders of magnitude. Hence, the second term in (3.12) is unlike to increase $N_{\rm hor,c}$ by much more than a factor of order unity.

The last term in (3.12) belongs to the main uncertainty. The duration of the reheating phase is not known and the reduction in energy density can span many orders of magnitude. In the extreme case in which reheating continues until BBN and with $H_I \sim 10^{-6}M_{\rm Pl}$, the last factor in (3.12) gives $1/12\ln\rho_{\rm reh}/\rho_{\rm end} \sim -15$. Hence, it is plausible to assume, for what concerns the thesis, that the correct value for $N_{\rm hor,c}$ is between $50 \leq N_{\rm hor,c} \leq 60$. This is consistent with what usually is assumed in the literature. However, under simple assumptions regarding the model, the expected number of e-folds can evade the previous range, see [111] for more details.

Inflation also solves the flatness problem. Indeed $1-\Omega$ is controlled by $(aH)^{-2}$ and in inflation the Hubble radius is decreasing, pushing $1-\Omega$ to zero. In other words, $\Omega = 1$ is an attractor during inflation. It is highly believed that inflation predicts Ω_0 to be close to one, $\Omega_0 = 1$.

3.4 Inflation

So far we use as a definition of inflation the shirking Hubble sphere since it is in direct connection with the horizon problem. In the literature, there are equivalent definitions of inflation

$$\frac{d}{dt}\frac{1}{aH} < 0 \iff \ddot{a} > 0 \iff \epsilon = -\frac{\dot{H}}{H^2} < 1 \iff P < -\frac{\rho}{3}, \tag{3.13}$$

and are all equivalent. We saw that we needed at least $N \sim 60$ to solve the previous puzzles. This means that ϵ should be smaller than one for a sufficiently long time. Hence, ϵ has to vary slowly in one Hubble time, to quantify this change we introduce

$$\eta = \frac{d\ln\epsilon}{dN} = \frac{\dot{\epsilon}}{H\epsilon}. \tag{3.14}$$

If $|\eta| < 1$, inflation can persist. Let us see which field theory can sustain an inflationary period in the following sub-section.

3.4.1 Scalar field

As a simple possible realization of inflation, we will study a scalar field as a source for the evolution of the FLRW metric (2.10). Moreover, in the rest of the thesis, we restrict to the case where the spatial curvature K, in (2.10), is set to zero. This assumption is consistent with the experiment and we assume the validity of GR and a single scalar field ϕ. The action of a real scalar field coupled minimally to gravity is given by

$$S_\phi = \int d^4x\sqrt{-g}\mathcal{L} = \int d^4x\sqrt{-g}\left(\frac{1}{2}\partial_\mu\phi\partial^\mu\phi - V(\phi)\right), \tag{3.15}$$

From S_ϕ we can derive the stress-energy tensor that is

$$T_{\mu\nu} = \partial_\mu\phi\partial_\nu\phi - g_{\mu\nu}\mathcal{L}. \tag{3.16}$$

From the Lagrangian in (3.15) we can read the component of the $T_{\mu\nu}$ that are

$$T_{00} = \rho_{\phi_b} = \dot{\phi}_b^2/2 + V(\phi_b), \tag{3.17}$$

$$P_{\phi_b} = T_i^i/3 = \dot{\phi}_b^2/2 - V(\phi_b), \tag{3.18}$$

where we used a fluid interpretation for ϕ and we restrict to homogeneous configuration, namely ϕ is a function only on time $\phi_b(t)$. From the Lagrangian in (3.15) we can derive the Klein-Gordon equation

$$\ddot{\phi}_b + 3H\dot{\phi}_b = -V_{,\phi_b}, \tag{3.19}$$

where $V_{,\phi_b} = \partial V/\partial\phi_b$ and the $3H\dot{\phi}_b$ plays the role of a friction term. If we insert (3.17) and (3.18) in (2.35) and (2.36) we obtain

$$M_{Pl}^2 H^2 = \frac{1}{3}\left[\dot{\phi}_b^2/2 + V(\phi_b)\right], \tag{3.20}$$

$$\frac{\ddot{a}}{a} = -\frac{1}{3M_{Pl}^2}\left(\dot{\phi}_b^2 - V(\phi_b)\right). \tag{3.21}$$

For an accelerated expansion the pressure satisfies $P_{\phi_b} < -\rho_{\phi_b}/3$. Putting (3.17) and (3.18) in $w_{\phi_b} = P_{\phi_b}/\rho_{\phi_b}$ we obtain

$$w_{\phi_b} = \frac{\dot{\phi}_b^2/2 - V(\phi_b)}{\dot{\phi}_b^2/2 + V(\phi_b)}. \tag{3.22}$$

If $\dot{\phi}_b^2 \ll V$, then relation (3.22) becomes $w_{\phi_b} \approx -1$ and we have an equation of state similar to vacuum energy that can sustain inflation.

We can obtain the same result starting from the definition of the ϵ parameter. If we take a time derivative of (2.35) and using (3.19) we get

$$\dot{H} = -\frac{\dot{\phi}_b^2}{2M_{Pl}^2}. \tag{3.23}$$

If we use (3.23) and (2.35) in (3.13) we obtain

$$\epsilon = \frac{3\dot{\phi}_b^2}{2\left(\dot{\phi}_b^2/2 + V(\phi_b^2)\right)}. \tag{3.24}$$

In order to have $\epsilon \ll 1$ we need $\dot{\phi}_b^2 \ll V(\phi_b^2)$, as we expected.

To maintain for a long time $\epsilon < 1$, we can introduce the dimensionless acceleration for Hubble time

$$\tilde{\delta} = -\frac{\ddot{\phi}_b}{H\dot{\phi}_b}, \tag{3.25}$$

and $\tilde{\delta}$ and η are related, in fact taking the derivative of (3.23) we obtain $\eta = 2(\epsilon - \tilde{\delta})$. If $\{\epsilon, |\tilde{\delta}|, |\eta|\} \ll 1$ then H, ϵ and ϕ_b change slowly in one Hubble time.

Let us now analyze a regime in which these parameters are small, such that inflation persists. The assumption that $\{\epsilon, |\tilde{\delta}|, |\eta|\}$ are small is called slow-roll approximation, and these parameters are called slow-roll parameters. From $\epsilon \ll 1$ we need $\dot{\phi}_b^2 \ll V$ and relation (2.35) becomes

$$3M_{Pl}^2 H^2 \simeq V(\phi_b). \tag{3.26}$$

From the slow-roll of ϕ_b, namely $\tilde{\delta} \ll 1$, we obtain

$$3H\dot{\phi}_b \simeq -V_{,\phi_b}, \tag{3.27}$$

that is the slow-roll version of the Klein-Gordon equation. If we insert (3.27) and (3.26) in the definition of ϵ we obtain

$$\epsilon \simeq \frac{M_{\rm Pl}^2}{2}\left(\frac{V_{,\phi_{\rm b}}}{V}\right)^2 = \epsilon_{\rm V}, \tag{3.28}$$

where the right-hand side is the definition of potential slow-roll parameter $\epsilon_{\rm V}$. Using (3.13) and (3.25) we can introduce the second potential slow-roll parameter $\eta_{\rm V}$ as

$$\tilde{\delta} + \epsilon = -\frac{\ddot{\phi}_{\rm b}}{H\dot{\phi}_{\rm b}} - \frac{\dot{H}}{H^2} \approx M_{\rm Pl}^2 \frac{V_{,\phi_{\rm b}\phi_{\rm b}}}{V} = \eta_{\rm V}, \tag{3.29}$$

where in going from left to right we estimate $\ddot{\phi}_{\rm b}$ using (3.27) and the most right-hand side is the definition of $\eta_{\rm V}$. Notice that $\eta_{\rm V}$ is related to η as $\eta_{\rm V} \approx 2\epsilon - \eta/2$. Of course, inflation requires that both $\epsilon_{\rm V}$ and $\eta_{\rm V}$ are small and the form of the potential is constrained to be sufficiently flat.

The amount of e-folds between two times $t_{\rm i}$ and $t_{\rm f}$ is defined as

$$N_{\rm t} = \int_{t_{\rm i}}^{t_{\rm f}} H dt. \tag{3.30}$$

If $t_{\rm i}$ and $t_{\rm f}$ satisfy $\epsilon(t_{\rm i}) = \epsilon(t_{\rm f}) = 1$ then $N_{\rm t}$ represents the total duration of inflation. It is important to stress that $N_{\rm t}$ and $N_{\rm hor,c}$ (see Section 3.3) are two different quantities and the exact value of $N_{\rm t}$ is not known but it is expected to be much larger than $N_{\rm hor,c}$, $N_{\rm t} \gg N_{\rm hor,c}$. If we use relation (3.27) and (3.28) in (3.30) we obtain

$$N_{\rm t} \simeq -\int_{\phi_{\rm i}}^{\phi_{\rm f}} \frac{1}{\sqrt{2\epsilon_{\rm V}}} \frac{d\phi}{M_{\rm Pl}}, \tag{3.31}$$

that is an integral over-the-field excursion during inflation.

Let us conclude this section by noting that based on the dynamics of the inflaton field, we can roughly have large-field or small-field models. In the first class, the inflaton field starts from a large field value and rolls down to the minimum of the potential. An example of this class is chaotic inflation [118]. In the second case, the inflaton initial value is small and the field rolls down to the potential minimum. New inflation [117] enters in this class. In both scenarios, the end of inflation is set when the kinetic energy of the inflaton field becomes comparable to the potential, namely $\epsilon(t_{\rm f}) = 1$. Hybrid inflation is an example of a model that can be both large-field or small-field, but with a different condition that sets the end of inflation, as stated in [119]. In this model, the end of inflation is established by a phase transition that is generated from an instability from a second field. Inflation may consist of different accelerated phases, each represented by a single-field model. For example, double inflation models involve two dynamical fields that provide two periods of inflation. An example is given by [142]. The presence of potential is a common feature among these models, but there are cases where inflation occurs without it [12].

Chapter 4

The perturbed Universe

So far our analysis has focused on the homogeneous Universe. We know that is not of course true at all scales and inhomogeneities are present and we introduced it in Section 4.1. We need to account for possible perturbations in the inflaton field that will become the seeds for the CMB perturbations, galaxies, and so on; this natural production mechanism of inhomogeneities is a strong motivation for the validity of the inflationary paradigm. Due to Einstein field equations these perturbations in ϕ source inevitably fluctuations in the metric. The gauge issue in GR reinforces the tight link between perturbations in the metric and the inflaton field that is discussed in Section 4.2. We will introduce gauge invariant quantities that mix perturbations in ϕ and $g_{\mu\nu}$ showing explicitly that they are ultimately linked. We will derive the linear equations of motion in Section 4.6 and from them we show the conservation of $\mathcal{R}$ (4.94) in Section 4.7. In Sections 4.9 and 4.10 we derived the power spectrum for $\mathcal{R}$ and the tensor modes. To practice with the tools just exposed we will analyze in Section 4.11 the model called Higgs Inflation. In Section 4.12, we derived the Lyth bound. In Section 4.13 we present the δN formalism. Other references on these topics include [26, 22, 127].

4.1 Perturbed metric tensor

Let us consider a small perturbation around a flat FLRW metric $\bar{g}_{\mu\nu}$ as

$$g_{\mu\nu} = \bar{g}_{\mu\nu} + \delta g_{\mu\nu}. \tag{4.1}$$

The general perturb line element is

$$ds^2 = a^2 \left[(1+2A)\, d\tau^2 - 2B_i dx^i d\tau - \left(\delta_{ij} + h_{ij}\right) dx^i dx^j \right], \tag{4.2}$$

where A, B, h are functions of (τ, x^i) and we will work with the conformal time τ. It is useful to introduce the so-called scalar-vector-tensor (SVT) decomposition. Within this decomposition and in linear theory, it has been proven that scalar, vector, and tensor perturbations evolve independently and they can be studied separately [102]. For vectors the SVT decomposition is simple, it consists of

$$B_i = \partial_i B + \hat{B}_i, \tag{4.3}$$

where $\hat{B}_i$ satisfies $\partial^i \hat{B}_i = 0$. B is the scalar part of B_i and $\hat{B}_i$ is the vector part and it is solenoidal. For the rank-two tensor we have

$$h_{ij} = 2C\delta_{ij} + 2\partial_{(i}\partial_{j)}E + 2\partial_{(i}\hat{E}_{j)} + 2\hat{E}_{ij}, \tag{4.4}$$

where

$$\partial_{(i}\partial_{j)}E = \left(\partial_i\partial_j - \frac{\delta_{ij}}{3}\nabla^2\right)E, \tag{4.5}$$

$$\partial_{(i}\hat{E}_{j)} = \frac{1}{2}\left(\partial_i\hat{E}_j + \partial_j\hat{E}_i\right). \tag{4.6}$$

A before $\partial^i \hat{E}_i = 0$ and $\hat{E}_{ij}$ represents gravitational waves in cosmology and satisfies $\hat{E}^i_i = 0$ and $\partial^i \hat{E}_{ij} = 0$. In this thesis, we are mainly interested in scalar and tensor perturbations. Vector perturbations are not produced during scalar-induced inflation and, even if they are present initially, they will decay quickly with the expansion of the Universe.

As we briefly mentioned the metric and matter perturbations are not only linked through the Einstein equations but also due to a redundancy of the description of the line element (4.2). In other words, not all perturbations are physical and a change of coordinate can change the values of the perturbations. We can introduce fictitious perturbations starting from an unperturbed FLRW metric. Let us take

$$ds^2 = a^2\left[d\tau^2 - \delta_{ij}dx^i dx^j\right], \tag{4.7}$$

and we perform the infinitesimal change x^i to $\tilde{x}^i = x^i + d^i(\tau, \vec{x})$ such that $dx^i = d\tilde{x}^i - d^{i,\prime}d\tau - d^i_{,j}dx^j$, where $d^{i,\prime} = \partial_\tau d^i$ and $d^i_{,j} = \partial_j d^i$. The line element (4.7) becomes

$$ds^2 = a^2\left[d\tau^2 - 2d^{i,\prime}d\tau d\tilde{x}^i - \left(\delta_{ij} + 2\partial_{(i}d_{j)}\right)d\tilde{x}^i d\tilde{x}^j\right], \tag{4.8}$$

where we neglect the second order term in d. We introduced two metric perturbations with the change of coordinates. Not only are metric perturbations affected by a change of coordinates but also matter quantities. Performing a time redefinition from τ to $\tau + \tilde{d}(\tau, \vec{x})$, the homogeneous energy density $\bar{\rho}(\tau)$ transforms in $\bar{\rho}(\tau) + \bar{\rho}(\tau)'\tilde{d}$. This tells us that even if we start from a uniform Universe we can introduce gauge modes that mimic perturbations. We can also revert the logic and remove real perturbations with an appropriate change of coordinates (hypersurface of constant energy for example). These very naive examples suggest we must introduce more fundamental quantities that are gauge (coordinate) invariant.

4.2 Gauge Transformations

We consider the following change of coordinates from x^μ to $\tilde{x}^\mu = x^\mu + d^\mu(\tau, \vec{x})$ and we define $d^0 = T$ and $d^i = \partial^i L + \hat{L}^i$. Using the invariance

of the line element we get the standard formula for the metric tensor in the two coordinates system

$$g_{\mu\nu}(x) = \frac{\partial \tilde{x}^\alpha}{\partial x^\mu}\frac{\partial \tilde{x}^\beta}{\partial x^\nu}\tilde{g}_{\alpha\beta}(\tilde{x}). \tag{4.9}$$

For example for $\mu = \nu = 0$ we get

$$g_{00}(x) = \frac{\partial \tilde{x}^\alpha}{\partial \tau}\frac{\partial \tilde{x}^\beta}{\partial \tau}\tilde{g}_{\alpha\beta}(\tilde{x}). \tag{4.10}$$

Using the parametrization (4.2), $\partial\tilde{\tau}/\partial\tau = 1 + T'$ and $\partial\tilde{x}^i/\partial\tau = \partial^i L' + \hat{L}^{i,'}$ we can deduce the change of A, at linear order, under the previous coordinates transformation, namely

$$\tilde{A} = A - T' - \mathcal{H}T, \quad \mathcal{H} = aH. \tag{4.11}$$

With the same logic we can derive the change of B_i and h_{ij} that are

$$\tilde{B}^i = B^i + \partial^i T - \hat{L}^{i,'} - \partial^i L', \tag{4.12}$$

$$\tilde{h}_{ij} = h_{ij} - 2\partial_{(i}L_{j)} - 2\mathcal{H}T\delta_{ij}. \tag{4.13}$$

$$\tag{4.14}$$

In terms of the variables used in the SVT decomposition we have

$$\tilde{B} = B + T - L', \tag{4.15}$$

$$\tilde{\hat{B}}^i = \hat{B}^i - \hat{L}^{i,'}, \tag{4.16}$$

$$\tilde{E} = E - L, \tag{4.17}$$

$$\tilde{C} = C - \mathcal{H}T - \frac{\nabla^2}{3}L, \tag{4.18}$$

$$\tilde{\hat{E}}_i = \hat{E}_i - \hat{L}_i, \tag{4.19}$$

$$\tilde{\hat{E}}_{ij} = \hat{E}_{ij}. \tag{4.20}$$

We notice that within the SVT decomposition, the tensor perturbations $\hat{E}_{ij}$ at linear order are gauge invariant.

We can introduce scalar, vector, and tensor perturbations Ψ, Φ, and $\hat{\Phi}$ that are gauge invariant at linear order and they are called Bardeen variables. They are defined as [21, 102]

$$\Psi = A + \mathcal{H}\left(B - E'\right) + \left(B - E'\right)', \tag{4.21}$$

$$\Phi = -C - \mathcal{H}\left(B - E'\right) + \frac{1}{3}\nabla^2 E, \tag{4.22}$$

$$\hat{\Phi}^i = \hat{E}^i - \hat{B}^i, \tag{4.23}$$

$$\hat{E}_{ij}. \tag{4.24}$$

These variables can not be removed via a gauge transformation.

As we said, contrary to working with gauge invariant quantities, we can fix the gauge and do the computations there. An example of a useful gauge is the Newtonian gauge which is defined when $B = E = 0$. In this gauge, $A = \Psi_N$ and $C = -\Phi_N$ can be seen directly from (4.21) and (4.22). Where Ψ_N and Φ_N are the Bardeen variables in the Newtonian gauge. Another useful gauge that we will use in this thesis is the spatially flat gauge where $C = E = 0$.

4.3 Perturbed stress-energy tensor

The unperturbed stress-energy tensor $\bar{T}^\mu_\nu = (\bar{\rho} + \bar{P})\bar{u}^\mu\bar{u}_\nu - \bar{P}\delta^\mu_\nu$ where $\bar{u}_\mu = a\delta^0_\mu$, $\bar{u}^\mu = a^{-1}\delta^\mu_0$ is now modified by a δT^μ_ν defined as

$$\delta T^\mu_\nu = (\delta\rho + \delta P)\,\bar{u}^\mu\bar{u}_\nu + (\bar{\rho} + \bar{P})\,(\delta u^\mu\bar{u}_\nu + \bar{u}^\mu\delta u_\nu) - \delta P\delta^\mu_\nu - \Pi^\mu_\nu, \tag{4.25}$$

where $\delta\rho$, δP, and δu^μ represent perturbations in the energy density, pressure and velocity. For the moment we keep track of Π, the anisotropic part of the stress-energy tensor, even if in this thesis we will neglect it.

Let us carry out the component of the δT. The perturb velocity has to respect the normalization condition $g_{\mu\nu}u^\mu u^\nu = -1$ and using the normalization condition for the unperturbed velocity and metric $\bar{g}_{\mu\nu}\bar{u}^\mu\bar{u}^\nu = -1$ we obtain

$$\delta g_{\mu\nu}\bar{u}^\mu\bar{u}^\nu + 2\bar{u}_\mu\delta u^\mu = 0. \tag{4.26}$$

If we use $\bar{u}^\mu = 1/a\delta^\mu_0$ and (4.2) in (4.26) we get $\delta u^0 = -A/a$. For the total velocity, we have

$$u^\mu = \bar{u}^\mu + \delta u^\mu = \left(1 - A, v^i\right)/a, \quad v^i = \frac{dx^i}{d\tau}, \tag{4.27}$$

and the velocity with the lower index is

$$u_\mu = a\left[1 + A, -\left(v_i + B_i\right)\right]. \tag{4.28}$$

From (4.25) we can evaluate all δT terms that are

$$\delta T^0_0 = \delta\rho, \tag{4.29}$$

$$\delta T^0_i = -\left(\bar{\rho} + \bar{P}\right)\left(v_i + B_i\right), \tag{4.30}$$

$$\delta T^i_0 = \left(\bar{\rho} + \bar{P}\right)v^i = q^i, \tag{4.31}$$

$$\delta T^i_j = -\delta P\delta^i_j - \Pi^i_j, \tag{4.32}$$

where we used $\Pi^0_0 = \Pi^0_i = 0$ and we defined the momentum density q^i as $q^i = (\bar{\rho} + \bar{P})\,v^i$. If there are present several contributions to the stress-energy tensor $T^{\mathrm{I}}_{\mu\nu}$, for the total stress-energy tensor we have $T_{\mu\nu} = \sum_{\mathrm{I}} T^{\mathrm{I}}_{\mu\nu}$. For the

components of $T_{\mu\nu}$ we obtain

$$\delta\rho = \sum_{\mathrm{I}} \delta\rho_{\mathrm{I}}, \tag{4.33}$$

$$\delta P = \sum_{\mathrm{I}} \delta P_{\mathrm{I}}, \tag{4.34}$$

$$q^i = \sum_{\mathrm{I}} q^i_{\mathrm{I}}, \tag{4.35}$$

$$\Pi^{ij} = \sum_{\mathrm{I}} \Pi^{ij}_{\mathrm{I}}. \tag{4.36}$$

We can decompose the components of δT using the SVT decomposition, for the vector q^i we have

$$q_i = \partial_i q + \hat{q}_i, \tag{4.37}$$

and for the anisotropic part, we have

$$\Pi_{ij} = \partial_{(i}\partial_{j)}\Pi + \partial_{(i}\hat{\Pi}_{j)} + \hat{\Pi}_{ij}. \tag{4.38}$$

Under the change of coordinates from x^μ to $\tilde{x}^\mu = x^\mu + d^\mu(\tau, \vec{x})$ where as before we define $d^0 = T$ and $d^i = \partial^i L + \hat{L}^i$. Under the change of coordinates for the stress-energy tensor $T_{\mu\nu}$ we obtain

$$T^\mu_\nu(x) = \frac{\partial x^\mu}{\partial \tilde{x}^\alpha}\frac{\partial \tilde{x}^\beta}{\partial x^\nu}\tilde{T}^\alpha_\beta(\tilde{x}). \tag{4.39}$$

For the component $\mu = \nu = 0$ we have

$$T^0_0(x) = \bar{\rho} + \delta\rho = \frac{\partial\tau}{\partial\tilde{\tau}}\frac{\partial\tilde{\tau}}{\partial\tau}\tilde{T}^0_0 = \bar{\rho} + \bar{\rho}' T + \delta\tilde{\rho}, \tag{4.40}$$

where going from left to right we used the definition of T^0_0, $\partial\tau/\partial\tilde{\tau} = 1 - T'$ and we worked at linear order. From (4.40) we obtain

$$\delta\tilde{\rho} = \delta\rho - \bar{\rho}' T, \tag{4.41}$$

that represents the change of $\delta\rho$ under the change of coordinates. For the other components of $T_{\mu\nu}$ we have

$$\delta\tilde{P} = \delta P - \bar{P}' T, \tag{4.42}$$

$$\tilde{v}_i = v_i + L_i^{'}\ , \tag{4.43}$$

$$\tilde{q}_i = q_i + (\bar{\rho} + \bar{P})\, L_i^{'}\ , \tag{4.44}$$

$$\tilde{\Pi}_{ij} = \Pi_{ij}. \tag{4.45}$$

From the last relations, we see that we need to introduce some gauge invariant variable that is composition of matter and metric perturbations. We define the comoving gauge density perturbation as

$$\bar{\rho}\Delta = \delta\rho + \bar{\rho}'\,(v + B)\,, \tag{4.46}$$

where v is the scalar part of v^i, namely $v^i = \partial^i v + \hat{v}^i$. Relation (4.46) is gauge invariant at linear order, indeed

$$\bar{\rho}\tilde{\Delta} = \delta\tilde{\rho} + \bar{\rho}'\left(\tilde{v} + \tilde{B}\right) = \delta\rho - \bar{\rho}'T + \bar{\rho}'\left(v + L' + B + T - L'\right) = \bar{\rho}\Delta, \quad (4.47)$$

where in going from left to right we used the transformation rules for $\delta\rho$, v, and B.

As before, instead of working with gauge invariant quantities, we can fix the gauge in the matter section. Famous gauge choices are

1. Uniform density gauge : $\delta\rho = 0$.

2. Comoving gauge: We put the scalar part of the momentum density to zero, $q = 0$.

Within these gauge choices, we have at our disposal the freedom to set other perturbations, A, B, or other to zero. Another property that characterizes matter perturbations is the type of these fluctuations. In this thesis, we will see two types: adiabatic and isocurvature perturbations.

4.4 Adiabatic perturbations

If the Universe is composed of multiple fluids, adiabatic perturbations correspond to perturbations induced by a common, local shift in time of all background quantities; we define adiabatic perturbations as

$$\delta\rho_{\mathrm{I}}(\tau, \vec{x}) = \bar{\rho}_{\mathrm{I}}(\tau + \delta\tau(\vec{x})) - \bar{\rho}_{\mathrm{I}}(\tau) = \bar{\rho}'_{\mathrm{I}}\delta\tau(\vec{x}), \quad (4.48)$$

where I indicates the particular species and $\delta\tau$ is the same for all. In a certain sense, we can view the presence of adiabatic perturbations as some parts of the Universe being "ahead" and the others "behind " in the evolution. Adiabatic perturbations imply

$$\delta\tau = \frac{\delta\rho_{\mathrm{I}}}{\bar{\rho}'_{\mathrm{I}}} = \frac{\delta\rho_{\mathrm{J}}}{\bar{\rho}'_{\mathrm{J}}}, \quad (4.49)$$

for all I, J. If there is no energy transfer between different species I, J, we can use $\bar{\rho}'_{\mathrm{I}} = -3\mathcal{H}(1 + w_{\mathrm{I}})\bar{\rho}_I$ and rewrite (4.49) as

$$\frac{\delta_{\mathrm{I}}}{1 + w_{\mathrm{I}}} = \frac{\delta_{\mathrm{J}}}{1 + w_{\mathrm{J}}}, \quad (4.50)$$

where $\delta_{\mathrm{I}} = \delta\rho_{\mathrm{I}}/\bar{\rho}_{\mathrm{I}}$.

From the last expression, we can deduce that, for adiabatic perturbations, all matter components have the same fractional perturbation; instead, all radiation components obey $\delta_{\mathrm{r}} = 4\delta_{\mathrm{m}}/3$. For adiabatic perturbations, it follows that the total energy density can be written as

$$\delta\rho_{\mathrm{TOT}} = \bar{\rho}_{\mathrm{TOT}}\delta_{\mathrm{TOT}} = \sum_I \bar{\rho}_I\delta_{\mathrm{I}}. \quad (4.51)$$

This quantity is dominated by the species that is dominant in the background since all $\delta_{\rm I}$ are comparable.

4.5 Isocurvature Fluctuations

Isocurvature fluctuations can be defined as the complement of adiabatic fluctuations. Isocurvature perturbations do not perturb the total energy density but are responsible for fluctuations between different components (I, J). We can use as a definition of isocurvature fluctuations the following expression

$$\mathrm{S}_{\rm IJ} = \frac{\delta_{\rm I}}{1+w_{\rm I}} - \frac{\delta_{\rm J}}{1+w_{\rm J}}. \tag{4.52}$$

Observations are consistent with a primordial spectrum of perturbations that are of adiabatic type.

4.6 Linearized Einstein Equations

We are going to derive the perturb continuity and Einstein equations at linear order in perturbation theory. We are going to use the spatially flat gauge ($C = E = 0$) from now on since it will be useful for later calculations of the evolution of $\delta\phi$.

The metric tensor in this gauge is

$$g_{\mu\nu} = a^2 \begin{pmatrix} 1+2A & -\partial_i B \\ -\partial_i B & -\delta_{ij} \end{pmatrix}, \tag{4.53}$$

where we neglect vector modes and gravitational waves ($\hat{E}_{ij}$) will be treated separately. In the rest of the thesis, we will neglect anisotropic stress in the stress-energy tensor, $\Pi_{ij} = 0$, and the vector modes inside $T_{\mu\nu}$. In other words, in the rest of the thesis, unless otherwise specified, we deal only with scalar perturbations both in the metric and matter sectors. The inverse metric is

$$g^{\mu\nu} = \frac{1}{a^2} \begin{pmatrix} 1-2A & -\partial^i B \\ -\partial^i B & -\delta^{ij} \end{pmatrix}. \tag{4.54}$$

With (4.53) and (4.54) we can evaluate the connection coefficients that are defined as

$$\Gamma^{\mu}_{\nu\rho} = \frac{1}{2} g^{\mu\lambda} \left(\partial_\nu g_{\lambda\rho} + \partial_\rho g_{\lambda\nu} - \partial_\lambda g_{\nu\rho} \right), \tag{4.55}$$

whose components are

$$\Gamma^0_{00} = \frac{1}{2}g^{00}\partial_\tau g_{00} = \frac{1-2A}{2a^2}\left[a^2(1+2A)\right]' = \mathcal{H} + A', \tag{4.56}$$

$$\Gamma^0_{0i} = \frac{1}{2}g^{00}\partial_i g_{00} = \partial_i A + \mathcal{H}\partial_i B, \tag{4.57}$$

$$\Gamma^i_{00} = \mathcal{H}\partial^i B + \partial^i B' + \partial^i A, \tag{4.58}$$

$$\Gamma^0_{ij} = \mathcal{H}\delta_{ij} - 2A\mathcal{H}\delta_{ij} - \partial_i\partial_j B, \tag{4.59}$$

$$\Gamma^i_{j0} = \mathcal{H}\delta^i_j, \tag{4.60}$$

$$\Gamma^i_{jk} = -\delta_{jk}\partial^i B\mathcal{H}. \tag{4.61}$$

The conservation of the $T_{\mu\nu}$, $\nabla_\mu T^\mu_\nu = 0$, gives the continuity and Euler equations. The $\nu = 0$ component is

$$\partial_\mu T^\mu_\nu + \Gamma^\mu_{\mu\alpha}T^\alpha_0 - \Gamma^\alpha_{\mu 0}T^\mu_\alpha = 0, \tag{4.62}$$

and at the background and first order we have

$$\bar{\rho}' + 3\mathcal{H}(\bar{\rho} + \bar{P}) = 0, \tag{4.63}$$

$$\delta\rho + 3\mathcal{H}(\delta\rho + \delta P) + (\bar{\rho} + \bar{P})\nabla^2 v = 0. \tag{4.64}$$

The Euler equation is the $\nu = i$ part and we get

$$(v+B)' - \frac{\bar{P}'}{\bar{\rho}'}3\mathcal{H}(v+B) + \frac{\delta P}{\bar{\rho}+\bar{P}} + A + \mathcal{H}B + \mathcal{H}v = 0. \tag{4.65}$$

Notice that this equation does not contain the $\nu = i$ index due to the SVT decomposition and having ignored vector modes. In (4.65), both v and B appear with a collective gradient that can be integrated by providing a scalar equation.

4.6.1 Perturbed Einstein Equations

The Ricci tensor is

$$R_{\mu\nu} = \partial_\rho\Gamma^\rho_{\mu\nu} - \partial_\nu\Gamma^\rho_{\rho\mu} + \Gamma^\alpha_{\alpha\rho}\Gamma^\rho_{\mu\nu} - \Gamma^\alpha_{\nu\rho}\Gamma^\rho_{\alpha\mu}, \tag{4.66}$$

whose components are

$$R_{00} = \mathcal{H}\nabla^2 B + \nabla^2 B' + \nabla^2 A - 3\mathcal{H}' + 3\mathcal{H}A, \tag{4.67}$$

$$R_{0i} = \mathcal{H}'\partial_i B + 2\mathcal{H}(\partial_i A + \mathcal{H}\partial_i B), \tag{4.68}$$

$$R_{ij} = \delta_{ij}\left(\mathcal{H}' + 2\mathcal{H}^2\right) - \delta_{ij}\left(A'\mathcal{H} + 2A\mathcal{H}' + \mathcal{H}\nabla^2 B + 4A\mathcal{H}\right) - \partial_i\partial_j(B' + A) - 2\mathcal{H}\partial_i\partial_j B. \tag{4.69}$$

The Ricci scalar is

$$R = g^{\mu\nu}R_{\mu\nu} = g^{00}R_{00} + g^{ij}R_{ij}, \tag{4.70}$$

and using the previous results for $R_{\mu\nu}$ we have

$$\begin{aligned} a^2R = &-6\mathcal{H}' - 6\mathcal{H}^2 + 6\mathcal{H}A' + 12A\mathcal{H}' + \\ &+ 6\mathcal{H}\nabla^2 B + 12A\mathcal{H}^2 + 2\nabla^2\left(B' + A\right). \end{aligned} \tag{4.71}$$

The Einstein tensor is defined as

$$G_{\mu\nu} = R_{\mu\nu} - \frac{g_{\mu\nu}}{2}R, \tag{4.72}$$

whose components are

$$G_{00} = 3\mathcal{H}^2 - 2\mathcal{H}\nabla^2 B, \tag{4.73}$$

$$G_{0i} = -2\mathcal{H}'\partial_i B - \mathcal{H}^2\partial_i B + 2\mathcal{H}\partial_i A, \tag{4.74}$$

$$\begin{aligned} G_{ij} = &-\delta_{ij}\left(\mathcal{H}^2 + 2\mathcal{H}'\right) - \partial_i\partial_j\left(B' + A\right) - 2\mathcal{H}\partial_i\partial_j B + \\ &+\delta_{ij}\left(\nabla^2 B' + \nabla^2 A + 2A\mathcal{H}^2 + 2\mathcal{H}\nabla^2 B + 4\mathcal{H}'A + 2A'\mathcal{H}\right) \end{aligned} \tag{4.75}$$

We are ready now to derive the Einstein equations that are

$$M_{\rm Pl}^2 G_{\mu\nu} = T_{\mu\nu}. \tag{4.76}$$

For the $\mu = \nu = 0$ component, in linear regime, we have

$$M_{\rm Pl}^2 G_{00} = g_{00}T_0^0. \tag{4.77}$$

Using (4.73) and (4.29) in (4.77) we obtain

$$M_{\rm Pl}^2\left(3\mathcal{H}^2 - 2\mathcal{H}\nabla^2 B\right) = a^2\bar{\rho}\left(1 + \delta + 2A\right), \tag{4.78}$$

and at the background and perturb level we have

$$M_{\rm Pl}^2 3\mathcal{H}^2 = a^2\bar{\rho}, \tag{4.79}$$

$$-2M_{\rm Pl}^2\mathcal{H}\nabla^2 B = a^2\bar{\rho}\left(2A + \delta\right). \tag{4.80}$$

Using (4.74) and (4.30), for the $\mu = i, \nu = 0$ components, we obtain

$$2M_{\rm Pl}^2\mathcal{H}\partial_i A = -a^2\left(\bar{\rho} + \bar{P}\right)\partial_i\left(v + B\right). \tag{4.81}$$

Using (4.75) and (4.32), for the diagonal part of the $\mu = i, \nu = j$ components, we get

$$M_{\rm Pl}^2\left(\mathcal{H}^2 + 2\mathcal{H}'\right) = -a^2\bar{P}, \tag{4.82}$$

$$\nabla^2 B' + \nabla^2 A + 2A\mathcal{H}^2 + 2\mathcal{H}\nabla^2 B + 4\mathcal{H}'A + 2A'\mathcal{H} = \frac{a^2\delta P}{M_{\rm Pl}^2}. \tag{4.83}$$

Instead from the off diagonal part of the $\mu = i, \nu = j$ components we obtain

$$B' + 2\mathcal{H}B = -A. \tag{4.84}$$

Relation (4.81) can be integrated, with the assumption that the perturbations decay at infinity, and we get

$$2M_{\rm Pl}^2 \mathcal{H} A = -a^2 \left(\bar{\rho} + \bar{P}\right)(v + B). \tag{4.85}$$

Using (4.85) in (4.80) we obtain

$$-2M_{\rm Pl}^2 \mathcal{H} \nabla^2 B = a^2 \left[\bar{\rho}\delta - 3\mathcal{H}\left(\bar{\rho} + \bar{P}\right)(v + B)\right] = a^2 \bar{\rho}\Delta, \tag{4.86}$$

where in going from left to right we used the definition of comoving-gauge density perturbation Δ. Using (4.84) in (4.83) we obtain

$$A'\mathcal{H} + A\left(\mathcal{H}^2 + 2\mathcal{H}'\right) = \frac{a^2 \delta P}{2M_{\rm Pl}^2}. \tag{4.87}$$

Relations (4.87), (4.86), (4.85), (4.64) and (4.65) form a consistent but redundant system.

4.7 Conserved curvature perturbation

To link the values of the primordial perturbations during and after inflation, it is crucial to introduce the so-called comoving curvature perturbation; which is conserved on super-Hubble ($k \ll \mathcal{H}$) scales for adiabatic fluctuations.

We start from the intrinsic curvature of surfaces at a constant time. We work in an arbitrary gauge for this section. The induced metric γ on the constant time surface is

$$\gamma_{iJ} = a^2 \left[(1 + 2C)\,\delta_{ij} + 2E_{ij}\right], \tag{4.88}$$

The associated induced connection is

$${}^{(3)}\Gamma^i_{jk} = \frac{\gamma^{il}}{2}\left(\partial_j \gamma_{kl} + \partial_k \gamma_{jl} - \partial_l \gamma_{jk}\right). \tag{4.89}$$

Since there are only spatial derivatives, the round bracket is already first order and we need γ^{ij} at zero order level $\gamma^{ij} = \delta^{ij}/a^2$. The associated Γ now is

$${}^{(3)}\Gamma^i_{jk} = \partial_j C\delta^i_k + \partial_j E^i_k + \partial_k C\delta^i_j + \partial_k E^i_j - \partial^i C\delta_{jk} - \partial^i E_{jk}. \tag{4.90}$$

The curvature of these leaves is

$${}^{(3)}R = \gamma^{ik}\partial_l {}^{(3)}\Gamma^l_{ik} - \gamma^{ik}\partial_k {}^{(3)}\Gamma^l_{il} + \ldots, \tag{4.91}$$

where dots represent terms that are second order in perturbation theory. The final expression for ${}^{(3)}R$ reads as follow

$$a^2 {}^{(3)}R = -4\nabla^2 C + 2\partial_i \partial_l E^{il}. \tag{4.92}$$

For E_{ij} we have the following expression $E_{ij} = \left(\partial_i \partial_j - \delta_{ij}\nabla^2/3\right) E$, where we used the SVT decomposition and we focused on scalar perturbations. Inserting the last relation in (4.92) we obtain

$$a^2 {}^{(3)}R = -4\nabla^2 \left(C - \frac{\nabla^2}{3} E \right). \tag{4.93}$$

We call the curvature perturbation $\mathcal{R}$ the following combination $\mathcal{R} = C - \nabla^2/3E$. We can give a gauge invariant definition of the comoving curvature perturbation that is

$$\mathcal{R} = C - \frac{\nabla^2 E}{3} + \mathcal{H}\left(B + v\right). \tag{4.94}$$

We will proceed now to show the conservation of $\mathcal{R}$. In the spatially flat gauge $C = E = 0$, $\mathcal{R}$ becomes

$$\mathcal{R} = \mathcal{H}\left(B + v\right) \tag{4.95}$$

Using (4.85) we can rewrite (4.95) as follow

$$\mathcal{R} a^2 \left(\bar{\rho} + \bar{P}\right) = -2\mathcal{H}^2 M_{\rm Pl}^2 A, \tag{4.96}$$

We derive (4.96) with respect to conformal time τ and we obtain

$$\mathcal{R}' a^2 \left(\bar{\rho} + \bar{P}\right) + \mathcal{R} a^2 \bar{P}' - \mathcal{R} a^2 \mathcal{H}\left(\bar{\rho} + \bar{P}\right) = -2M_{\rm Pl}^2 \mathcal{H}\left(\mathcal{H}A' + 2\mathcal{H}'A\right), \tag{4.97}$$

where we used the continuity equation at the background level.

Using (4.87), (4.85) and (4.95) in the last relation we get

$$\mathcal{R}' a^2 \left(\bar{\rho} + \bar{P}\right) + \mathcal{R} a^2 \bar{P}' = -a^2 \mathcal{H} \delta P. \tag{4.98}$$

Using (4.95), (4.85), (4.86) and the background continuity equation we can rewrite (4.98) as follow

$$\mathcal{R}' a^2 \left(\bar{\rho} + \bar{P}\right) = -\frac{a^2 \mathcal{H}}{M_{\rm Pl}^2} \left(\delta P - \frac{\bar{P}'}{\bar{\rho}'} \delta\rho \right) + 2\frac{\bar{P}'}{\bar{\rho}'} \mathcal{H}^2 \nabla^2 B, \tag{4.99}$$

where $\delta P - \bar{P}'/\bar{\rho}'\delta\rho$ can be checked to be gauge invariant and it can be used as a definition of a gauge invariant pressure density perturbation.

For barotropic fluid, where $P(\rho)$, the combination $\delta P - \bar{P}'/\bar{\rho}'\delta\rho = 0$ and we have

$$\mathcal{R}' a^2 \left(\bar{\rho} + \bar{P}\right) \simeq 2\frac{\bar{P}'}{\bar{\rho}'} \mathcal{H}^2 \nabla^2 B. \tag{4.100}$$

Using (4.84) and (4.96) we can estimate B as follow

$$B \sim \frac{a^2(\bar{\rho}+\bar{P})}{2\mathcal{H}^2 M_{\rm Pl}^2}\frac{\mathcal{R}}{\mathcal{H}}. \tag{4.101}$$

Inserting (4.101) in (4.100) and going in Fourier space, we obtain (neglecting time coefficients)

$$\frac{d\ln\mathcal{R}}{d\ln a} \sim \frac{k^2}{\mathcal{H}^2} \sim 0, \tag{4.102}$$

where in the last step we use the super-horizon limit. This derivation shows that $\mathcal{R}$, for adiabatic perturbations and on super-horizon scales, is conserved and provides a crucial ingredient for the study of the inflationary fluctuations [128].

4.8 Perturbed stress-energy tensor for a scalar field

Let us perturb the stress-energy tensor in (3.16), we obtain

$$\delta T_{\mu\nu} = \partial_\mu\delta\phi\partial_\nu\bar{\phi} + \partial_\mu\bar{\phi}\partial_\nu\delta\phi - \delta g_{\mu\nu}\left(\frac{\bar{\phi}'^2}{2a^2} - V\right) - \bar{g}_{\mu\nu}\left(-A\frac{\bar{\phi}^2}{a^2} + \frac{\bar{\phi}\delta\phi'}{a^2} - V_{,\phi}\delta\phi\right), \tag{4.103}$$

where we expand $\phi = \bar{\phi} + \delta\phi$ and we assumed the spatially flat gauge. The components of δT are

$$\delta T_{00} = \bar{\phi}'\delta\phi' + 2a^2AV + a^2V_{,\phi}\delta\phi \tag{4.104}$$

$$\delta T_{0i} = \bar{\phi}'\partial_i\delta\phi + \frac{\bar{\phi}'^2}{2}\partial_i B - a^2V(\bar{\phi})\partial_i B, \tag{4.105}$$

$$\delta T_{ij} = \delta_{ij}\left(-A\bar{\phi}'^2 + \bar{\phi}'\delta\phi' - V_{,\phi}a^2\delta\phi\right). \tag{4.106}$$

With the previous expression, we can obtain the Einstein equations with the perturb scalar stress-energy tensor and we obtain

$$-2M_{\rm Pl}^2\mathcal{H}\nabla^2 B = \bar{\phi}'\delta\phi' + 2a^2AV + a^2V_{,\phi}\delta\phi, \tag{4.107}$$

$$M_{\rm Pl}^2\left(2\mathcal{H}\partial_i A - \mathcal{H}^2\partial_i B - 2\mathcal{H}'\partial_i B\right) = \bar{\phi}'\partial_i\delta\phi + \partial_i B\left(\frac{\bar{\phi}'^2}{2} - a^2V\right), \tag{4.108}$$

$$\nabla^2 B' + \nabla^2 A + 2A\mathcal{H}^2 + 2\mathcal{H}\nabla^2 B + 4\mathcal{H}'A + 2A'\mathcal{H} = = \frac{\bar{\phi}'\delta\phi' - A\bar{\phi}'^2 - V_{,\phi}\delta\phi a^2}{M_{\rm Pl}^2}, \tag{4.109}$$

$$B' + 2\mathcal{H}B = -A. \tag{4.110}$$

Using (4.110) and the background Einstein equations we can rewrite (4.108) and (4.109) as follow

$$2M_{\rm Pl}^2\mathcal{H}A = \bar{\phi}'\delta\phi, \tag{4.111}$$

$$2M_{\rm Pl}^2A'\mathcal{H} + 2a^2AV = \bar{\phi}'\delta\phi' - a^2V_{,\phi}\delta\phi. \tag{4.112}$$

These steps will be useful for the derivation of the perturbed equation of motion for ϕ.

4.9 Perturbed Klein-Gordon Equation

We are now ready to derive the perturbed Klein-Gordon equation that we have to solve coupled with the Einstein equations. The Klein-Gordon equation is

$$\partial_\mu\left(\sqrt{-g}g^{\mu\nu}\partial_\nu\phi\right) = -\frac{\partial V}{\partial\phi}\sqrt{-g}. \tag{4.113}$$

At the perturbed level, we have

$$\begin{aligned}&\partial_\mu\left(\delta\sqrt{-g}\bar{g}^{\mu\nu}\partial_\nu\bar{\phi} + \sqrt{-\bar{g}}\delta g^{\mu\nu}\partial_\nu\bar{\phi} + \sqrt{-\bar{g}}\bar{g}^{\mu\nu}\partial_\nu\delta\phi\right) = \\ &-\sqrt{-\bar{g}}V_{,\phi\phi}\delta\phi - V_{,\phi}\delta\sqrt{-\bar{g}},\end{aligned} \tag{4.114}$$

and working in the spatially flat gauge and using $\bar{\phi}'' + 2\mathcal{H}\bar{\phi}' = -V_{,\phi}a^2$ we obtain

$$\delta\phi'' + 2\mathcal{H}\delta\phi' - \nabla^2\delta\phi - A'\bar{\phi}' - \bar{\phi}'\nabla^2B - 2a^2AV_{,\phi} = -a^2V_{,\phi\phi}\delta\phi - 4a^2AV_{,\phi}. \tag{4.115}$$

From now on we will use the slow-roll approximations, namely $3\mathcal{H}\bar{\phi}' \simeq -a^2V_{,\phi}$ and $3M_{\rm Pl}^2\mathcal{H}^2 \simeq a^2V(\bar{\phi})$. Using (4.107), (4.111) and (4.112) we can rewrite (4.115) as

$$\delta\phi'' + 2\mathcal{H}\delta\phi' - \nabla^2\delta\phi - \frac{a^2}{\mathcal{H}M_{\rm Pl}^2}V_{,\phi}\bar{\phi}'\delta\phi = -a^2V_{,\phi\phi}\delta\phi - 4a^2AV_{,\phi}. \tag{4.116}$$

In slow-roll we have

$$-a^2V_{,\phi\phi}\delta\phi = -3\eta_{\rm V}\mathcal{H}^2\delta\phi, \tag{4.117}$$

$$-4a^2AV_{,\phi} = 12\mathcal{H}^2\epsilon_{\rm V}\delta\phi, \tag{4.118}$$

$$-\frac{a^2}{\mathcal{H}M_{\rm Pl}^2}V_{,\phi}\bar{\phi}'\delta\phi = 6\epsilon_{\rm V}\mathcal{H}^2\delta\phi, \tag{4.119}$$

and (4.116) becomes

$$\delta\phi'' + 2\mathcal{H}\delta\phi' - \nabla^2\delta\phi = -3\eta_{\rm V}\mathcal{H}^2\delta\phi + 6\mathcal{H}^2\epsilon_{\rm V}\delta\phi. \tag{4.120}$$

We are going to solve (4.120) in Fourier space. We expand $\delta\phi$ as

$$\delta\phi = \int \frac{d^3k}{(2\pi)^{3/2}} e^{-i\vec{k}\cdot\vec{x}} \mu_{\vec{k}}(\tau), \tag{4.121}$$

and μ satisfies

$$\mu_{\vec{k}}'' + 2\mathcal{H}\mu_{\vec{k}}' + k^2\mu_{\vec{k}} + \left(3\eta_V\mathcal{H}^2 - 6\epsilon_V\mathcal{H}^2\right)\mu_{\vec{k}} = 0. \tag{4.122}$$

With an appropriate field redefinition $\mu_{\vec{k}} = \hat{\mu}_{\vec{k}}/a$, we can recast the last expression as

$$\hat{\mu}_{\vec{k}}'' + \left(k^2 - \frac{a''}{a} + 3\eta_V\mathcal{H}^2 - 6\epsilon_V\mathcal{H}^2\right)\hat{\mu}_{\vec{K}} = 0, \tag{4.123}$$

that is an equation for a harmonic oscillator with time-dependent frequency. We quantize the operator $\delta\phi$ by expanding $\hat{\mu}$ as

$$\hat{\mu}_{\vec{k}} = v_{\vec{k}}a_{\vec{k}} + v_{\vec{k}}^* a_{\vec{k}}^\dagger, \tag{4.124}$$

where a, $a^\dagger$ are the annihilation and creation operators that satisfy the following commutation relations

$$\left[a_{\vec{k}}, a_{\vec{k}'}^\dagger\right] = \delta\left(\vec{k} - \vec{k}'\right), \left[a_{\vec{k}}, a_{\vec{k}'}\right] = \left[a_{\vec{k}}^\dagger, a_{\vec{k}'}^\dagger\right] = 0. \tag{4.125}$$

The mode functions v are normalized as follows

$$\mathrm{W}\left[v_{\vec{k}}, v_{\vec{k}}^*\right] = v_{\vec{k}}'v_{\vec{k}}^* - v_{\vec{k}}v_{\vec{k}}^{*\prime} = -\imath. \tag{4.126}$$

The vacuum state is destroyed by the operator a such that $a_{\vec{k}}|0\rangle = 0$.

In slow-roll, we have $a(\tau) = -1/\tau H\left(1 - \epsilon_V\right)$ and working at first order in the slow-roll parameters we can evaluate a''/a as

$$\frac{a''}{a} = a^2H^2\left(2 - \epsilon_V\right) \simeq \frac{2 + 3\epsilon_V}{\tau^2}. \tag{4.127}$$

Using (4.124) and (4.127) in (4.123) we obtain

$$v_k'' + \left(k^2 - \frac{\nu^2 - 1/4}{\tau^2}\right)v_k = 0, \quad \nu^2 = 9/4 + 9\epsilon_V - 3\eta_V. \tag{4.128}$$

Relation (4.128) can be solved exactly to give

$$v_k(\tau) = \sqrt{-\tau}\left[\alpha \mathrm{H}_\nu^{(1)}(-k\tau) + \beta \mathrm{H}_\nu^{(2)}(-k\tau)\right], \tag{4.129}$$

where $\mathrm{H}_\nu^{(1,2)}$ are the Hankel functions of the first and second kind. Usually, as initial conditions, in the sub-horizon regime $k/aH \sim k\tau \gg 1$, are imposed

the Bunch-Davis vacuum conditions that are

$$\lim_{k\tau\to-\infty} v_k(\tau) = \frac{e^{-\imath k\tau}}{\sqrt{2k}}. \tag{4.130}$$

The physical motivation of these conditions resides in focusing on modes that are sub-horizon and, due to the equivalence principle, they do not feel the expansion of the Universe. Hence, the solutions of (4.128) follow the Minkowski solutions that are plane waves.

The limits of the Hankel functions are

$$\lim_{k\tau\to-\infty} \mathrm{H}_\nu^{(1)}(-k\tau) \approx \sqrt{\frac{2}{\pi}}\frac{1}{\sqrt{-k\tau}}e^{-\imath k\tau}, \quad \lim_{k\tau\to-\infty} \mathrm{H}_\nu^{(2)}(-k\tau) \approx \sqrt{\frac{2}{\pi}}\frac{1}{\sqrt{-k\tau}}e^{\imath k\tau}, \tag{4.131}$$

where we dropped irrelevant phases. Using (4.131) in (4.129) we obtain

$$\lim_{k\tau\to-\infty} v_k(\tau) \sim \alpha\sqrt{\frac{2}{\pi k}}e^{-\imath k\tau} + \beta\sqrt{\frac{2}{\pi k}}e^{\imath k\tau}, \tag{4.132}$$

and from (4.130) we have $\beta = 0$ and $\alpha = \sqrt{\pi}/2$. The Bunch-Davis modes function to first order in slow-roll are

$$v_k(\tau) = \frac{\sqrt{\pi}}{2}\sqrt{-\tau}\mathrm{H}_\nu^{(1)}(-k\tau). \tag{4.133}$$

From the evolution of v, we can calculate the zero-point fluctuations of the operator $\delta\phi$. Indeed, for $\delta\phi$ we have

$$\delta\phi(\tau,\vec{x}) = \int \frac{d^3k}{(2\pi)^{2/3}}\frac{e^{-\imath\vec{k}\cdot\vec{x}}}{a}\left[v_k(\tau)a_k + v_k^*(\tau)a_k^\dagger\right], \tag{4.134}$$

and the variance of the inflaton field is

$$\begin{aligned}\langle|\delta\phi|^2\rangle &= \langle 0|\delta\phi^\dagger(\tau,0)\delta\phi(\tau,0)|0\rangle = \\ &= \int \frac{d^3k}{(2\pi)^3}\frac{d^3k'}{a^2}\left\langle 0\left|\left[v_{k'}^*a_{k'}^\dagger + v_{k'}a_{k'}\right]\left[v_ka_{k'} + v_k^*a_k^\dagger\right]\right|0\right\rangle,\end{aligned} \tag{4.135}$$

where we used (4.134). Using $\langle 0|a_ka_{k'}^\dagger|0\rangle = \delta(\vec{k}-\vec{k}')$ in (4.135) we obtain

$$\langle|\delta\phi|^2\rangle = \int d\ln k\frac{k^3}{2\pi^2}\frac{|v_k(\tau)|^2}{a^2}. \tag{4.136}$$

We define the dimensionless power spectrum of the inflaton field as

$$\Delta^2_{\delta\phi}(k,\tau) = \frac{k^3}{2\pi^2}\frac{|v_k(\tau)|^2}{a^2}. \tag{4.137}$$

Let us evaluate (4.137) on super-horizon scales $-k\tau \ll 1$. The asymptotic expression for the Hankel function is

$$\mathrm{H}_{\nu}^{(1)}(x \ll 1) \approx \sqrt{\frac{2}{\pi}} e^{-\imath\pi/2} 2^{\nu-3/2} \frac{\Gamma(\nu)}{\Gamma(3/2)} x^{-\nu}, \tag{4.138}$$

and using the last formula in (4.137) we get

$$\Delta^2_{\delta\phi}(-k\tau \ll 1) \approx \frac{H^2}{4\pi^2} 2^{2\nu-3} \frac{|\Gamma(\nu)|^2}{\Gamma(3/2)^2} \left(\frac{k}{aH}\right)^{3-2\nu}. \tag{4.139}$$

At the lowest order in slow-roll parameters we have $\nu \simeq 3/2 + 3\epsilon_{\mathrm{V}} - \eta_{\mathrm{V}}$ and (4.139) becomes

$$\Delta^2_{\delta\phi}(-k\tau \ll 1) \approx \frac{H^2}{4\pi^2} \left(\frac{k}{aH}\right)^{2\eta_{\mathrm{V}} - 6\epsilon_{\mathrm{V}}}. \tag{4.140}$$

Having obtained (4.140), we are ready to compute the power spectrum of $\mathcal{R}$ on super-horizon scales. It is important to compute $\mathcal{R}$ since it is directly linked to observables. The curvature perturbation in spatially flat gauge is

$$\mathcal{R} = \mathcal{H}(B + v), \tag{4.141}$$

where $B + v$ is the δT^0_i part of the stress-energy tensor as visible in (4.30). Relation (4.30) for a scalar field is

$$\delta T^0_i = -\frac{\bar{\phi}'^2}{a^2} \partial_i (B + v), \tag{4.142}$$

and from the comparison of the last expression with the δT^0_i component of the stress-energy tensor of the scalar field, $\delta T^0_i = \bar{\phi}' \partial_i \delta\phi / a^2$, we obtain

$$B + v = -\frac{\delta\phi}{\bar{\phi}'}. \tag{4.143}$$

Using (4.143) in (4.141) we get

$$\mathcal{R} = -\frac{\mathcal{H}\delta\phi}{\bar{\phi}'}, \tag{4.144}$$

and the power spectrum of $\mathcal{R}$ on super-horizon scales is

$$\Delta^2_{\mathcal{R}}(-k\tau \ll 1) \approx \frac{\mathcal{H}^2}{\bar{\phi}'^2} \Delta^2_{\delta\phi}(-k\tau \ll 1) \approx \frac{H^2}{8\pi^2 M^2_{\mathrm{Pl}} \epsilon_{\mathrm{V}}} \left(\frac{k}{aH}\right)^{2\eta_{\mathrm{V}} - 6\epsilon_{\mathrm{V}}}, \tag{4.145}$$

where in going from left to right we used (4.144), (4.140) and (3.28). Since $\mathcal{R}$ is constant upon horizon exits, we can evaluate it at horizon crossing $k = aH$

and (4.145) becomes

$$\Delta^2_{\mathcal{R}}\left(k=aH\right)=\left.\frac{H^2}{8\pi^2 M^2_{\rm Pl}\epsilon_{\rm V}}\right|_{k=aH}. \tag{4.146}$$

The spectral index is defined as

$$n_s-1=\frac{d\ln\Delta^2_{\mathcal{R}}}{d\ln k}\simeq 2\eta_{\rm V}-6\epsilon_{\rm V}, \tag{4.147}$$

where we used (4.145).

Let us introduce a new gauge invariant quantity ξ that will be useful later. We define ξ as

$$\xi=C-\frac{1}{3}\nabla^2 E+\mathcal{H}\frac{\delta\rho^{(1)}}{\bar{\rho}'}, \tag{4.148}$$

and represents the curvature variable on the uniform energy density slices. It can be shown that $\mathcal{R}$ and ξ are related as follow

$$-\xi=\mathcal{R}+\frac{2\bar{\rho}}{9\left(\bar{\rho}+\bar{P}\right)}\left(\frac{k}{aH}\right)^2 A. \tag{4.149}$$

Relation (4.149) shows that on large scales $k\ll aH$ we get $\mathcal{R}\approx-\xi$; such that the power spectrums of $\mathcal{R}$ and ξ are the same on super-horizon scales and are both conserved.

4.10 Gravitational waves from Inflation

A clear prediction of the inflationary paradigm is the formation of a background of gravitational waves. Gravitational waves are tensor modifications of the metric and the line element reads

$$ds^2=a^2\left[d\tau^2-\left(\delta_{ij}+2\hat{E}_{ij}\right)dx^i dx^j\right]. \tag{4.150}$$

If we insert (4.150) in the Einstein-Hilbert action, at second order, we have

$$S^2_{\hat{E}}=\frac{M^2_{\rm Pl}}{8}\int d\tau d^3x a^2\left[\left(\hat{E}_{ij}\right)^2-\left(\nabla\hat{E}_{ij}\right)^2\right]. \tag{4.151}$$

It is convenient to pass in Fourier space writing $\hat{E}$ as follow

$$\hat{E}_{ij}\left(\tau,\vec{x}\right)=\int\frac{d^3k}{\left(2\pi\right)^{3/2}}\sum_{\gamma=+,\times}\epsilon^{\gamma}_{ij}(\vec{k})\mathrm{E}_{\vec{k},\gamma}(\tau)e^{-\imath\vec{k}\cdot\vec{x}}, \tag{4.152}$$

where $\epsilon_i^{i,\gamma} = k^i \epsilon_{ij}^{\gamma} = 0$ and $\epsilon_{ij}^{\gamma} \epsilon^{ij,\gamma'} = 2\delta_{\gamma\gamma'}$. Using (4.152) in (4.151) we obtain

$$S^2_{\hat{E}} = \sum_{\gamma} \int d\tau d^3k \frac{M_{\rm Pl}^2 a^2}{4} \left[\left(\mathrm{E}'_{\vec{k},\gamma} \right)^2 - k^2 \left(\mathrm{E}_{\vec{k},\gamma} \right)^2 \right]. \tag{4.153}$$

In order to canonically normalize E we introduce $\mathrm{E}_{\vec{k},\gamma} = \sqrt{2}\mathrm{u}_{\vec{k},\gamma}(\tau)/M_{\rm Pl} a$ and we obtain

$$S^2_{\hat{E}} = \sum_{\gamma} \int d\tau d^3k \frac{1}{2} \left[\left(\mathrm{u}_{\vec{k},\gamma}(\tau)' \right)^2 - \left(k^2 + \frac{a''}{a} \right) \mathrm{u}_{\vec{k},\gamma}(\tau)^2 \right], \tag{4.154}$$

where a''/a comes from an integration by part when passing from E to u.

The canonical field u satisfies the following equation of motion

$$\mathrm{u}''_{\vec{k},\gamma} + \left(k^2 - \frac{a''}{a} \right) \mathrm{u}_{\vec{k},\gamma} = 0. \tag{4.155}$$

The canonical field u, for both γ, obeys an equation that resembles the one of $\delta\phi$. In slow-roll, relation (4.155) becomes

$$\mathrm{u}''_{\vec{k},\gamma} + \left(k^2 - \frac{\nu_{\rm T}^2 - 1/4}{\tau^2} \right) \mathrm{u}_{\vec{k},\gamma} = 0, \tag{4.156}$$

where $\nu_{\rm T}^2 = 9/4 + 3\epsilon_{\rm V}$.

We quantize the operator $\hat{E}$ by expanding u as

$$\mathrm{u}_{\vec{k},\gamma} = \mathrm{v}_{\vec{k},\gamma} a_{\vec{k},\gamma} + v^*_{\vec{k},\gamma} a^{\dagger}_{\vec{k},\gamma}, \tag{4.157}$$

and the mode functions v have solutions that are consistent with the Bunch-Davis vacuum conditions and respect the Wronskian (4.126) normalization; whose expression is

$$\mathrm{v}_{k,\gamma} = \frac{\sqrt{2}}{\pi} \sqrt{-\tau} \mathrm{H}^{(1)}_{\nu_{\rm T}} (-k\tau). \tag{4.158}$$

The operator $\hat{E}$ has the following expansion

$$\hat{E}_{ij}(\tau, \vec{x}) = \int \frac{d^3k}{(2\pi)^{3/2}} \sum_{\gamma=+,\times} \epsilon_{ij}^{\gamma} \frac{\sqrt{2}}{a M_{\rm Pl}} e^{-i\vec{k}\cdot\vec{x}} \left(\mathrm{v}_{\vec{k},\gamma} a_{\vec{k},\gamma} + \mathrm{v}^*_{\vec{k},\gamma} a^{\dagger}_{\vec{k},\gamma} \right), \tag{4.159}$$

and the variance of $\hat{E}$ is

$$\begin{aligned} &\langle 0 | \hat{E}^{\dagger}_{ij}(\tau, 0) \hat{E}^{ij}(\tau, 0) | 0 \rangle = \\ &\int \frac{d^3k d^3k'}{(2\pi)^3} \sum_{\gamma,\gamma'} \epsilon_{ij}^{\gamma}(\vec{k}) \epsilon^{\gamma',ij}(\vec{k}') \frac{2}{a^2 M_{\rm Pl}^2} \mathrm{v}_{\vec{k}',\gamma'} \mathrm{v}^*_{\vec{k},\gamma} \langle 0 | a_{\vec{k}',\gamma'} a^{\dagger}_{\vec{k},\gamma} | 0 \rangle; \end{aligned} \tag{4.160}$$

where we used (4.159) and $a_{\vec{k},\gamma}|0\rangle = 0$. Inserting $\langle 0|a_{\vec{k}',\gamma'}a^{\dagger}_{\vec{k},\gamma}|0\rangle = \delta\left(\vec{k}-\vec{k}'\right)\delta_{\gamma,\gamma'}$ in (4.160) we obtain

$$\langle 0|\hat{E}^{\dagger}_{ij}(\tau,0)\hat{E}^{ij}(\tau,0)|0\rangle = \int d\ln k \frac{k^3}{2\pi^2}\frac{8|\mathrm{v}|^2_{k,\gamma}}{a^2 M^2_{\mathrm{Pl}}}. \tag{4.161}$$

The dimensionless power spectrum for the tensor modes is

$$\Delta^2_{\hat{E}}(k,\tau) = \frac{k^3}{2\pi^2}\frac{8}{a^2 M^2_{\mathrm{Pl}}}|\mathrm{v}|^2_{k,\gamma}. \tag{4.162}$$

On super-horizon scales and at the lowest order in the slow-roll parameters, relation (4.162) becomes

$$\Delta^2_{\hat{E}}(-k\tau \ll 1) \approx \frac{2H^2}{M^2_{\mathrm{Pl}}\pi^2}\left(\frac{k}{aH}\right)^{3-2\nu_{\mathrm{T}}}, \tag{4.163}$$

and at horizon crossing we have

$$\Delta^2_{\hat{E}} = \left.\frac{2H^2}{M^2_{\mathrm{Pl}}\pi^2}\right|_{k=aH}. \tag{4.164}$$

The tensor tilt can be calculated as follows

$$n_{\mathrm{T}} = \frac{d\ln\Delta^2_{\hat{E}}}{d\ln k} \simeq -2\epsilon_{\mathrm{V}}, \tag{4.165}$$

where we used (4.163).

From an observational point of view, a crucial quantity is the tensor-to-scalar ratio defined as

$$r = \frac{\mathrm{A_T}}{\mathrm{A_S}}, \tag{4.166}$$

where $\mathrm{A_{T,S}}$ are the amplitudes of the dimensionless power spectrum $\Delta^2_{\hat{E}}$ and $\Delta^2_{\mathcal{R}}$ respectively. From (4.145) and (4.163) we obtain

$$\mathrm{A_S} = \frac{H^2}{8\pi^2 M^2_{\mathrm{Pl}}\epsilon_{\mathrm{V}}}, \quad \mathrm{A_T} = \frac{2H^2}{M^2_{\mathrm{Pl}}\pi^2}. \tag{4.167}$$

Using (4.167) in (4.166) we obtain

$$r = 16\epsilon_{\mathrm{V}}, \tag{4.168}$$

that is a clear prediction for all single-field models of inflation.

In 2018, the Planck mission released data on the measurement of the CMB anisotropies, which updated the constraints on cosmic inflation. The Planck collaboration presented updated bounds on the spectral index, scalar power spectrum amplitude, and an updated upper limit on the tensor-to-scalar ratio. It is important to note that the scope of this thesis does not involve

Parameter	TT+low E	EE+low E	TE+low E	TT,TE,EE+low E	TT,TE,EE+low E+lensing
$\ln 10^{10} A_S$	3.040 ± 0.016	3.052 ± 0.022	$3.018^{0.002}_{-0.0018}$	3.045 ± 0.016	3.044 ± 0.014
n_s	0.9626 ± 0.0057	0.980 ± 0.015	0.967 ± 0.011	0.9649 ± 0.0044	0.9649 ± 0.0042

TABLE 4.1: 68 % confidence limits for A_S and n_s from Planck data[9]. The different columns present temperature (TT), polarization (EE), and temperature-polarization (TE) cross-correlation both separately and combined. Furthermore, it shows the combined constraint with EE measurement at low multipoles (low E) and the Planck lensing. A_S and n_s are evaluated at the pivot scale $k_* = 0.05\text{Mpc}^{-1}$.

discussing the details of the analysis conducted by the Planck collaboration. However, we report the updated bounds that were used and will be extensively used in the rest of the manuscript.

In Table 4.1 we reported the 68 % confidence limit (C.L.) for A_S and n_s based on different data that are taken both separately and combined in the analysis. From a practical point of view, our interest belongs to the last column where the data from temperature (TT), polarization (EE), temperature-polarization (TE) cross-correlation together with the EE measurement at low multiples and the Planck lensing are combined. In the thesis, we used these values for A_S and n_s when we confronted the theoretical prediction of a model with observations.

The bounds concern two parameters that play fundamental roles in the primordial universe. Depending on the inflation model chosen this will produce different values of A_S and n_s. One can then test the predictions of these models with observations, and in general this is done in the $r - n_s$ plane. In Fig. 4.1, we present the constraint from Planck data in combination with BICEP/Keck 2015 (BK15) [6] and BK15 plus Baryonic acoustic oscillations (BAO)[139]. The Planck collaboration has tested several inflationary models shown in the panel against observational data. The R^2 model agrees with Planck data, see Fig. 4.1, confirming what was previously found in 2013 and 2015. In Section 4.11, we will discuss Higgs inflation and its agreement with Planck. The predictions are shown in (4.185). Monomial potentials predict a value too large for r, disfavored by data with respect to R^2. In Chapter 7, we will discover a vital ingredient that can lower the value of r, ultimately making the monomial models compatible with Planck data once again. This crucial ingredient involves the use of non-minimal coupling to gravity, which is similar to what we will do with Higgs inflation. As far as the thesis is concerned, another model of interest would be natural inflation (see Section 6.7). However, this model is heavily disfavoured by the Plank plus BK15 data.

For our purposes, we do not discuss the other models in the panel, for more details see [9]. In Chapter 7, it is important to note that we will be utilizing an observational upper limit on r of $r < 0.036$ at $k = 0.05\text{Mpc}^{-1}$ (95% C.L., BICEP/Keck [7]). This is an updated bound and the numerical simulations' initial conditions are fixed at that scale.

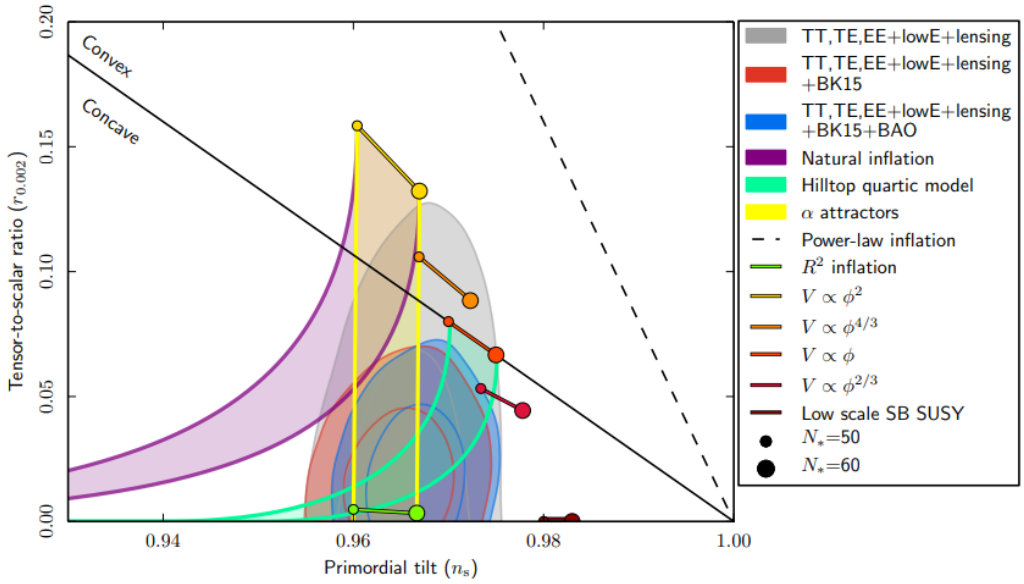

FIGURE 4.1: Joint 68 % and 95 % C.L. regions for n_s and r from Planck and in combination with BICEP/Keck 2015 (BK15) and BK15 plus Baryonic acoustic oscillations (BAO) data. Overlaid the theoretical predictions of selected inflationary models. r and n_s are evaluated at the pivot scale $k_* = 0.002\text{Mpc}^{-1}$. Figure taken from [9].

4.11 The Higgs boson as the inflaton

Generically the models of inflation present in the literature introduce additional DOF to the standard model of particle physics. It seems that a possible explanation of inflation requires models beyond the standard model, indeed in Gran Unified Theory, supersymmetry, string theory, extra-dimension, etc this new particle may appear naturally. Without invoking some UV complete model we can take a more phenomenological approach and the simplest realization of a model of inflation is what we studied in Section 3.4, given by a single scalar field. In [29] it has been shown that no extra new particles are necessary to explain inflation and the role of the inflaton field is played by the Higgs boson. A necessary ingredient for this model as we will see is a non-minimal coupling of the Higgs field with the Ricci scalar R. Hence, the model is slightly different from what we studied in Section 3.4, but with an appropriate conformal transformation, we will go back to a setup similar to (3.15).

To present the main features of this model, let us start with the following Lagrangian density

$$L_{\text{tot}} = L_{\text{SM}} - \frac{M^2}{2}R - \xi \text{H}^\dagger \text{H} R, \tag{4.169}$$

where L_{SM} is the SM Lagrangian, M is some mass parameter, R is the Ricci scalar, H is the Higgs field, and ξ is an arbitrary constant. As we discussed

in the introductory part, the last term in (4.169) is expected to exist from the point of view of an effective field theory in curved space [137]. The minimal coupling to gravity of the scalar field is restored when $\xi = 0$ and M can be identified with the Planck mass $M_{\rm Pl}$. Since the self-coupling of the Higgs is large the model is not able to sustain inflation even if it has a "good" particle physics phenomenology. In the case in which M is set to zero, the electroweak scale generates the Planck mass if $\sqrt{\xi} \sim M_{\rm Pl}/M_{\rm W} \sim 10^{17}$, where $M_{\rm W}$ is the W boson mass. This scenario, called the "induced" gravity model [181, 161, 152], can sustain inflation but it fails to reproduce the particle physics experiments.

Hence, the intermediate regime, in which $1 \leq \sqrt{\xi} \ll 10^{17}$, possesses the SM as a low energy theory with the usual Higgs boson, and being $\xi \geq 1$ the behavior during inflation changes with respect to $\xi = 0$ and inflation may become possible. In this range, the scale M, with very good accuracy, is approximated by $M \simeq M_{\rm Pl}$. We focus only on the Higgs field in the unitary gauge in which the Higgs doublet is $\mathrm{H} = h/\sqrt{2}$ and the Lagrangian (4.169) becomes

$$S_{\rm J} = \int d^4x\sqrt{-g}\left[-\frac{M^2+\xi h^2}{2}R + \frac{1}{2}\partial_\mu h\partial^\mu h - \frac{\lambda}{4!}\left(h^2-v^2\right)^2\right], \tag{4.170}$$

where v is the Higgs vacuum expectation value. Non-minimally coupled scalar field theory was originally studied in [152, 90]. We can pass from the Jordan to the Einstein frame with a conformal transformation as follows

$$\hat{g}_{\mu\nu} = \Omega^2 g_{\mu\nu}, \;\; \Omega^2 = 1 + \frac{\xi h^2}{M_{\rm Pl}^2}. \tag{4.171}$$

The action in the Einstein frame is

$$S_{\rm E} = \int d^4x\sqrt{-\hat{g}}\left[-\frac{M_{\rm Pl}^2}{2}\hat{R} + \frac{1}{2}\partial_\mu\chi\partial^\mu\chi - U(\chi)\right], \tag{4.172}$$

where $\hat{R}$ is calculated with $\hat{g}$ metric, χ is the canonical Higgs field that is linked to the previous h as follows

$$\frac{d\chi}{dh} = \sqrt{\frac{\Omega^2 + 6\xi^2h^2/M_{\rm Pl}^2}{\Omega^4}}, \tag{4.173}$$

$U(\chi)$ is the potential in the Einstein frame and it reads

$$U(\chi) = \frac{1}{\Omega^4}\frac{\lambda}{4!}\left(h(\chi)^2 - v^2\right)^2, \tag{4.174}$$

where the Ω^4 factor comes from the conformal transformation. In the large field limit $\xi h^2 \gg M_{\rm Pl}^2 \gg v^2$, the potential U becomes

$$U \simeq \frac{\lambda M_{\rm Pl}^4}{4!\xi^2}, \tag{4.175}$$

The potential at large-field values becomes constant due to the conformal transformation, and it is this flattening of the potential that can sustain inflation.

The next question is to check if the model is consistent with the Planck data. The slow-roll analysis of Section 3.4 can be applied in the Einstein frame. Hence, the slow-roll parameters (3.28), (3.29) are constructed with the U potential

$$\epsilon_{\rm U} = \frac{M_{\rm Pl}^2}{2}\left(\frac{U_{,\chi}}{U}\right)^2, \quad \eta_{\rm U} = M_{\rm Pl}^2\frac{U_{,\chi\chi}}{U}. \tag{4.176}$$

With the potential (4.174) and in the large-field regimes the slow-roll parameters become

$$\epsilon_{\rm U} \simeq \frac{4M_{\rm Pl}^4}{3\xi^2 h^4}, \tag{4.177}$$

$$\eta_{\rm U} \simeq -\frac{4M_{\rm Pl}^2}{3\xi h^2}, \tag{4.178}$$

where, as assumed in the first part of the section, we restrict our analysis to regime $1 \ll \sqrt{\xi} \ll 10^{17}$. The slow-roll parameters obey a hierarchical condition that is $|\eta_{\rm U}| \gg \epsilon_{\rm U}$. The end of inflation is given by $\epsilon_{\rm U} \simeq 1$, and for $h_{\rm end}$ we obtain

$$h_{\rm end} \simeq \left(\frac{4}{3}\right)^{1/4}\frac{M_{\rm Pl}}{\sqrt{\xi}}. \tag{4.179}$$

The scalar power spectrum amplitude, scalar spectral index, and the tensor-to-scalar ratio at some wave number of interest k_* are written, from (4.146), (4.147) and (4.168), as

$$A_s \simeq \frac{U_*}{24\pi^2 M_{\rm Pl}^4 \epsilon_{{\rm U},*}}, \quad n_s - 1 \simeq 2\eta_{{\rm U},*} - 6\epsilon_{{\rm U},*}, \quad r \simeq 16\epsilon_{{\rm U},*}. \tag{4.180}$$

The subscript $*$ denotes that the quantities are evaluated when the mode k_* exits the Hubble horizon. Relation (4.180) with the potential (4.174), (4.177) and (4.178) becomes

$$A_s \simeq \frac{\lambda h_*^4}{768\pi^2 M_{\rm Pl}^4}, \quad h_*^2 \simeq \frac{8M_{\rm Pl}^2}{3\xi(1-n_s)}, \quad r \simeq \frac{64M_{\rm Pl}^4}{3\xi^2 h_*^4}. \tag{4.181}$$

Relation (3.31) evaluated between h_* and $h_{\rm end}$ gives us

$$N_* = \int_{h_{\rm end}}^{h_*}\frac{1}{M_{\rm Pl}}\frac{1}{\sqrt{2\epsilon_{\rm U}}}\frac{d\chi}{dh}dh \simeq \frac{3\xi}{4}\frac{h_*^2 - h_{\rm end}^2}{M_{\rm Pl}^2}, \tag{4.182}$$

where we used (4.177), (4.173). From (4.181) and (4.179) we see that $h_* \gg h_{\rm end}$ and (4.182) becomes

$$\frac{h_*^2}{M_{\rm Pl}^2} \simeq \frac{4N_*}{3\xi}. \tag{4.183}$$

We can use (4.183) to rewrite (4.181) as

$$A_s \simeq \frac{\lambda N_*^2}{432\pi^2\xi_*^2}, \quad N_* \simeq \frac{2}{(1-n_s)}, \quad r \simeq \frac{12}{N_*^2}. \tag{4.184}$$

If we specialize on the specific scale $k_* = 0.05{\rm Mpc}^{-1}$, where the CMB observables are fixed, we can adjust the scalar power spectrum amplitude to take the best-fit value $A_s = 2.1 \times 10^{-9}$. From the solution of the horizon and flatness problems, we know that $50 \leq N_* \leq 60$ and (4.184) becomes

$$\xi \simeq 5815, \;\; n_s = 0.964, \;\; r \simeq 0.005, \tag{4.185}$$

where we used $N_* = 55$, $A_s = 2.1 \times 10^{-9}$ and $\lambda \simeq 0.1$ for the self-coupling of the Higgs field. The predicted values for n_s and r are within one sigma of the current Planck measurements [9], see Table 4.1 and Fig. 4.1. En route, we note that $\epsilon_{\rm U}$, $\eta_{\rm U}$, and N_* do not depend on v such that the inflationary dynamics and observables are insensitive to the exact value of v until $\sqrt{\xi} \ll 10^{17}$. Inflation can be a natural consequence of the standard model of particle physics. The predictions of this model are different from a $\lambda\phi^4$ or $m^2\phi^2$ model and can be distinguished in future experiments.

4.11.1 EFT aspects of Higgs Inflation

The large value of ξ required to fix the amplitude of the scalar power spectrum poses a problem for the validity of Higgs inflation as an effective field theory [20]. The plateau in the potential for $h \gg M_{\rm Pl}/\sqrt{\xi}$ with energy density given by (4.175) suggests that the energy scale controlling inflation is given by $\Lambda_I = M_{\rm Pl}/\sqrt{\xi}$. Instead, the actual cut-off of the theory is lower than this scale.

The cut-off of the theory, in the Jordan frame, can be derived from the operator h^2R, which gives a term like

$$\frac{\xi h^2}{M_{\rm Pl}}\eta^{\mu\nu}\partial^2\gamma_{\mu\nu} + \ldots, \tag{4.186}$$

where in the weak-field limit we expand $g_{\mu\nu} = \eta_{\mu\nu} + \gamma_{\mu\nu}/M_{\rm Pl}$, η is the Minkowski metric and dots stand for other terms present in R. From (4.186) we identify the cut-off scale to be $\Lambda = M_{\rm Pl}/\xi$[1] and the same result can be derived in the Einstein frame. Working at small field values relation (4.173)

[1] In the expansion there are operators that are suppressed by $M_{\rm Pl}/\sqrt{\xi}$, which is a higher energy sale respect to Λ for $\xi \gg 1$.

gives us

$$h = \chi \left[1 - \left(\frac{\xi \chi}{M_{\rm Pl}} \right)^2 \right] + \dots , \tag{4.187}$$

where dots represent higher terms in the expansion of the field redefinition (4.173). Plugging (4.187) into the Higgs potential term h^4 we obtain the following dimension-six operator

$$\chi^6 \frac{\xi^2}{M_{\rm Pl}^2}, \tag{4.188}$$

showing the same cut-off scale as derived in the Jordan frame.

An effective field theory can make reliable predictions only up to a certain cut-off scale. In Higgs Inflation, the Hubble parameter sets the inflationary energy scale, which is in the same order as the cut-off scale for $\xi \gg 1$, as shown in equation (4.175). This implies that the theory's predictability is compromised because of the large value of λ. The literature suggests various ways to solve this problem, as proposed in [71, 17]. It is worth noting that by using equation (4.184), we can conclude that if λ is considered a free parameter, then we can achieve $\xi \sim 1$ by selecting a very small value for λ i.e., $\lambda \ll 1$. This possibility occurs in PQ inflation, and we will explore it further in Chapter 7.

4.12 Lyth bound

Having obtained the tensor-to-scalar ratio we can derive the so-called Lyth bound that is

$$\frac{\Delta \phi}{M_{\rm Pl}} \simeq \mathcal{O}(1) \sqrt{\frac{r}{0.01}}, \tag{4.189}$$

where r is the tensor-to-scalar ratio at the CMB scale $k_* = 0.05 \text{Mpc}^{-1}$ and $\Delta\phi$ is the excursion of the field during inflation. Relation (4.189) linked large values of r ($r > 0.01$) to excursions of the field that are super Plankian ($\Delta\phi > M_{\rm Pl}$). In other words, large values of r require large-field inflation models.

It is easy to derive relation (4.189), indeed from (4.168) we have

$$r = 16\epsilon_{\rm V} = \frac{8}{M_{\rm Pl}^2} \left(\frac{d\phi}{dN} \right)^2, \tag{4.190}$$

where we used (3.28) and we passed from conformal time τ to number of e-folds N. We can integrate (4.190) from N_{CMB}, horizon exit of k_*, to the end of inflation $N_{\rm end}$

$$\int_{\phi_{\rm end}}^{\phi_{CMB}} \frac{d\phi}{M_{\rm Pl}} = \int_{N_{rmend}}^{N_{CMB}} dN \sqrt{\frac{r}{8}}. \tag{4.191}$$

If we assume that, during inflation, r does not evolve we obtain

$$\frac{\phi_{CMB}-\phi_{\rm end}}{M_{\rm Pl}}=\frac{\Delta\phi}{M_{\rm pl}}=\sqrt{\frac{r}{8}}\left(N_{CMB}-N_{\rm end}\right). \tag{4.192}$$

Relation (4.192) is the Lyth bound and the order unity factor comes from $\sqrt{0.01/8}\left(N_{CMB}-N_{\rm end}\right)\sim\sqrt{0.01/8}\times 60\sim\mathcal{O}(1)$ where we assumed $N_{CMB}-N_{\rm end}=60$.

4.13 δ N formalism

In this section we will derive the δN formalism which is a popular and powerful technique for computing the nonlinear evolution of cosmological perturbations on large scales, following mainly [155]. In particular, it enables us to compute the curvature perturbation, $\mathcal{R}$, on large scales without actually solving perturbed field equations.

Let us take $\{\mathcal{U}(\tau)\}$ as a foliation of the spacetime with hypersurfaces $\mathcal{U}$ and q^μ be the unit vector normal to $\mathcal{U}$. The volume expansion of these hypersurfaces along the integral curve $\gamma(s)$ of q^μ is define as

$$\subseteq=\nabla_\mu \mathrm{q}^\mu, \tag{4.193}$$

From (4.193), we can introduce for each integral curve the number of e-folds as

$$\mathcal{N}=\int_{\gamma(s)}\frac{\subseteq}{3}ds, \tag{4.194}$$

where s is the proper time along the curve. From [102], at linear order in perturbation theory, it is shown

$$\frac{\subseteq}{3}=\frac{\mathcal{H}}{a}\left(1-A+\frac{\mathcal{R}'}{\mathcal{H}}+\frac{1}{3\mathcal{H}a}\nabla^2 S_g\right), \tag{4.195}$$

where S_g is a combination of the E and B perturbations. In the absence of anisotropic perturbations in the stress-energy tensor, the off-diagonal part of the Einstein equations gives $S_g\sim A/\mathcal{H}\sim\mathcal{R}/\mathcal{H}$. Given this scaling, the last term in (4.195) is negligible compared to the other terms on super-horizon scales $k^2\ll\mathcal{H}^2$. From now on let us work on super-horizon scales and (4.194) becomes

$$\mathcal{N}=\int_{\gamma(s)}d\tau\mathcal{H}\left(1+A\right)\left(1-A+\frac{\mathcal{R}'}{\mathcal{H}}\right)=\int_{\gamma(s)}d\tau\left(\mathcal{H}+\mathcal{R}'\right), \tag{4.196}$$

where $ds=a\left(1+A\right)d\tau$ and we worked at linear order. If we define the unperturbed number of e-folds, N, as

$$\mathrm{N}=\int_{\gamma(s)}d\tau\mathcal{H}, \tag{4.197}$$

we can introduce the following quantity

$$\delta \mathrm{N} = \mathcal{N} - \mathrm{N} = \delta\mathcal{R}, \tag{4.198}$$

where we used (4.196) and $\delta\mathcal{R}$ is the difference between the values of the curvature perturbation $\mathcal{R}$ on the final and initial hypersurfaces $\mathcal{U}$.

If we choose the initial (τ_1) hypersurface as flat and the final (τ_2) comoving, we obtain

$$\delta \mathrm{N}\left(\mathcal{U}_f(\tau_1), \mathcal{U}_c(\tau_2); \gamma(s)\right) = \mathcal{R}_c(\tau_2), \tag{4.199}$$

for a given curve $\gamma(s)$.

We assume τ_1 to be some time during inflation when the relevant scale that we are interested in has passed outside the horizon and τ_2 to be some time when $\mathcal{R}_c$ has become constant. From assumption $\mathcal{U}_f(\tau_1)$ is flat and all fluctuations are inside the fields present at τ_1. Then one can see $\mathcal{N}$ as a function of the field configuration $\phi^a(\tau_1, \vec{x})$ and the time τ_2 as

$$\mathcal{N} = \mathcal{N}\left(\phi^a(\tau_1, \vec{x}), \tau_2\right). \tag{4.200}$$

In principle, $\mathcal{N}$ is a function also of ϕ'^a but we used the slow-roll approximations at τ_1 to eliminate ϕ'^a. We write ϕ^a as

$$\phi^a(\tau_1, \vec{x}) = \bar{\phi}^a(\tau_1) + \delta\phi^a(\tau_1, \vec{x}), \tag{4.201}$$

and for N we have

$$\mathrm{N} = \mathrm{N}(\bar{\phi}^a(\tau_1), \tau_2). \tag{4.202}$$

Using (4.200), (4.201) and (4.202) in (4.199) we have

$$\mathcal{R}_c\left(\tau_2, \vec{x}_2\right) = \frac{\partial \mathrm{N}}{\partial \bar{\phi}^a} \delta\phi_f^a\left(\tau_1, \vec{x}_1\right), \tag{4.203}$$

where $\vec{x}_1$ and $\vec{x}_2$ are the spatial coordinates of γ on $\mathcal{U}_f(\tau_1)$ and $\mathcal{U}_c(\tau_2)$, respectively. The index a represents the multiple fields present in the theory. In the case in which $B = 0$ then the two spatial coordinates $\vec{x}_1$ and $\vec{x}_2$ coincide. It turns out that the perturbations in both $\subseteq$ and the density are negligible on comoving hypersurfaces on super-horizon scales, $\mathcal{U}_c(\tau_2)$ may be regarded as a hypersurface of constant Hubble parameter or constant energy density.

The δN formalism enables us to compute the curvature perturbations in terms of the derivative of the unperturbed number of e-folds, viewed as a function of the initial background fields configurations, and the fluctuations of the field on the initial flat hypersurface $\mathcal{U}_f(\tau_1)$.

Chapter 5

The Reheating phase

So far, we have examined the inflationary phase and the behavior of the axion during and after inflation. However, we have not yet explored how we can pass from inflation to the standard radiation-dominated Universe, which is known as reheating. This process is explained in Sections 5.1 and 5.2. In Section 5.3, we will discuss the complexity of preheating, which can be viewed as a quantum field theory in a classical time-dependent background. Other references on these topics include [104, 23]

5.1 Set up for Reheating

As we know the end of inflation is set by the time when ϵ, relation (3.13), reaches one. At this moment the kinetic energy of the inflaton is not anymore negligible and the field rolls rapidly to the minimum of the potential V. Inflation is a powerful tool to homogenize the Universe, leaving it empty and cold. To avoid this cataclysm the inflaton energy has to be converted into the matter that will provide the primordial bath. To understand this complicated phase that the Universe went through let us take a simple model described by

$$\mathcal{L} = \frac{1}{2}\left(\partial_\mu \phi\right)^2 - V\left(\phi\right) - g^2\phi^2\chi^2. \tag{5.1}$$

Here, ϕ plays the role of the inflaton and we introduce an additional boson χ; that is a proxy for SM fields or any hidden sector. We assume that the potential V has a minimum located at $\phi = \sigma$. We restrict the analysis near the minimum such that the potential can be expanded as

$$V\left(\phi\right) = \frac{m^2}{2}\left(\phi - \sigma\right)^2 + \ldots, \tag{5.2}$$

where m is the inflaton mass. If we absorbed σ into ϕ the interaction term in (5.1) becomes

$$2g^2\sigma\phi\chi^2 + g^2\phi^2\chi^2. \tag{5.3}$$

Thanks to the field redefinition we have generated two types of interactions that can contribute to the decay of the inflaton.

In the next section, we will study the effects of these interactions, which are characterized by the decay rate Γ, on the inflaton field dynamics. These interactions drain energy from ϕ to the field χ and we can model this transfer

of energy by an additional friction term Γ as follows

$$\ddot{\phi} + 3H\dot{\phi} + \Gamma\dot{\phi} + m^2\phi = 0. \tag{5.4}$$

The reheating completes when $\Gamma = H$.

This treatment ignores crucial effects. The interaction term in (5.1) of the classical inflaton field ϕ and quantum field χ leads to χ-particles production due to the oscillating effective mass of χ. As we will see the mode function of χ satisfies

$$\ddot{\chi}_k + 3H\dot{\chi}_k + \left(\frac{k^2}{a^2} + g^2\phi^2(t)\right)\chi_k = 0, \tag{5.5}$$

and the oscillating ϕ^2 term can lead to resonance phenomena, called preheating, that can enormously enhance the reheating efficiency. The resonance of an interaction can be narrow or broad, depending on its strength. When it is narrow, only a small range of momenta is excited. However, when it is broad, a wider range of momenta is excited. According to current theories, reheating after inflation starts in a broad resonance regime but never completes in a stage of parametric resonance. This is because the initial amplitude of the inflaton field is of the order of Planck. Eventually, the phenomenological and perturbative treatment can be applied. This simple treatment does not have to be applied to the original coherently oscillating inflaton field, but to its decay products and to the residual part of the inflationary energy left by the preheating processes.

5.2 Reheating as a perturbative processes

As we already said, after inflation, the inflaton field oscillates around the minimum of the potential. The field ϕ follows

$$\ddot{\phi} + 3H\dot{\phi} + m^2\phi = 0, \;\; H^2 = \frac{1}{3M_{\rm Pl}^2}\left(\frac{\dot{\phi}^2}{2} + \frac{m^2\phi^2}{2}\right), \tag{5.6}$$

where we ignored for the moment the field χ. An approximate solution for (5.6) is given by

$$\phi(t) \approx \Phi(t)\sin mt, \;\; \Phi(t) \sim \frac{M_{\rm Pl}}{3mt}. \tag{5.7}$$

Having ϕ we can take an average of the Hubble parameter over many oscillations of the inflaton field and we obtain

$$\rho_\phi \sim a^{-3}, \;\; a \sim t^{2/3}, \tag{5.8}$$

showing the well-known matter behavior of a scalar field that is oscillating in a quadratic potential.

Equation (5.6) is modified by the interaction term with χ. We consider the coupling $2g^2\sigma\phi\chi^2$ that represents the decay of the inflaton field. The decay

rate can be computed and its form is

$$\Gamma_{\phi\to\chi\chi} = \frac{g^4\sigma^2}{8\pi m}. \tag{5.9}$$

Note that the scattering process $\phi\phi \to \chi\chi$ can not lead to an efficient reheating since its decay rate Γ scales as $\Gamma \sim 1/t^2$ and the decay rate never catches up with the expansion of the Universe. We can model the evolution of the number density of ϕ and χ as follows

$$\frac{1}{a^3}\frac{d\left(a^3 n_\phi\right)}{dt} = -\Gamma_{\phi\to\chi\chi} n_\phi, \quad \frac{1}{a^3}\frac{d\left(a^3 n_\chi\right)}{dt} = +2\Gamma_{\phi\to\chi\chi} n_\chi, \tag{5.10}$$

where the right-handed sides of (5.10) represent the decay effects.

As we said the decay processes start to become important when $H \simeq \Gamma$ and assuming that thermodynamic equilibrium is reached quickly after this moment we have

$$\frac{\pi^2}{30} g\left(T_{\rm R}\right) T_{\rm R}^4 = 3\Gamma_{\phi\to\chi\chi}^2 M_{\rm Pl}^2, \tag{5.11}$$

where $T_{\rm R}$ is the reheating temperature. Having obtained $T_{\rm R}$ we have completed the analysis of reheating since from now on the standard radiation-dominated Universe begins. Note that $T_{\rm R}$ does not depend on the initial position of the field ϕ; it is completely determined by the parameter $\Gamma_{\phi\to\chi\chi}$, which contains information regarding the underlying elementary particle theory.

5.3 Preheating

The previous treatment assumes that a superposition of free asymptotic single states can describe the inflaton. Instead at the onset of the oscillation, thanks to the large occupation number, the inflaton ϕ is a coherently oscillating homogeneous field. The presence of this time-dependent background provides a way to produce χ-particles.

Let us consider the quantum field χ in the classical background $\phi(t)$,

$$\hat{\chi}\left(t,\vec{x}\right) = \int \frac{d^3k}{(2\pi)^{3/2}}\left(\hat{a}_{\vec{k}}\chi_k(t)e^{\imath\vec{k}\cdot\vec{x}} + \hat{a}^\dagger_{\vec{k}}\chi_k(t)^* e^{-\imath\vec{k}\cdot\vec{x}}\right), \tag{5.12}$$

where $\hat{a}$ and $\hat{a}^\dagger$ are the creation and annihilation operators respectively, and the modes function $\chi_k(t)$ satisfy (5.5). Ignoring, for the moment, the expansion of the Universe, relation (5.5) becomes

$$\ddot{\chi}_k + \left(k^2 + g^2\Phi^2 \sin\left(mt\right)^2\right)\chi_k = 0. \tag{5.13}$$

Using $z = mt$, relation (5.13) becomes

$$\frac{d^2}{dz^2}\chi_k + \left(A_k - 2q\cos 2z\right)\chi_k = 0, \tag{5.14}$$

where

$$A_k = \frac{k^2}{m^2} + 2q, \quad q = \frac{g^2\Phi^2}{4m^2}. \tag{5.15}$$

Relation (5.14) is called the Mathieu equation and the main characteristic of the solutions is exponential instability within certain resonance bands Δk,

$$\chi_k \approx e^{\mu_k z}, \tag{5.16}$$

where μ_k are called Floquet exponents. This implies an exponential enhancement of the number density

$$n_k = |\chi_k|^2 \approx e^{2\mu_k z}. \tag{5.17}$$

Relation (5.16) has two important regimes:

1. $q \ll 1$ narrow resonance
2. $q > 1$ broad resonance

5.3.1 Adiabaticity parameters

Before going into the analysis of these two different regimes, let us discuss some other important ingredients for the study of particle creation, the so-called adiabaticity conditions. In the Fock space of a quantum field theory, the vacuum state $|0\rangle$ is annihilated by the number operator N, which is defined as $N = a^\dagger a$. An observer does not detect any particles in this state. This property continues to hold also for all observers linked together by a Pioncarè transformation. This property ceases to hold in a curved space since the vacuum state is not invariant under general coordinate transformations. This inequivalence between vacua is the basis of the production of particles by a time-dependent potential or a curved spacetime.

This inequivalence can be formulated by studying the evolution of the mode functions of the theory we are considering. Let us consider a free scalar field theory in Minkowski spacetime whose Hamiltonian H in the basis given by equation (5.12) reads

$$\mathrm{H} = \frac{1}{2}\int d^3k \left[\hat{a}_k \hat{a}_{-k} F_k^* + \hat{a}_k^\dagger \hat{a}_{-k}^\dagger F_k + \left(2\hat{a}_k^\dagger \hat{a}_k + \delta(0)\right) E_k\right], \tag{5.18}$$

where

$$E_k = |\dot{\chi}_k|^2 + k^2|\chi_k|^2, \tag{5.19}$$

$$F_k = \dot{\chi}_k^2 + k^2\chi_k^2. \tag{5.20}$$

A unique definition of the vacuum state of a quantum field theory can be given through the Hamiltonian of the system H. We can evaluate the Hamiltonian (5.18) on the vacuum of the theory and we obtain

$$\langle 0|\mathrm{H}|0\rangle = \frac{\delta(0)}{2}\int d^3k E_k. \tag{5.21}$$

The last expression represents the energy of the theory and the minimization of (5.21) fixes the form of $\chi_k(t)$. The result is

$$\chi_k = \frac{1}{\sqrt{2k}} e^{-\imath k t}, \tag{5.22}$$

that is the preferred modes function (that satisfies the Wronskian condition) in which H is diagonal in the basis of the operator N ($F_k = 0$, $E_k = k$).

This prescription can not be generalized directly to a time-dependent background. In general, the equation for the modes χ_k involves time-dependent frequencies ω_k, and the minimum energy state depends on the specific moment t_0. In line with the previous discussion, we can find the modes function that minimize H instantaneously and we can define the vacuum state ($|0\rangle_{t_0}$) at the moment t_0. The required χ_k satisfies

$$\chi_k(t_0) = \frac{1}{\sqrt{2\omega_k(t_0)}} e^{-\imath \omega_k(t_0) t_0} \ , \dot{\chi}_k(t_0) = -\imath \omega_k(t_0) \chi_k(t_0). \tag{5.23}$$

As time progresses, the value of ω_k changes, meaning that at time t_1, there will be a different mode function that satisfies the conditions (5.23). This difference implies that the vacuum at time t_1 is not equivalent to the vacuum at time t_0. The rate at which ω_k changes determines the difference between these vacuums. If ω_k changes slowly, then we do not expect any rapid particle production since the vacuum remains mostly the same and the mode function remains in the vacuum state. However, if ω_k changes suddenly, the opposite occurs. Adiabatic parameters can be used to quantify the speed at which ω_k changes.

In general χ_k obeys the following equation

$$\ddot{\chi}_k + \omega_k^2 \chi_k(t) = 0, \tag{5.24}$$

which represents the equation for a harmonic oscillator with time-dependent frequency ω_k. An approximate solution of the previous equation is given by

$$\chi_k = \frac{1}{\sqrt{2\omega_k(t)}} e^{-\imath \int dt \omega_k(t)} + \text{h.c} \ , \tag{5.25}$$

the so-called Wentzel-Kramers-Brillouin (WKB) approximation [109, 176]. Inserting the last expression into equation (5.24) shows that (5.25) provides an approximation to (5.24) if:

$$\mathrm{R} = \frac{\dot{\omega}_k(t)}{\omega_k^2(t)} \ll 1, \tag{5.26}$$

$$\mathrm{R}_1 = \frac{\ddot{\omega}_k}{\omega_k^3} \ll 1, \tag{5.27}$$

are much smaller than unity. These factors are called adiabaticity parameters. For details on the error between the true and the WKB approximate solutions see [178].

Let us conclude this section by making an important observation. The narrow and broad regimes correspond to situations where R and R_1 are much smaller than 1 and much larger than 1, respectively. When R and R_1 are small, particle production is not violent and the increment of χ_k is determined by a Bose effect. On the other hand, when R and R_1 are much larger than 1, we can expect violent particle production to occur instantly.

5.3.2 Narrow resonance

The theory of the instability/stability bands of the Mathieu equation shows that, for $q \ll 1$, resonances occur when $A_k \approx n^2$, where $n \in \mathbb{Z}$. The widths of the bands are $\Delta k \sim m q^n$. For $q < 1$, the most relevant band is the first one for which the range of exited k is

$$k = m\left(1 \pm \frac{q}{2}\right). \tag{5.28}$$

In the first band, the instability parameter is

$$\mu_k = \sqrt{\left(\frac{q}{2}\right)^2 - \left(\frac{k}{m} - 1\right)}. \tag{5.29}$$

The maximum of (5.29) is obtained in $k = m$ and we have

$$\mu_{\max} = \mu_{k=m} = \frac{q}{2} = \frac{g^2\Phi^2}{8m^2}. \tag{5.30}$$

Parametric resonances occur when perturbative decays are inefficient, resulting in $qm > \Gamma$, where $t_{\mathrm{PR}} \sim 1/qm$ represents the time of the resonances. It is important to check if t_{PR} is shorter than the Hubble expansion because if it is, then the parametric resonances will be inefficient. Another factor to consider is the redshift of momenta k away from the resonance band, which can prevent parametric resonances. The time Δt during which a given mode goes outside this band can be estimated by q/H. During this interval, the number of particles changes by a factor of $\exp\left(q^2 m/H\right)$, and the decays are efficient if $q^2 m > H$. In the narrow resonance regime, this condition is stronger than the condition resulting from the Hubble expansion, $qm > H$. The parametric resonances dominate over the perturbative decays and are efficient if:

1. $qm > \Gamma$,
2. $q^2 m > H$.

By referring to Equation (5.15), we can easily understand that parametric resonances (PR) can be effective when the value of Φ is high enough. However, it's important to note that the preheating stage doesn't lead to the end of reheating since the amplitude of oscillations eventually decreases, and PR comes to a halt. The primary goal of the preheating stage is to establish a different setup for the final stage of reheating.

It's crucial to mention the rescattering and backreaction effects, which can push modes out of the resonance band. Backreaction refers to the impact of the produced χ-particle on the classical inflaton field, following the Hartree approximation. This means that the effect of χ is represented in the variance $\langle\chi^2\rangle$, and the classical inflaton field obtains a mass of approximately $m^2_{\phi,\text{eff}} \sim g^2\langle\chi^2\rangle$. We're computing the primary correction on the dynamics of ϕ arising from the energy depleted by χ. When the mass $g^2\langle\chi^2\rangle$ reaches the inflaton's bare mass m^2, PR terminates, since the parameter q is decreasing as a result of the increase in $m_{\phi,\text{eff}}$. Based on (5.17), we can determine the time when PR stops as $t_{\text{end}} \sim 1/\mu m \ln m/g$.

The Hartree approximation is an incomplete method of considering preheating because it assumes that the inflaton field is homogeneous. However, if we take into account the inflaton fluctuations, then interactions such as $\phi^2\chi$ or $\phi\chi^2$ in Fourier space can result in mode coupling. In the Hartree approximation, ϕ is considered a function of t, which in Fourier space is equivalent to a delta function that collapses the convolution and eliminates mode coupling. The mode-mode coupling between different momentum modes is known as rescattering, which becomes increasingly important during the final nonlinear stages of preheating. This indicates that parametric resonance is a complex process that requires detailed numerical simulations, including all relevant effects, in order to determine its occurrence.

5.3.3 Broad Resonance

It's important to note that if the value of Φ is large, not only will the parametric resonance (PR) be efficient, but the value of q will also satisfy $q \gg 1$, which leads to a broad regime rather than a narrow one. This phenomenon can be observed in many models of inflation where Φ remains large at the end of inflation.

In the toy model that we're working with, the Planck normalization suggests that $m \sim 10^{-6} M_{\text{Pl}}$ and $\Phi \sim M_{\text{Pl}}$. These two results indicate a value for $q \sim g^2 10^{12}$ according to equation (5.15). With the exception of an extremely small g, we can achieve large values for q.

From equation (5.15), we can see that the ranges of k excited are larger in the broad case than in the narrow case. Moreover, the instability coefficients μ_k will be large, and reheating will be very efficient.

In the regime where q is much greater than 1, the field χ_k undergoes many oscillations for every oscillation of the field ϕ. Numerical simulations in a Minkowski background reveal that the production of χ particles occurs at points where $\phi(t)$ equals 0, while production is suppressed away from these points. This behavior leads to a sudden change in the evolution of n_k at $\phi = 0$, while it remains constant elsewhere.

From this lesson, we now understand that the frequency of χ changes adiabatically away from $\phi = 0$, and there n_k remains constant. Instead, particle

production happens when the adiabatic condition (5.26) is violated, namely

$$\mathrm{R} = \frac{|\dot{\hat{w}}_k|}{\hat{w}_k^2} \geq 1, \tag{5.31}$$

where $\hat{w}_k = \sqrt{k^2 + g^2\phi^2}$ comes from (5.5). For small values of k, relation (5.31) becomes

$$\mathrm{R} \simeq \frac{\dot{\phi}}{g\phi^2}. \tag{5.32}$$

From the last relation, we can understand that R diverges whenever ϕ approaches zero. In the moment where $\phi \approx 0$ we expect χ-particles production. For finite values of k, relation (5.31) becomes

$$\mathrm{R} = \frac{g^2\phi\dot{\phi}}{(k^2 + g^2\phi^2)^{3/2}} \sim \frac{g^2\phi m\Phi}{(k^2 + g^2\phi^2)^{3/2}}, \tag{5.33}$$

where in the second equality we used $\dot{\phi} \sim \Phi m \cos mt \sim \Phi m$, that holds near the origin $\phi = 0$ where we can use (5.7). From (5.33), the adiabaticity condition is broken for those wavevector that satisfy

$$k^2 \lesssim \left(g^2\phi m\Phi\right)^{2/3} - g^2\phi^2. \tag{5.34}$$

From relation (5.34), we can understand that, in the broad regime, there is a wide range of k that are excited; they form a sphere in the k space rather than shells as in the narrow case. In the regime of small k, relation (5.34) start to be satisfied for ϕ smaller than $\phi_{\max} = \sqrt{m\Phi/g}$. To find the maximum range of k that are excited we take a ϕ derivative of the right-hand side of (5.34) and search for the zeros of this equation. The maximum ϕ_* turns out to be given by the following estimate $\phi_* \sim \phi_{\max}/2$. Inserting ϕ_* in (5.34) we obtain

$$k^2 \lesssim k_*^2 = gm\Phi, \tag{5.35}$$

where the second step is the definition of k_*. Including the expansion of the Universe, relation (5.35) becomes

$$\frac{k^2}{a^2(t)} \lesssim k_*^2(t) = gm\Phi(t). \tag{5.36}$$

Due to the scaling of a as $a \sim t^{2/3}$ and Φ as $\Phi \sim 1/t$ we see that the expansion makes broad resonance more effective since more k-modes are pushed into the instability band.

Including the expansion of the Universe modifies the modes equation (5.13) with the inclusion of an addition term

$$\ddot{\chi}_k + \omega_k^2\chi_k = 0, \tag{5.37}$$

where

$$\omega_k^2 = \frac{k^2}{a^2} + g^2\Phi^2 \sin^2 mt + \Delta, \quad \Delta = -\frac{3}{4}\left(3H^2 + 2\dot{H}\right). \tag{5.38}$$

It has been shown in [104] that the system, in broad regime, can be analyzed as a successive sequence of Schrodinger scattering of the wavefunction χ against an inverted quadratic potential. Indeed, the χ-particles production happen near $\phi = 0$ and there the modes function χ_k deviate from and adiabatic evolution $e^{\pm i\int \omega_k dt}$. This bring us to study (5.38) near $\phi(t_0) = 0$ where we can expand $g^2\Phi^2 \sin^2 mt \sim g^2\Phi^2 m^2 (t - t_0)^2$ at leading order. From this approximation, the quadratic potential pops out. In broad regime $q \gg 1$, the phase θ, $\theta = \int dt\omega_k$, is rapidly changing with time due to ω_k and its value is practically stochastic. In [104], it is shown that in the 75% of all scattering events the amplitude of χ_k grows after passing through $\phi = 0$. Over a long period, the occupation number of χ-particles therefore grows. Of course, this treatment is only an approximation of the full analysis and considering back-reaction and rescattering, point toward an analysis that requires numerical simulations.

Chapter 6

The landscape of Axions

In this chapter, we review the main properties of axion in Section 6.1 and how it behaves during inflation in Sections 6.2 and 6.3. We pass to study the possible type of production mechanisms in Section 6.4. We discuss both the natural inflation and axion quality issues in Sections 6.7 and 6.6, respectively. Other references on these topics include [131, 159].

6.1 Motivations for the Axions

The motivation of the axion comes from the presence of the strong CP problem in the strong sector of the standard model. In this part of the Lagrangian is present a topological term that is

$$\mathcal{L}_{QCD} \subset \frac{g_s^2 \theta}{32\pi^2} G_{\mu\nu} \tilde{G}^{\mu\nu}, \tag{6.1}$$

where $\tilde{G}$ is $\tilde{G}_{\mu\nu} = \epsilon_{\mu\nu\rho\gamma} G^{\rho\gamma}$ and ϵ is the totally anti-symmetric tensor. Moreover, g_s is the strong coupling constant and θ is a constant term. Due to the ϵ tensor the last term breaks CP-invariance. Moreover, we have to be precise by adding the fact that the quark mass term is CP-violating for non-zero phases. The quark fields can always be redefined by a chiral transformation. This redefinition not only affects the mass matrix but due to a change in the path integral measure changes the value of θ [67]. It can be shown that the following quantity

$$\bar{\theta} = \theta - \arg\det Y_u Y_d, \tag{6.2}$$

where Y_u, Y_d are the Yukawa mass matrices for the quarks, and it is the correct physical combination to account for a possible CP violation.

Notably, it gives rise to a neutron electric dipole moment

$$d_{\mathrm{N}} = \left(5.2 \times 10^{-16} e \cdot cm\right) \bar{\theta}. \tag{6.3}$$

Current experimental upper bounds on the dipole moment give an upper bound of $d_{\mathrm{N}} < 10^{-16} e \cdot cm$ [15, 5], which requires $\bar{\theta} < 10^{-10}$. The strong CP problem is why $\bar{\theta}$ is so small.

The Peccei–Quinn (PQ) mechanism, [138], based on a global $\mathrm{U}(1)_{\mathrm{PQ}}$ symmetry, provides a solution to the strong CP problem by promoting the QCD $\bar{\theta}$ angle to a dynamical axion field [174, 177]. The axion can be interpreted as

the phase of a complex scalar—the PQ field $\Phi = \varphi e^{ia/f}$. When the temperature T is of order the decay constant of the axion f, the radial field φ acquires a vacuum expectation value, of order f, and the global $U(1)_{PQ}$ symmetry is broken. The axion is the Goldstone boson of the $U(1)_{PQ}$ and is massless at all orders in perturbation theory. The axion potential is induced by non-perturbative effects, as instantons, at temperature T_{NP}. The axion is an angular DOF and it has to satisfy a residual discrete symmetry, that is a going in $a + 2\pi n f$, where n is an integer number. The last symmetry restricts the potential of the axion to be periodic. A prototypical example for the potential $\tilde{V}_{NP}$ of the axion is

$$\tilde{V}_{NP}(a) = f^2 m_{QCD}^2(T)\,(1 - \cos a/f)\,, \tag{6.4}$$

where the mass m_{QCD} is temperature dependent and it is set by the topological susceptibility χ as follows

$$m_{QCD}(T) = \frac{\sqrt{\chi}}{f}, \quad \chi(T) = \chi_0 \left(\frac{T_{QCD}}{T}\right)^n, \quad T_{QCD} = 200\text{MeV}. \tag{6.5}$$

Where in the relation (6.5), $\chi_0 = (75.5\text{MeV})^4$ comes from a QCD calculation, and if we assume the dilute instanton gas approximation we have $n = 8$, [33, 34]. Relation (6.4) is not unique and the exact form of the potential requires detailed knowledge of the non-perturbative physics.

One interesting property of the axion a is that the self-interaction and interaction with matter are suppressed by f, due to the shift symmetry. The weak interactions of the axion a promote it to be a light and long-lived particle. All these axion properties promote it to provide a candidate for inflation, dark matter, and dark energy. In this thesis, we explore the axion as a dark matter candidate. A crucial aspect of the axion is when the $U(1)_{PQ}$ is broken or not. It is important to study the role of the axion during inflation and there are two different cases [1]

1. The PQ symmetry is unbroken during inflation if $f < H/2\pi$
2. The PQ symmetry is broken during inflation if $f > H/2\pi$

6.2 PQ symmetry unbroken during inflation

The De Sitter spacetime can be viewed as having a temperature $T_H = H/2\pi$ and the axion a acquires thermal fluctuations of order $\delta a \sim H/2\pi$. These temperature fluctuations are large enough that the $U(1)_{PQ}$ symmetry is unbroken and φ has zero vacuum expectation value. After inflation, the temperature drops below the scale f, breaking the symmetry. The temperature, at which the breaking happens, is larger than the temperature at which non-perturbative effects switch on. Hence, the axion has no potential and there

[1] To be precise, the condition would be $max(T_R, H/2\pi)$, where T_R is the reheating temperature. The symmetry can be thermally restored, but we avoid this possibility for the moment, which would require a complete reheating model.

are no preferred values that the axion can acquire. In each casually disconnected patch, the axion picks a value from a random uniform distribution on $[-\pi, \pi]$. Each causally disconnected patch is of order the horizon size $1/H$ and the axion has different values. This means that the axion varies on horizon scales and has $\mathcal{O}(1)$ fluctuations when non-perturbative effects switch on $1/H \sim 10$pc (QCD scale). These fluctuations are non-adiabatic, but are not scale invariant and give rise to additional power on scales that are sub-horizon at the PQ symmetry breaking; these perturbations may give rise to axion mini-cluster[37].

A breaking of global symmetry generates topological defects, in the case of a global $\mathrm{U}(1)_{\mathrm{PQ}}$ we may have to deal with cosmic strings, and if $N_{\mathrm{DW}} \neq 1$, the domain wall number, also domain walls. These latter defects, if they are not removed, tend to dominate the energy budget of the Universe since their energy density scales as $1/a^2$. Instead if $N_{\mathrm{DW}} = 1$, the domain wall problem can be avoided. Anyway, both cosmic strings and domain walls provide a rich phenomenology.

Since a_{in}, the initial axion value, varies from patch to patch we can calculate $\langle a_{\mathrm{in}}^2 \rangle$ as follows

$$\langle \theta_{\mathrm{in}}^2 \rangle = \frac{1}{2\pi} \int_{-\pi}^{\pi} \theta^2 = \frac{\pi^2}{3}, \tag{6.6}$$

where

$$\theta_{\mathrm{in}} = \frac{a_{\mathrm{in}}}{f}, \tag{6.7}$$

and we assumed a uniform density distribution for θ. The last relation will be useful later for the calculation of the relic abundance of dark matter. As we will see, in the next scenario, θ_{in} is not predicted and is an environmental parameter.

6.3 PQ symmetry broken during inflation

In this case, the PQ symmetry is broken before or during inflation and all topological defects are red-shifted away by the expansion. In particular the value of the initial angle θ_{in} is stretched on super-horizon scales and each single patch, our Universe, has a single value for θ_{in}. The axion in this scenario is a homogeneous field and its initial value is arbitrary, there is no reason to choose 0 or π, except for personal taste or anthropic reasons.

In this scenario, the axion exits during inflation as a massless field. Massless fields acquire fluctuations of order Hubble. The axion has no potential and its perturbations do not alter the energy density ρ, in other words, its fluctuations are of isocurvature type. If axion provides a dark matter candidate these isocurvature perturbations are then imprinted in the spectrum of dark matter. The Planck experiment severely constrains the isocurvature perturbations in the dark matter component. Indeed, the Planck collaboration [9] puts, at the CMB scale $k_* = 0.05\mathrm{Mpc}^{-1}$, for uncorrelated axion-type

isocurvature perturbations the following constraint

$$\frac{P_{iso}}{A_S} \leq 0.038, \tag{6.8}$$

where $P_{\rm iso} = \delta\Omega_{\rm DM}/\Omega_{\rm DM}$ is the isocurvature dark matter power spectrum and $A_S \sim 10^{-9}$ from observation. To compute the last formula we need an explicit expression for the relic abundance of axion that will be our next task.

6.4 Axion's production mechanisms

In this Chapter, we will discuss the abundance of axion relics, denoted as Ω_a, which can be produced through several ways such as the decay of topological defects, vacuum realignment, kinetic misalignment, thermal population and decay of parent particles. In particular, we will focus on the first three methods and provide a brief overview of each.

6.4.1 The axion as decay product of topological defects

As introduced before we are referring to the case of the PQ symmetry unbroken during inflation. Let us stress immediately that the evolution of the string networks/ domain walls is hardly complicated, see [108, 159] and analytically calculations lack. In the rest of the thesis, we will not touch the dark matter production mechanism since as we will see in the future chapter, Chapter 7, the evolution of the symmetry after Peccei-Quinn inflation requires numerical simulations.

Nevertheless, within this scenario, the production mechanism of the strings network is the so-called Kibble mechanism [97]. In this scenario, there is at least one string per horizon. This string is created when the random value of the axion field wraps from zero to $2\pi f$ along a closed path in physical space. If this closed path has a size larger than the horizon the string perforates the surface subtend by the closed path. Moreover, this string network consists of string loops that emit axions while tightening, oscillating, reconnecting, and collapsing during the Universe's expansion.

The final amount of axions from string decay is a long-standing controversy and the relic abundance can be written as

$$\Omega_a h^2 = \Omega_{\rm mis} h^2 \left(1 + \alpha_{\rm dec}\right), \tag{6.9}$$

where $\Omega_{\rm mis} h^2$ is the misalignment result and the value of $\alpha_{\rm dec}$ oscillates from 0.16 to 186, [78, 55, 24, 86]. The degree of ignorance, parameterized as $\alpha_{\rm dec}$, lies in the form of the spectrum of the axions emitted from strings. A slice of this ignorance resides in how the string system is simulated. This is a very important area of research because the uncertainties present are directly related to possible observations of axion since a large contribution from strings points toward small values of f.

6.4.2 Vacuum realignment

This process is present in the cases of PQ symmetry which is broken after or before inflation. In the broken scenario, the vacuum realignment consists of zero and higher modes contributions since the axion is inhomogeneous, besides the aforementioned defects. When the axion is homogeneous only the zero mode contributes and topological defects are not present.

In the standard vacuum misalignment scenario, the axion starts at some random initial place $a_{\text{in}} = f\theta_{\text{in}}$ with $\dot{a}_{\text{in}} = 0$. Recently, the study of the scenario in which axion has a non-zero initial velocity has received much attention in the literature. If this initial velocity is sizeable it can affect the evolution of the axion, postponing its oscillation time and therefore changing its relic abundance. This is the core of the so-called kinetic misalignment model[46]. We have to mention also the so-called "axion kination" that is based on the same logic where a spinning axion dominates the energy budget of the Universe providing an equation of state w equal to $w = 1$. The interest of this mechanism lies, to name one, in the boost that the gravitational wave spectrum, originating from inflation, receives if this phase with $w = 1$ is present. From the observation or not of this signal, one can put constraints on the UV models that generate this phase that are principally based on supersymmetry [49, 73].

But let us go back to the case in which $\dot{a}_{\text{in}} = 0$. If the axion is homogeneous over the entire Hubble patch its evolution is governed by (3.19). The axion is stuck to a_{in} by Hubble friction until the oscillation temperature T_* that is the moment when

$$3H\left(T_*\right) \approx m_{\text{QCD}}\left(T_*\right). \tag{6.10}$$

In the rest of the chapter, we will assume that the onset of oscillation starts in radiation domination and the subsequent evolution is adiabatic; moreover, we assume for simplicity $N_{\text{DW}} = 1$. After oscillation (neglecting anharmonic effects) the axion behaves as non-relativistic matter and the production of dark matter axion is non-thermal[2].

The calculation of the relic abundance proceeds as follows, we start from

$$\Omega_{\text{a}} h^2 = \frac{\rho(T_0)_{\text{a}} h^2}{\rho_{\text{crit},0}}, \tag{6.11}$$

where we used (2.39). Since the axion is non-relativistic from oscillation until now, we know that

$$\rho(T_0)_{\text{a}} = m_{\text{QCD}}\left(T_0\right) n_{\text{a}}\left(T_*\right) \left(\frac{a_*}{a_0}\right)^3. \tag{6.12}$$

[2]The field is described by a classical condensate of particles at rest $\vec{k} = 0$ that oscillate coherently with the same phases

The ratio of scale factors can be evaluated using the conservation of entropy and we obtain

$$\left(\frac{a_*}{a_0}\right)^3 = \frac{g\left(T_0\right)}{g\left(T_*\right)}\frac{T_0^3}{T_*^3}. \tag{6.13}$$

Using (6.13) and (6.12) in (6.11) we get

$$\Omega_a h^2 \approx \frac{m_{\rm QCD}\left(T_0\right) h^2 f^2 \langle\theta_{\rm in}^2\rangle}{2\rho_{\rm crit,0}} \frac{3g\left(T_0\right) T_0^3}{M_{\rm Pl} g\left(T_*\right) T_*} \sqrt{\frac{\pi^2 g\left(T_*\right)}{90}}, \tag{6.14}$$

where we used (6.7), $n_a\left(T_*\right) \approx \frac{m_{\rm QCD}(T_*) f^2 \langle\theta_{\rm in}^2\rangle}{2}$ since the axion is stuck until T_*, (6.10) and radiation domination $3M_{\rm Pl}^2 H^2\left(T_*\right) = \frac{\pi^2 g(T_*) T_*^4}{30}$.

For the temperature T_* we can use (6.10), (6.5), radiation domination and we obtain

$$\sqrt{\frac{\pi^2 g\left(T_*\right)}{90}} \frac{T_*^2}{M_{\rm Pl}} = \frac{\sqrt{\chi_0}}{3f} \left(\frac{T_{QCD}}{T_*}\right)^{n/2}. \tag{6.15}$$

The last steps are to substitute (6.15) in (6.14) and we obtain

$$\Omega_a \sim 0.1 \langle\theta_{\rm in}^2\rangle \left(\frac{f}{10^{12}{\rm GeV}}\right)^{7/6}, \tag{6.16}$$

where we also used (6.5), and

$$\rho_{\rm crit,0} \simeq 10^{-5} h^2 {\rm GeV cm}^{-3}, \;\; {\rm n_{fl}} \simeq 410 {\rm cm}^{-3}, \;\; {\rm g\left(T_0\right)} \simeq 4, \;\; {\rm n} = 8, \;\; {\rm g\left(T_*\right)} \simeq 62, \tag{6.17}$$

the most right expression represents the relativistic standard model degree of freedom just above the QCD scale.

Relation (6.16) implicitly assumed that the axion oscillations start when $T_* \gtrsim T_{\rm QCD}$. From (6.15) and (6.17) we have

$$T_* \sim T_{\rm QCD} \left(\frac{10^{16}{\rm GeV}}{f}\right)^{1/6}. \tag{6.18}$$

Relation (6.18) is telling us that (6.16) holds for $f \lesssim 10^{15}$GeV. Instead for $f \gtrsim 10^{17}$GeV the oscillations begin when $T \lesssim T_{\rm QCD}$ and the relic abundance changes. In this case, the axion starts to oscillate with the zero temperature mass, hence we can take in (6.15) the $n = 0$ case and we obtain

$$\Omega_a h^2 \sim 0.1 \langle\theta_{\rm in}^2\rangle \left(\frac{f}{10^{13}{\rm GeV}}\right)^{3/2}. \tag{6.19}$$

In the range $10^{15}{\rm GeV} \lesssim {\rm f} \lesssim 10^{17}{\rm GeV}$, oscillations begin during the QCD epoch, and the dilute instanton gas approximation breaks down; in this regime the estimation of the relic abundance is complicated.

Both in (6.16) and (6.18) we approximate the potential to be quadratic but when $\theta_{\rm in} \sim 1$ anharmonic effects start to be important. In this regime, there is an increment of the relic abundance of dark matter. The first analytical

estimate of these effects is presented in [122], and they can be included by the replacement of $\theta_{\rm in}$ with

$$\theta_{\rm in}^2 \left[\ln \frac{1}{1-\theta_{\rm in}/\pi} \right]^{1.175} . \tag{6.20}$$

The author's choice for the dependence of mass on temperature ($n \neq 8$) results in the numerical value 1.175. This is only a glimpse to show that the actual calculation is complicated and many approximations are used; such that one has not to rely on these computations for a more realistic result. The interested reader can find in [169], a full numerical computation of the relic abundance valid for all f, with g temperature dependents and all anharmonic effects accounted.

Let us consider $\theta_{\rm in}$ as a free parameter and analyze the consequence of (6.16), we further specialize to the case $f \lesssim 10^{15}$GeV. In particular, high and low scale f point towards a tuning of the initial angle $\theta_{\rm in}$ in the $\theta_{\rm in} \ll 1$ and $\theta_{\rm in} \sim \pi$ regions respectively. There is a "sweet" spot where $\theta_{\rm in} \sim 1$ and the total dark matter abundance is reproduced, from (6.16), for $f \sim 10^{12}$GeV. In the unbroken scenario, thanks to (6.6) and (6.16) we can put a bound on $f \lesssim 10^{11}$GeV in order not to overproduce dark matter. In the unbroken scenario all values of $f \lesssim 10^{11}$GeV are possible. This freedom reflects the uncertainty in the production mechanism, in other words, the ignorance of the exact amount of axions from topological defects.

6.4.3 Kinetic Misalignment Mechanism

As we anticipated in Section 6.4.2 there can be the possibility of changing the evolution of the axion field through a non-vanishing velocity $\dot{\theta}$, leading to axion dark matter for larger values of $m_{\rm QCD}$ respect to the standard misalignment scenario. The so-called "kinetic misalignment" (KM) mechanism is at play when the kinetic energy of the axion is larger than the potential energy at the usual oscillation temperature T_* (6.18). The non-zero velocity for the axion can be induced, for example, with a higher-dimensional operator, that breaks the $U(1)_{\rm PQ}$ symmetry and provides an angular kick for the axion, similar to the Affleck-Dine mechanism [8]. Let us review this scenario as proposed in [46].

The $U(1)_{\rm PQ}$ symmetry is associated with a conservation of a Noether charge due to the shift symmetry of the axion $\theta \to \theta + \alpha$. The charge can be read from the action and we get

$$\varphi^2 \dot{\theta} a^3 = L, \tag{6.21}$$

where L is a constant and represents the angular momentum. For the estimation of the relic abundance is useful to work with red-shift invariant quantities. In order to do that we call $n_\theta = \varphi^2 \dot{\theta}$ and we introduce a yield Y_θ defined as

$$Y_\theta = \frac{n_\theta}{s}, \tag{6.22}$$

where s is the entropy density and scales as a^{-3}. Hence, Y_θ is constant and its value is model-dependent.

Let us assume to be in radiation domination and the radial field is stuck to the minimum $\varphi = f$. If the kinetic energy of the axion $f^2\dot{\theta}^2/2$ at the usual oscillation temperature T_* (6.18) is greater than the potential energy given by relation (6.4), then the axion will overcome the potential barrier and θ will continue to change. This evolution ceases when the kinetic energy reaches the height of the potential barrier

$$|\dot{\theta}(T')| = 2m_{\rm QCD}(T'), \tag{6.23}$$

where T' is the temperature of this moment. After this moment the axion is trapped in the minimum and the onset of oscillations is delayed if $T' < T_*$.

We assume that the mass of the axion changes adiabatically and that the energy density of the axion redshifts as matter after the onset of the oscillation. Today's energy density of axion normalized to the entropy density reads

$$\frac{\rho_a}{s} = m_{\rm QCD}(T_0)\frac{n_a(T')}{s(T')}, \tag{6.24}$$

where $m_{\rm QCD}$ is the vacuum axion mass. For $n_a(T')/s(T')$ we have

$$\frac{n_a(T')}{s(T')} \simeq \frac{f^2\dot{\theta}(T')}{s(T')} = Y_\theta, \tag{6.25}$$

where we used $n_a = V_{NP}/m_{\rm QCD}$, (6.22) and (6.23). However, this computation is not entirely correct since we assumed that $\rho_a \sim a^{-3}$ immediately after the onset of the oscillations. Since the axion oscillates near the maximum, anharmonic effects become important, causing a delay in the oscillation and boosting the relic abundance. This non-linearities correct relation (6.24) by a factor of two, leading to[46]

$$\frac{\rho_a}{s} = 2m_{\rm QCD}(0)Y_\theta. \tag{6.26}$$

The condition for kinetic misalignment to be relevant, namely $|\dot{\theta}(T_*)| > m_{\rm QCD}(T_*)$, can be rewritten as

$$Y_\theta > Y_{\rm crit}, \quad Y_{\rm crit} = \frac{n_a(T_*)}{s(T_*)} \sim \frac{f^2}{M_{\rm Pl}T_*}, \tag{6.27}$$

where we used $n_a(T_*) \sim m_{\rm QCD}(T_*)f^2$, $m_{\rm QCD}(T_*) \sim H(T_*)$, $H(T_*) \sim T_*^2/M_{\rm Pl}$ and $s(T_*) \sim T_*^3$ and dropped numerical factors.

Using (6.18) in (6.27) we obtain

$$Y_{\rm crit} = 0.11\left(\frac{f}{10^9{\rm GeV}}\right)^{13/6}. \tag{6.28}$$

Assuming $Y_\theta \gg Y_{\rm crit}$, the axion abundance is given by the kinetic misalignment mechanism and we get

$$\Omega_a h^2 \simeq \Omega_{DM} h^2 \left(\frac{f}{10^9 \text{GeV}}\right) \left(\frac{Y_\theta}{40}\right), \tag{6.29}$$

which is independent of the axion mass evolution. Comparing (6.29) and (6.28) we get $Y_\theta < Y_{\rm crit}$ for $f \gtrsim 1.5 \times 10^{11}$GeV . Hence, kinetic misalignment can provide all the dark matter for smaller values of f compared to the standard misalignment. In equation (6.29), all model dependence is contained within Y_θ. In Chapter 8, we will investigate whether potential (7.23) can maintain kinetic misalignment.

6.5 Isocurvature perturbations in the vanilla Axion scenario

In the unbroken scenario, the axion does not exist during inflation and it does not acquire isocurvature perturbations on large scales where we have strong constraints from Planck. As we said in Section 6.2, non-adiabatic perturbations may be present at small scales, and spectral distortions and mini-clusters may impose interesting additional constraints [45, 37].

We turn our attention to the broken scenario where the axion acquires fluctuations during inflation. Inflation can be tested by combining the isocurvature constraint and the properties of the axion to be a DM candidate. Within the broken scenario, the relic abundance is given by the vacuum realignment, relation (6.16). If the axion provides the totality of the dark matter then $\Omega_{\rm DM} = \Omega_{\rm a}$ and we can estimate $P_{\rm iso}$ as

$$P_{\rm iso} \sim \left(\frac{2\delta\theta_{\rm in}}{\theta_{\rm in}}\right)^2 \sim \left(\frac{H}{\pi f \theta_{\rm in}}\right)^2, \tag{6.30}$$

where in going from left to right we used $\delta\theta \sim H/2\pi f$. From $\Omega_{\rm DM} = \Omega_{\rm a}$ and (6.16) we get

$$\theta_{\rm in}^2 \sim \left(\frac{f}{10^{12}\text{GeV}}\right)^{-7/6}. \tag{6.31}$$

With the help of (4.167), (4.168) and (6.31) we can rewrite (6.8) as follows

$$r \lesssim 5 \times 10^{-11} \left(\frac{f}{10^{16}\text{GeV}}\right)^{5/6}. \tag{6.32}$$

With future $r \sim 10^{-3}$ and futuristic sensitivity, from 21cm lensing, $r \sim 10^{-9}$ [32, 158] we can probe in detail both the axion and the inflationary paradigms. Assuming the totality of the dark matter is given by the axion, the last relation highlights that any scale f, that is smaller than Planck, is excluded with an observation of r within the previous range. Relaxing the

assumption that the axion provides the totality of the DM, we can simultaneously reach $r \sim 10^{-4}$ and satisfy the bound from isocurvature but at the precise of tuning $\theta_{\rm in} \sim 10^{-7}$, where $\Omega_a h^2 < 10^{-6}$. There is no possible tuning with $f < M_{\rm Pl}$ that can bring us to a value of $r \sim 10^{-3}$. Hence, observation of large tensor modes forces the axion to live in the unbroken scenario where $f \lesssim 10^{11}$GeV.

If some of the assumptions are relaxed the previous conclusions are not expected to hold. In the previous treatment, we implicitly assumed that the radial part of the PQ field was stuck in the minimum f. As we will see in Appendix C by promoting the radial field to be the inflaton we can simultaneously obtain an $r \sim 10^{-3}$, providing all the DM and satisfying the isocurvature bound. Note how, in this case, the symmetry always breaks, and the axion always acquires isocurvature perturbations. The parameter that affects the evolution of PQ symmetry is only the reheating temperature.

We conclude this section by reporting the observational bounds on axion which are mainly driven by astrophysics. For f close to $f \sim M_{\rm Pl}$ meaning $m_{\rm QCD}$ of order $m_{\rm QCD} \sim 10^{-11}$eV the strongest bound is given by the modification of the gravitational wave emission of rapidly rotating astrophysical black holes through the Penrose superradiance process. The non-observation of this effect for the rapidly rotating black hole in the X-ray binary LMC X-1 puts an upper bound for the QCD axion on f, which is $f \leq 2 \times 10^{17}$GeV [13]. On the other side, for small f meaning large $m_{\rm QCD}$ the axion starts to be coupled more strongly to the SM particles and can affect the cooling behavior of stars or supernovae. The non-observation of anomalous cooling puts a lower bound on f, which is $f \geq 10^{9}$GeV. The axion can reproduce the observed DM abundance for a wide range of f, $10^{9}\text{GeV} \leq \text{f} \leq 10^{17}$GeV.

6.6 Axion quality problem

As we have seen the main motivation for the axion is that it provides a natural solution to the strong CP problem, see Section 6.1. The Wafa-Witten theorem [171] guarantees the axion to relax to the minimum of its potential in which CP is preserved, $\bar{\theta} = 0$. This theorem does not ensure the perseverance of the solution in the case in which there are UV violations of the $U(1)_{\rm PQ}$ symmetry in addition to those given by the non-perturbative effects. The latter effects appear at scales of the order of $T \sim$ Gev which is much smaller than the usual values of f. This makes the solution to the strong CP problem an IR effect. In the (KSVZ) and (DFSZ) models [98, 157, 57, 182] the dynamics in the UV is reflected in the IR only through the coupling that the axion has with the SM, but the dynamics of the axion is unchanged. Is the naturalness of the solution preserved even if in the UV we have operators that break the $U(1)_{\rm PQ}$ symmetry? How sensitive is the solution to the strong CP problem which is an IR effect to the presence of these operators?

In [93, 87, 91] we find answers to these questions. The purpose of this section is to review these works since Chapter 7, the original part of the thesis,

shares many similarities with these papers. These $U(1)_{\rm PQ}$-breaking operators are induced at the Planck scale due to quantum gravity, which is supposed to violate all global symmetries. Wormholes and black holes [82, 70, 51, 68] show that Planck-scale physics can lead to violation of global symmetries. At energy scales smaller than the Planck one these effects are described by higher-dimensional symmetry-breaking operators suppressed by an appropriate power of the Planck mass. These operators will favor values of the minimum of the potential of the axion which leads to an invalidation of the solution of the strong CP problem, ($\bar{\theta} \neq 0$). This is often referred to as the axion quality problem. Let us derive the necessary suppression of these higher-dimensional operators, induced by quantum gravity, to not spoil the solution of the strong CP provided by the axion.

We add to the standard wine bottle potential $V_{\rm PQ} \sim \lambda_{\rm PQ}\left(|\Phi|^2 - f^2\right)$ the following term

$$g\frac{|\Phi|^{2m}\Phi^n}{M_{\rm Pl}^{2m+n-4}} + \text{h.c.}, \tag{6.33}$$

with $g = |g|e^{i\delta}$ being a dimensionless and complex constant. We used $M_{\rm Pl}$ as the suppression scale of the operator, by considering that some new physics must intervene at or below $M_{\rm PL}$. One may thus expect $|g| \gtrsim 1$, however, we will later show that the solution of the strong CP problem generically requires a much smaller $|g|$. After the radial field has stabilized to the minimum of the Mexican hat potential $|\Phi| = f$, the higher-dimensional operator induced a mass for the axion

$$m_\theta^2 = n^2|g|M_{\rm Pl}^2\left(f/\sqrt{2}M_{\rm Pl}\right)^{l-2}, \tag{6.34}$$

where $l = 2m + n$.

As seen in Section 6.1, the axion obtains a potential at temperatures below the QCD scale of the form,

$$V(\theta) = \frac{m_{\rm QCD}^2 f^2}{N_{\rm DW}^2}\left[1 - \cos(N_{\rm DW}\theta)\right] - \frac{m_\theta^2 f^2}{n^2}\cos\left(n\theta + \delta\right), \tag{6.35}$$

where we inserted $N_{\rm DW}$ to keep the treatment general and we used $a = f\theta$. Here we have taken the CP-conserving vacuum as $\theta = 0$ modulo $2\pi/N_{\rm DW}$ without loss of generality, and $m_{\rm QCD}$ is the mass arising from QCD non-perturbative effects given by [53, 34],

$$m_{\rm QCD} \simeq 5.7\mu{\rm eV}\left(\frac{10^{12}{\rm GeV}}{{\rm f/N_{DW}}}\right). \tag{6.36}$$

The second term in (6.35) is induced by the higher-dimensional operator after QCD confinement and m_θ is given by (6.34).

The axion at the minimum of the potential (6.35) needs to satisfy $|N_{\rm DW}\theta_{\rm min}| \lesssim$

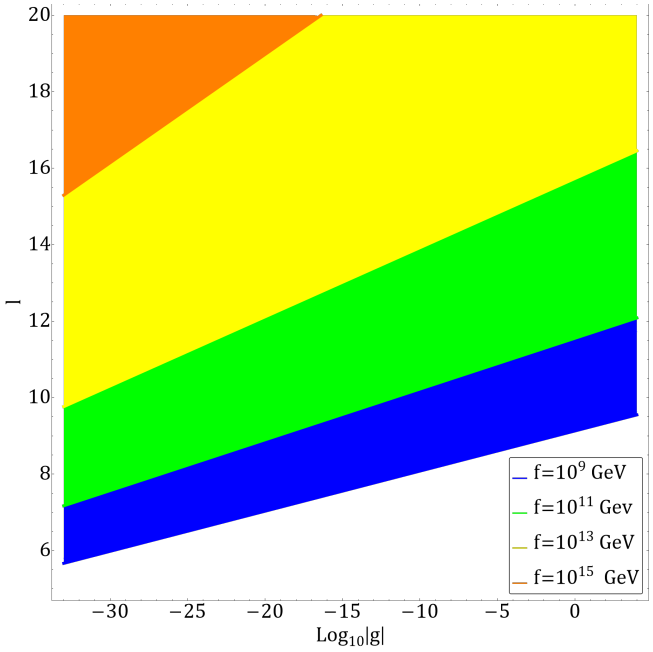

FIGURE 6.1: Axion quality constraint on the coupling constant $|g|$ and dimension l of higher-dimensional operators for the PQ field to solve the strong CP problem. The colored lines show the axion quality constraint on $\mathrm{U}(1)_{\mathrm{PQ}}$-breaking operators, for $f = 10^9\,\mathrm{GeV}$ (blue), $f = 10^{11}\,\mathrm{GeV}$ (green), $f = 10^{13}\,\mathrm{GeV}$ (yellow), $f = 10^{15}\,\mathrm{GeV}$ (orange). The colored regions show where the constraint is satisfied; for $f = 10^9$GeV this happens in the blue and the rest of the colored regions, for $f = 10^{11}$GeV the regions move to green, yellow, and orange, for $f = 10^{13}$geV they further move to yellow and orange, and for $f = 10^{15}$GeV only the orange region is allowed.

10^{-10} (modulo 2π) as implied by experimental bounds on the neutron electric dipole moment [15, 5]. This requirement imposes

$$\frac{N_{\mathrm{DW}}}{n}\frac{m_\theta^2}{m_{\mathrm{QCD}}^2}\left|\sin\left(n\theta_{\mathrm{min}}+\delta\right)\right| \lesssim 10^{-10}. \tag{6.37}$$

Supposing $|\sin(n\theta_{\mathrm{min}}+\delta)| \sim 1$, then this translates into a bound on $|g|$ as

$$|g| \lesssim 10^{-88}\,\frac{N_{\mathrm{DW}}}{n}\left(\frac{\sqrt{2}M_{\mathrm{Pl}}}{f}\right)^l. \tag{6.38}$$

In Fig. 6.1 the axion quality constraint (6.38) is shown in the $|g|$ - l plane as the colored lines, for the parameter choice of $N_{\mathrm{DW}} = n$ with for $f = 10^9\,\mathrm{GeV}$ (blue), $f = 10^{11}\,\mathrm{GeV}$ (green), $f = 10^{13}\,\mathrm{GeV}$ (yellow), $f = 10^{15}\,\mathrm{GeV}$ (orange). The allowed regions, where we solve the strong CP problem, are given: for $f = 10^9$GeV this happens in the blue and the rest of the colored regions, for $f = 10^{11}$GeV the regions move to green, yellow, and orange, for $f = 10^{13}$geV they further move to yellow and orange, and for $f = 10^{15}$GeV only

the orange region is allowed.

As we have seen at the end of Section 6.5 the minimum allowed value for f is $f \sim 10^9$GeV. With this scale, from Fig. 6.1 a possible higher-dimensional operator, that is already Planck suppressed, needs to be further suppressed by a coupling $|g|$ of order $|g| \sim 10^{-30}$. Hence, we substitute the mystery of the smallness of $\bar{\theta}$ with an even more big conundrum, the smallness of $|g|$. From Fig. 6.1 we appreciate how the strong CP problem, which is an IR process, is influenced by the unknown UV physics (parameterized by the higher-dimensional operators). Relation (6.38) shows how the naturalness of the strong CP problem solution given by the axion is challenged. In fact, from IR physics we can put very strong bounds on operators living at the UV scales. In Chapter 7 we will see that our analysis of the inflationary dynamics shares close analogies with the above discussion. We are going to see how these operators, given by relation (6.33), affect the inflaton dynamics and make the inflationary predictions sensitive to the unknown UV physics. In this sense, the two works share many similarities even if they probe, as we will see, two different energy scales, and the solution of the strong CP problem is substituted by the flatness of the potential; which is being accused by these operators (6.33).

6.7 Natural Inflation

Our main goal in this section is to examine the possibility of driving inflation with the axion field. The axion is the Goldstone boson of the $U(1)_{\rm PQ}$ symmetry and the shift symmetry $a \to a +$ const implies that the axion potential vanishes. For driving inflation the axion must have a sufficiently flat potential. The shift symmetry of the axion is broken at the non-perturbative level generating the potential (6.4). The non-perturbative nature of the rupture portends that the potential can remain sufficiently flat to sustain inflation.

In this section, we focus on the original version of natural inflation (NI)[66] where there is a single rolling field with potential

$$V_{\rm NI} = \Lambda^4 \left(1 + \cos a/f\right), \tag{6.39}$$

where Λ is a constant with the dimension of an energy scale. The slow-roll parameters, relations (3.28) and (3.29), with the choice of the previous potential read

$$\epsilon_{\rm V} = \frac{M_{\rm Pl}^2 \sin^2 a/f}{2f^2\left(1+\cos a/f\right)^2}, \quad \eta_{\rm V} = -\frac{M_{\rm Pl}^2 \cos a/f}{f^2\left(1+\cos a/f\right)} \ , \tag{6.40}$$

When these two parameters satisfy $\epsilon_{\rm V}, |\eta_{\rm V}| \ll 1$, the dynamic of the axion is governed by the slow-roll equations of motion

$$3H\dot{a} \simeq -\frac{\partial V_{\rm NI}}{\partial a}, \quad 3M_{\rm Pl}^2 H^2 \simeq V_{\rm NI}, \tag{6.41}$$

where a dot represents a cosmic time (t) derivative. The end of inflation is roughly sets by the condition $\epsilon_V(a_{\rm end}) = 1$, which for $a_{\rm end}$ gives

$$a_{\rm end} = 2f \arctan\left(\frac{\sqrt{2}f}{M_{\rm Pl}}\right). \tag{6.42}$$

Relation (3.31) evaluated between a generic scale a_*, corresponding to time when the mode k_* exits the Hubble horizon, and the end of inflation $a_{\rm end}$ gives us the following number of e-folds

$$N_* = -\int_{a_*}^{a_{\rm end}} \frac{V_{\rm NI}}{V'_{\rm NI}} \frac{da}{M_{\rm Pl}^2} = \int_{a_*}^{a_{\rm end}} \frac{f}{M_{\rm Pl}^2} \frac{(1+\cos a/f)}{\sin a/f} da, \tag{6.43}$$

where in going from left to right we used (6.39) and $V'_{\rm NI} = -\Lambda^4/f \sin a/f$. The previous integral can be computed, yielding

$$N_* = \frac{2f^2}{M_{\rm Pl}^2} \ln\left(\frac{\sin a_{\rm end}/2f}{\sin a_*/2f}\right), \tag{6.44}$$

notice that $a_{\rm end} \geq a_*$ since we restrict our analysis to $0 \leq a/f \leq \pi$. Relation (6.44) can be solved for the initial position a_*

$$\sin a_*/2f = \sin\left(\arctan\frac{\sqrt{2}f}{M_{\rm Pl}}\right) \exp\left(-\frac{N_* M_{\rm Pl}^2}{2f^2}\right), \tag{6.45}$$

where we used (6.42).

The scalar power spectrum amplitude, scalar spectral index, and the tensor-to-scalar ratio at the wave number of interest k_* are written, from (4.146), (4.147) and (4.168), as

$$A_S \simeq \frac{V_{\rm NI,*}}{24\pi^2 M_{\rm Pl}^4 \epsilon_{V,*}}, \quad n_s - 1 \simeq 2\eta_{V,*} - 6\epsilon_{V,*}, \quad r \simeq 16\epsilon_{V,*}. \tag{6.46}$$

The subscript $*$ denotes that the quantities are evaluated when the mode k_* exits the Hubble horizon. Using (6.39), (6.40) and (6.45) in (6.46) we get

$$A_S = \frac{f^2\Lambda^4\left[1-\sin^2\left(\arctan\frac{\sqrt{2}f}{M_{Pl}}\right)\exp\left(-\frac{N_*M_{Pl}^2}{f^2}\right)\right]^2}{6\pi^2 M_{Pl}^6\sin^2\left(\arctan\frac{\sqrt{2}f}{M_{Pl}}\right)\exp\left(-\frac{N_*M_{Pl}^2}{f^2}\right)} \tag{6.47}$$

$$n_s - 1 = \frac{M_{Pl}^2}{f^2} - \frac{2M_{Pl}^2}{f^2}\frac{1}{\left[1-\sin^2\left(\arctan\frac{\sqrt{2}f}{M_{Pl}}\right)\exp\left(-\frac{N_*M_{Pl}^2}{f^2}\right)\right]} \tag{6.48}$$

$$r = \frac{8M_{Pl}^2}{f^2}\frac{\sin^2\left(\arctan\frac{\sqrt{2}f}{M_{Pl}}\right)\exp\left(-\frac{N_*M_{Pl}^2}{f^2}\right)}{\left[1-\sin^2\left(\arctan\frac{\sqrt{2}f}{M_{Pl}}\right)\exp\left(-\frac{N_*M_{Pl}^2}{f^2}\right)\right]} \tag{6.49}$$

If set $k_* = 0.05\text{Mpc}^{-1}$ from the last column of Table 4.1 we know that the best fit values for n_s and A_S are $n_s = 0.965$ and $A_S = 2.1\times10^{-9}$. Furthermore, if we set $N_* = 60$ we can fix f from (6.48) and we obtain

$$f_{60} = 8.5M_{Pl}, \tag{6.50}$$

where the sub-script 60 represents the value of f which generates $N_* = 60$ and $n_s = 0.965$ at the pivot scale k_*. From (6.47) we fix Λ as follows

$$\Lambda = M_{Pl}\left(\frac{6\pi^2M_{Pl}^2A_S}{f_{60}^2}\right)^{1/4}\frac{\sqrt{\sin\left(\arctan\frac{\sqrt{2}f_{60}}{M_{Pl}}\right)\exp\left(-\frac{N_*M_{Pl}^2}{4f_{60}^2}\right)}}{\sqrt{1-\sin^2\left(\arctan\frac{\sqrt{2}f}{M_{Pl}}\right)\exp\left(-\frac{N_*M_{Pl}^2}{f^2}\right)}} \sim 10^{16}\text{GeV}, \tag{6.51}$$

where in going from left to right we used the values of f_{60}, A_S and $N_* = 60$. This analysis reveals that natural inflation can reproduce the CMB observables but at the price of working with super-Planckian values for f and Λ is forced to be at the GUT scale. Since Λ sets the amplitude of the potential we expect a large value for the tensor-to-scalar ratio. Indeed, from (6.49) we get

$$r_{60} = \frac{8M_{Pl}^2}{f_{60}^2}\frac{\sin^2\left(\arctan\frac{\sqrt{2}f_{60}}{M_{Pl}}\right)\exp\left(-\frac{N_*M_{Pl}^2}{f_{60}^2}\right)}{\left[1-\sin^2\left(\arctan\frac{\sqrt{2}f_{60}}{M_{Pl}}\right)\exp\left(-\frac{N_*M_{Pl}^2}{f_{60}^2}\right)\right]} \sim 0.08, \tag{6.52}$$

in going from left to right we used the value of f_{60} and $N_* = 60$. This value exceeds the upper bound from Planck and makes the model strongly disfavoured against observational data. The model remains ruled out even if we change N_* or n_s although the values of f, Λ, and r may change.

Chapter 7

UV sensitivity of PQ inflation

The original motivation of the Peccei–Quinn (PQ) mechanism [138], based on a global $\mathrm{U}(1)_{\mathrm{PQ}}$ symmetry, is to provide a possible solution to the strong CP problem by promoting the QCD θ angle to a dynamical axion field [174, 177]. The axion can be interpreted as the phase of a complex scalar—the PQ field. When the PQ field settles down to the minimum of a Mexican hat potential, the $\mathrm{U}(1)_{\mathrm{PQ}}$ symmetry is spontaneously broken and the axion plays the role of a pseudo Nambu–Goldstone boson. Axions also provide a viable candidate for the dark matter of our Universe [143, 1, 56].

In itself, the PQ field has nothing to do with the physics of the primordial universe but was introduced to solve a problem related to the nature of the strong interaction. Taking inspiration from the case of Higgs inflation we can promote the radial field of the PQ field to be the inflation. This makes the PQ model capable of explaining inflation, dark matter, and the strong CP problem. The simplicity and cost-effectiveness of the model are some of the reasons that pushed us to analyze it in detail.

Another is linked, as we will see, to the fact that the model can be falsified. It predicts a value of $r \sim 10^{-3}$ which will be tested with future experiments. PQ inflation shares many similarities with Higgs inflation but theoretically has better virtues. As we saw in Section 4.11.1, Higgs inflation has a validity problem as an EFT linked to the value of ξ being too large. In PQ inflation this problem does not arise because the self-coupling of the PQ field is a free parameter and can be chosen to accommodate $\xi \sim 1$ values. On the other hand, values of $\xi \sim \mathcal{O}(1)$ pose a problem with the possible impact of higher-dimensional operators on the background dynamics. The nature of these operators depends on the details of the ultraviolet completion of the theory, bringing us back to a situation similar to Higgs inflation.

Considering the reasons cited above, it becomes important to try to understand whether the model's predictions are preserved or whether a UV sensitivity is present instead. In this chapter, we tackle this issue by evaluating the effects of higher-dimensional operators on PQ inflation. By calculating their impact on curvature perturbations and the duration of inflation, we derive constraints on Planck-suppressed operators. (See also [89] which performed a similar study for a Higgs-like real inflaton.)

We will see that the size of these operators is highly constrained by the flatness of the potential. The ultraviolet sensitivity of PQ inflation is reminiscent of the so-called axion quality problem [93, 87, 91], which is based on the observation that $\mathrm{U}(1)_{\mathrm{PQ}}$-breaking higher-dimensional operators can

spoil the axion as a solution to the strong CP problem by displacing the axion field from the CP-conserving vacuum. While this vacuum displacement is an effect sourced by higher-dimensional operators at low energies where the PQ field is localized at the potential minimum, the effects on PQ inflation are at the inflationary scale where the PQ field is largely displaced from its minimum. Hence the two effects induced by higher-dimensional operators have different natures, and we find that the resulting constraints are complementary to each other, excluding a wide range of operators when combined. This result exacerbates the impact of unknown physics at the Planck scale on experimentally testable IR physics.

It has been claimed in [61, 35] that after PQ inflation ends, axion dark matter is produced due to the misalignment of the nearly homogeneous axion field from the vacuum, and also that the isocurvature fluctuation of the axions is suppressed by the large PQ field displacement during inflation [116, 115]. On the other hand in the specific PQ(-like) inflation model of [17], the oscillation of the inflaton about its origin induces a resonant amplification of the field fluctuation, which leads to a restoration of the PQ symmetry. (See [167, 96, 95, 166, 79, 100, 48, 16] for related works). The subsequent symmetry breaking thus yields a highly inhomogeneous axion field as well as axionic strings, whose decay contributes to the axion production. Here, one may expect that $\mathrm{U}(1)_{\mathrm{PQ}}$-breaking higher-dimensional operators should suppress resonant effects since they can source an angular momentum to the PQ field and prevent the field from oscillating violently along its radial direction. However, we show that with higher-dimensional operators allowed for a consistent PQ inflation, a resonant amplification of the PQ field fluctuation is inevitably triggered. Our finding thus implies that axion production after PQ inflation does not proceed as in the vanilla vacuum misalignment scenario.

The plan of this chapter is as follows. In Section 7.1 we review the basic properties of the PQ inflation model. In Section 7.2 we derive constraints on higher-dimensional operators by numerically solving the PQ field dynamics during inflation. We then analytically derive an approximate expression for the constraints in Section 7.3. In our calculations we treat PQ inflation as an effectively single-field model; we justify this treatment in Section 7.4. In Section 7.5 we study the PQ field dynamics after inflation and show that a resonant amplification of field fluctuations is unavoidable. In Section 7.6 we compare the constraint on higher-dimensional operators from PQ inflation with that from axion quality arguments.

7.1 Peccei–Quinn inflation

We consider a PQ field Φ that is coupled to the Ricci scalar,

$$S = \int d^4x\sqrt{-g}\left[-\left(\frac{M^2}{2}+\xi\Phi\Phi^*\right)R + g^{\mu\nu}\partial_\mu\Phi\partial_\nu\Phi^* - V(\Phi)\right], \tag{7.1}$$

with V being a Mexican hat potential,

$$V(\Phi) = \frac{\lambda}{6}\left(|\Phi|^2 - \frac{f^2}{2}\right)^2, \tag{7.2}$$

and f is the axion decay constant. The self-coupling constant λ and gravitational coupling ξ are assumed to be non-negative. At the symmetry-breaking vacuum, i.e. $|\Phi| = f/\sqrt{2}$, the mass scale M is related to the reduced Planck mass, $M_{\rm Pl} \approx 2.4 \times 10^{18}\,{\rm GeV}$, by

$$M_{\rm Pl}^2 = M^2 + \xi f^2. \tag{7.3}$$

We assume

$$\xi f^2 \ll M_{\rm Pl}^2, \tag{7.4}$$

so that $M_{\rm Pl} \simeq M$. Rewriting Φ in terms of its radial and phase (axion) directions as

$$\Phi = \frac{\varphi}{\sqrt{2}} e^{i\theta}, \tag{7.5}$$

where $\varphi \geq 0$, then the above action becomes

$$S = \int d^4x\sqrt{-g}\left[-\frac{M^2 + \xi\varphi^2}{2}R + \frac{1}{2}g^{\mu\nu}\partial_\mu\varphi\partial_\nu\varphi + \frac{1}{2}\varphi^2 g^{\mu\nu}\partial_\mu\theta\partial_\nu\theta - V\right], \tag{7.6}$$

with

$$V = \frac{\lambda}{4!}\left(\varphi^2 - f^2\right)^2. \tag{7.7}$$

Performing a conformal transformation $\tilde{g}_{\mu\nu} = \Omega^2 g_{\mu\nu}$ with conformal factor

$$\Omega^2 = 1 + \xi\frac{\varphi^2}{M_{\rm Pl}^2}, \tag{7.8}$$

one goes to the Einstein frame where the action takes the form

$$S = \int d^4x\sqrt{-\tilde{g}}\left[-\frac{M_{\rm Pl}^2}{2}\tilde{R} + \frac{1}{2}\tilde{g}_{\mu\nu}\partial_\mu\chi\partial_\nu\chi + \frac{1}{2}\frac{\varphi^2}{\Omega^2}\tilde{g}_{\mu\nu}\partial_\mu\theta\partial_\nu\theta - U\right]. \tag{7.9}$$

Here $U = V/\Omega^4$, and χ is an almost canonically normalized field defined as

$$d\chi = I\,d\varphi, \quad I = \frac{\sqrt{1 + \xi(1+6\xi)\frac{\varphi^2}{M_{\rm Pl}^2}}}{1 + \xi\frac{\varphi^2}{M_{\rm Pl}^2}}. \tag{7.10}$$

Hereafter we carry out the analyses in the Einstein frame, and consider a flat Friedmann–Robertson–Walker background, $\tilde{g}_{\mu\nu}dx^\nu dx^\mu = dt^2 - a(t)^2dx^2$. The $\mathrm{U}(1)_{\rm PQ}$ symmetry allows the axion to stay fixed to its initial position. As a result, inflation takes place along the radial direction, which makes the model similar to Higgs inflation (refer to Section 4.11). The key differences

between the two are that λ is a free parameter in PQ and there is no assumption that ξ is very large. The results of PQ inflation are more general, and by taking the limit $\xi \gg 1$, we obtain Higgs inflation. Thanks to the $\mathrm{U}(1)_{\mathrm{PQ}}$ symmetry we treat the model as effectively single-field and introduce the slow-roll parameters, relations (3.28) and (3.29), in terms of the canonical radial field as

$$\epsilon = \frac{M_{\mathrm{Pl}}^2}{2}\left(\frac{1}{U}\frac{\partial U}{\partial \chi}\right)^2, \quad \eta = \frac{M_{\mathrm{Pl}}^2}{U}\frac{\partial^2 U}{\partial \chi^2}. \tag{7.11}$$

When these are both smaller than unity, the radial field drives slow-roll inflation with its dynamics described by

$$3H\dot{\chi} \simeq -\frac{\partial U}{\partial \chi}, \quad 3M_{\mathrm{Pl}}^2 H^2 \simeq U. \tag{7.12}$$

Here an overdot denotes a derivative in terms of the physical time t, and $H = \dot{a}/a$ is the Hubble rate. The scalar power spectrum amplitude, scalar spectral index, and the tensor-to-scalar ratio at some wave number of interest k_* are written, from (4.146), (4.147) and (4.168), as

$$A_s \simeq \frac{U_*}{24\pi^2 M_{\mathrm{Pl}}^4 \epsilon_*}, \quad n_s - 1 \simeq 2\eta_* - 6\epsilon_*, \quad r \simeq 16\epsilon_*. \tag{7.13}$$

The subscript $*$ denotes that the quantities are evaluated when the mode k_* exits the Hubble horizon.

Ignoring the decay constant f in the potential (7.7) and using $V = \lambda\varphi^4/4!$, the slow-roll parameters are obtained as

$$\epsilon = \frac{8\frac{M_{\mathrm{Pl}}^2}{\varphi^2}}{1+\xi(1+6\xi)\frac{\varphi^2}{M_{\mathrm{Pl}}^2}}, \quad \eta = \frac{12\frac{M_{\mathrm{Pl}}^2}{\varphi^2} + 4\xi(1+12\xi) - 8\xi^2(1+6\xi)\frac{\varphi^2}{M_{\mathrm{Pl}}^2}}{\left\{1+\xi(1+6\xi)\frac{\varphi^2}{M_{\mathrm{Pl}}^2}\right\}^2}. \tag{7.14}$$

The amplitudes of the two parameters become unity for similar field values. We thus roughly estimate the field value when inflation ends by solving $\epsilon = 1$, giving,

$$\left(\frac{\varphi_{\mathrm{end}}}{M_{\mathrm{Pl}}}\right)^2 \sim \frac{16}{1+\sqrt{(1+8\xi)(1+24\xi)}} \simeq \begin{cases} 8 & \text{for } \xi \ll 10^{-1}, \\ \dfrac{2}{\sqrt{3\xi}} & \text{for } \xi \gg 10^{-1}. \end{cases} \tag{7.15}$$

Hence as long as the decay constant satisfies both $f^2 \ll M_{\mathrm{Pl}}^2$ and (7.4), it follows that $f^2 \ll \varphi_{\mathrm{end}}^2$. This justifies our neglecting of f during inflation.

In particular, if the radial field value is large enough such that

$$\xi\frac{\varphi^2}{M_{\mathrm{Pl}}^2} \gg 1, \tag{7.16}$$

then the slow-roll parameters become

$$\epsilon \simeq \frac{8M_{\rm Pl}^4}{\xi(1+6\xi)\varphi^4}, \quad \eta \simeq -\frac{8M_{\rm Pl}^2}{(1+6\xi)\varphi^2}. \tag{7.17}$$

As expected if $\xi \gg 1$ we get back relations (4.177) and (4.178). These satisfy a hierarchical relation of $\epsilon \ll |\eta| \ll 1$, and using (7.13) we obtain

$$A_s \simeq \frac{\lambda(1+6\xi)\varphi_*^4}{4608\pi^2\xi M_{\rm Pl}^4}, \quad n_s - 1 \simeq -\frac{16M_{\rm Pl}^2}{(1+6\xi)\varphi_*^2}, \quad r \simeq \frac{128M_{\rm Pl}^4}{\xi(1+6\xi)\varphi_*^4}. \tag{7.18}$$

The slow-roll approximations (7.12) in the large-field regime (7.16) take the forms,

$$3H\dot{\varphi} \simeq -\frac{\lambda}{6\xi^2(1+6\xi)}\frac{M_{\rm Pl}^4}{\varphi}, \tag{7.19}$$

$$H^2 \simeq \frac{\lambda M_{\rm Pl}^2}{72\xi^2}. \tag{7.20}$$

Relation (3.30) can be used to obtain the number of e-folds between the exit of the k_* mode and the end of inflation as

$$N_* = \int_{t_*}^{t_{\rm end}} dt\, H \simeq \frac{1+6\xi}{8M_{\rm Pl}^2}\left(\varphi_*^2 - \varphi_{\rm end}^2\right), \tag{7.21}$$

where we assumed the field condition (7.16) to (at least marginally) hold until the end of inflation. Supposing $\varphi_*^2 \gg \varphi_{\rm end}^2$, then (7.18) is rewritten in terms of N_* as,

$$A_s \simeq \frac{\lambda N_*^2}{72\pi^2\xi(1+6\xi)}, \quad n_s - 1 \simeq -\frac{2}{N_*}, \quad r \simeq \frac{2(1+6\xi)}{\xi N_*^2}. \tag{7.22}$$

We have also numerically computed the inflationary predictions and model parameters of PQ inflation, which are shown in Fig. 7.1 as functions of ξ. Here λ and φ_* are fixed using the expressions (7.13), such that the scalar power spectrum amplitude takes the best-fit value $A_s = 2.1 \times 10^{-9}$, and the spectral index lies within the 68% confidence region $n_s = 0.9649 \pm 0.0042$ from the Planck constraints at the pivot scale $k_* = 0.05\,{\rm Mpc}^{-1}$ [9]. The initial field velocity $\dot{\varphi}_*$ is fixed from the slow-roll expression (7.19). The equation of motion of φ and the Friedmann equation are then numerically solved until the end of inflation, namely when $-\dot{H}/H^2 = 1$. The axion field θ is fixed to a constant in this computation. We show in the plots the values[1] of the self-coupling λ, the radial field values at horizon exit φ_* and at the end of inflation $\varphi_{\rm end}$, e-folding number N_* from when the pivot scale exits the horizon until the end of inflation, and tensor-to-scalar ratio r at the pivot scale.

[1] The values of λ and ξ should be considered as those at the inflation scale. Throughout this paper, we ignore the renormalization group running of the couplings during inflation, by considering the logarithmic corrections to be small.

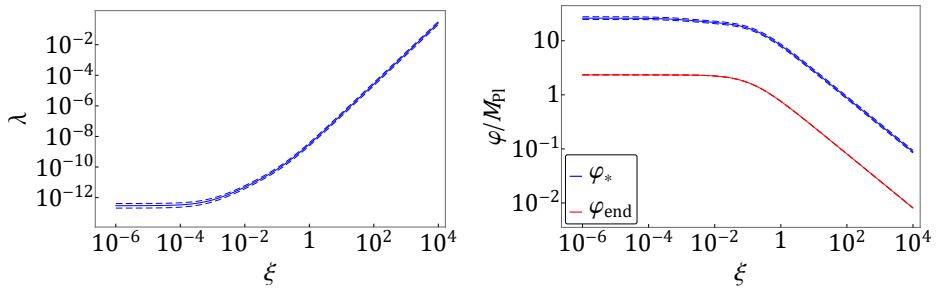

(a) Self-coupling (b) Field values

(c) Number of e-folds (d) Tensor-to-scalar ratio

FIGURE 7.1: Inflationary predictions and model parameters of PQ inflation, as functions of the non-minimal gravitational coupling. Between the dashed lines, the scalar spectral index takes values within the Planck 68% C.L. region $n_s = 0.9649 \pm 0.0042$, with the solid line corresponding to the central value. In Fig. 7.1(d) the orange line shows the BICEP/Keck upper limit for r.

The blue solid and dashed lines indicate values derived from, respectively, the best-fit and 1σ uncertainty for n_s. (These are barely distinguishable in the log plots for φ_* and λ.) The red line in Fig. 7.1(b) shows the field at the end of inflation $\varphi_{\rm end}$, which also barely depends on the detailed value of n_s. In Fig. 7.1(d) we also show the observational upper limit $r < 0.036$ (95% C.L., BICEP/Keck [7]) by the orange line.

For $\xi \lesssim 10^{-4}$, the model reduces to a simple φ^4 inflation which is strongly disfavoured by the Planck data [9]. The exclusion is explicitly seen in the plots as r exceeding its upper limit, as well as N_* far exceeding 60. At $\xi \gtrsim 1$, the values of N_* and r approach those of Higgs inflation which invokes $\lambda \sim 10^{-1}$ and $\xi \sim 10^4$, see Section 4.11. The results of Higgs inflation, relations (4.182) and (4.184), are reproduced in (7.21) and (7.22) by taking the large ξ limit. In Figure 7.1, the region of Higgs inflation is reproduced in the far right portions of the graphs. Here the central value of the number of e-folds becomes $N_* \approx 56.5$. Moreover, the tensor-to-scalar ratio approaches $r \approx 0.004$, which can be tested in upcoming experiments such as [10]. The upper limit on r requires $\xi \gtrsim 10^{-2}$.

With the scale of inflation for this model, and assuming that inflation is followed by a phase of inflaton oscillation, and then by radiation domination, the number of inflationary e-folds from the horizon exit of the pivot scale

$k_* = 0.05\,\mathrm{Mpc}^{-1}$ should satisfy $N_* \lesssim 56$; here the upper limit corresponds to the case of instantaneous reheating. One sees in Fig. 7.1(c) that if n_s takes a value that is $+1\sigma$ away from the best fit, the upper limit on N_* is violated for any value of ξ.

One can hope to avoid a breakdown of the effective field theory by choosing a set of sufficiently small couplings λ and ξ, as shown in Fig. 7.1(a). However Fig. 7.1(b) indicates that for $\xi \lesssim 10^2$, the field value φ_* exceeds $M_{\rm Pl}$. It should also be noted that, independently of ξ, the excursion of the canonical field (7.10) obeys[2] $\Delta\chi > M_{\rm Pl}$. The large field excursions would make the inflationary predictions sensitive to operators suppressed by $M_{\rm Pl}$. We look into this in detail in the next section.

7.2 Impact of higher-dimensional operators

We now study how the naive picture of PQ inflation described above is affected by higher-dimensional operators, and show that such operators need to be strongly suppressed during inflation. As we are going to see this part has close analogies with Section 6.6.

7.2.1 Higher-dimensional operators

We include an operator of dimension $2m + n$ in the Jordan frame such that the potential (7.2) is modified to

$$V(\Phi) = \frac{\lambda}{6}\left(|\Phi|^2 - \frac{f^2}{2}\right)^2 + \Lambda - \left(g\frac{|\Phi|^{2m}\Phi^n}{M_{\rm Pl}^{2m+n-4}} + \text{h.c.}\right), \tag{7.23}$$

with g being a dimensionless and complex constant. We used $M_{\rm Pl}$ as the suppression scale of the operator, by considering that some new physics must intervene at or below $M_{\rm Pl}$. One may thus expect $|g| \gtrsim 1$, however we will later show that PQ inflation generically requires a much smaller $|g|$. Operators that are suppressed instead by the effective Planck scale $(M_{\rm Pl}^2 + \xi\varphi^2)^{1/2}$ are studied in Appendix A. See also [20, 39, 84, 28, 40] for discussions on the suppression scales of higher-dimensional operators in the context of Higgs inflation.

The parameter Λ has mass dimension four and its value is chosen such that the vacuum energy at the potential minima vanishes. At leading order in g, its amplitude is of

$$|\Lambda| \sim 2|g|M_{\rm Pl}^4\left(\frac{f}{\sqrt{2}M_{\rm Pl}}\right)^{2m+n}. \tag{7.24}$$

[2] This can also be understood from the Lyth bound [124] for a canonical inflaton, $|d\chi/dN| \simeq \sqrt{r/8}\,M_{\rm Pl}$, combined with the values of r shown in Fig. 7.1(d).

We also write the dimension of the operator as

$$l = 2m + n, \tag{7.25}$$

and the coupling as $g = |g|e^{i\delta}$ with a real phase δ. Rewriting the complex scalar as (7.5), the above potential becomes

$$V = \frac{\lambda}{4!}\left(\varphi^2 - f^2\right)^2 + \Lambda - 2|g|M_{\rm Pl}^4\left(\frac{\varphi}{\sqrt{2}M_{\rm Pl}}\right)^l \cos(n\theta + \delta). \tag{7.26}$$

If $n = 0$ the axion remains massless. On the other hand if $n \neq 0$, the $\mathrm{U}(1)_{\rm PQ}$ symmetry is broken and the axion acquires a mass; the presence of such operators is also suggested by the breaking of global symmetries due to quantum gravity [3, 18, 80]. In the following we will consider both PQ-breaking and preserving operators.

The homogeneous equations of motion and the Friedmann equation in the presence of the higher-dimensional operator are

$$0 = \ddot{\chi} + 3H\dot{\chi} + \frac{1}{\Omega^4\sqrt{\Omega^2 + 6\xi^2\frac{\varphi^2}{M_{\rm Pl}^2}}}\left[\left(1 + \xi\frac{f^2}{M_{\rm Pl}^2}\right)\frac{\lambda}{6}(\varphi^2 - f^2)\varphi - \frac{4\xi\varphi\Lambda}{M_{\rm Pl}^2} - \Omega^2\varphi\dot{\theta}^2 - \left\{l\Omega^2 - 4\xi\frac{\varphi^2}{M_{\rm Pl}^2}\right\}\frac{\Omega^2\varphi m_\theta^2}{n^2}\cos(n\theta + \delta)\right], \tag{7.27}$$

$$0 = \ddot{\theta} + 3H\dot{\theta} + \frac{2\dot{\theta}\dot{\varphi}}{\Omega^2\varphi} + \frac{m_\theta^2}{n}\sin(n\theta + \delta), \tag{7.28}$$

$$3M_{\rm Pl}^2H^2 = \frac{\dot{\chi}^2}{2} + \frac{\varphi^2\dot{\theta}^2}{2\Omega^2} + \frac{1}{\Omega^4}\left\{\frac{\lambda}{4!}(\varphi^2 - f^2)^2 + \Lambda - \frac{\Omega^2\varphi^2 m_\theta^2}{n^2}\cos(n\theta + \delta)\right\}. \tag{7.29}$$

Here m_θ represents the mass of the angular direction around its potential minima, which is defined as

$$m_\theta^2 = \frac{1}{\varphi^2\Omega^2}\frac{\partial^2 V}{\partial\theta^2}\bigg|_{n\theta+\delta=0} = \frac{n^2|g|M_{\rm Pl}^2}{\Omega^2}\left(\frac{\varphi}{\sqrt{2}M_{\rm Pl}}\right)^{l-2}. \tag{7.30}$$

The mass induced by higher-dimensional operators depends on the inflaton field value. In particular when the inflaton reaches its potential minimum, the axion mass becomes $m_\theta^2 \simeq n^2|g|M_{\rm Pl}^2\left(f/\sqrt{2}M_{\rm Pl}\right)^{l-2}$.

7.2.2 Constraints from number of e-folds

Higher-dimensional operators change the tilt of the inflaton potential, which in turn affects the number of inflationary e-folds N. We compute N by numerically solving the set of equations (7.27), (7.28), and (7.29), from the time when the pivot scale k_* exits the horizon until the end of inflation at $-\dot{H}/H^2 =$

1. The scalar power spectrum amplitude and spectral index are fixed to the central values $A_s = 2.1 \times 10^{-9}$ and $n_s = 0.965$; we impose this condition by evaluating the observables using the slow-roll expressions (7.13) with V given by (7.26), and choosing the values of λ and φ_* accordingly.[3]

We also use the slow-roll approximations to fix the field velocities at the horizon exit of the pivot scale, namely, (7.12) for the radial field and

$$3H\dot{\theta} \simeq -\frac{m_\theta^2}{n}\sin(n\theta+\delta) \tag{7.31}$$

for the axion. The solution (7.31) assumes $m_\theta^2 \ll H^2$. In particular for $n = 0$, the right-hand side vanishes and thus the axion is fixed to a constant value during inflation. On the other hand if $m_\theta^2 \gtrsim H^2$, the axion does not follow (7.31), but quickly becomes stabilized at one of its potential minima. Hence instead of treating θ_* as a free parameter, we write it as

$$n\theta_* + \delta = (n\theta_i + \delta)\exp\left(-\frac{m_{\theta*}^2}{H_*^2}\right), \tag{7.32}$$

in terms of an 'initial' angle θ_i, which represents the axion field value a few e-foldings before the pivot scale exits the horizon. If $m_{\theta*}^2 \ll H_*^2$ then $\theta_* \simeq \theta_i$, while if $m_{\theta*}^2 \gg H_*^2$ then $n\theta_* + \delta$ is effectively zero independently of the value of θ_i. We also note that for $m_{\theta*}^2 \gg H_*^2$, the parametrization (7.32) combined with (7.31) yields $\dot{\theta}_* \simeq 0$, corresponding to an axion at rest in a minimum. Hence (7.31) and (7.32) allow us to systematically analyze the range of possibilities arising from higher-dimensional operators.

Since the inflationary dynamics is insensitive to the precise values of f and Λ, we are thus left with five free parameters: $|g|$, l, n, $n\theta_i + \delta$, and ξ. In Fig. 7.2 we show constraints on higher-dimensional operators in the $|g|$ - l plane. (We performed computations also for fractional l.) As a rough guide, we require the number of e-folds from when the pivot scale k_* exits the horizon until the end of inflation, to lie within the range[4] $50 \leq N_* \leq 60$. The regions on the right sides of the lines are excluded since there the number of e-folds N_* is either larger than 60 or smaller than 50, and/or A_s and n_s cannot simultaneously take the observed values. In each line the non-minimal coupling is taken as $\xi = 10^{-1}$ (blue), 1 (green), 10 (yellow), 10^2 (orange), 10^3 (red). Each of these are further classified by whether the $\mathrm{U}(1)_{\mathrm{PQ}}$ is broken or conserved, and whether $\cos(n\theta_i + \delta)$ is positive (if $n \neq 0$ this corresponds to starting close to a minimum of the axion potential) or negative (close to a hilltop); we took the combinations of $n = 1$ and $\theta_i + \delta = \pi - 0.5$ (solid), $n = 0$ and $\delta = \pi - 0.5$ (dotted), $n = 1$ and $\theta_i + \delta = 0.5$ (dashed), $n = 0$ and $\delta = 0.5$ (dashed). The last two cases are both shown by the same dashed

[3] We will show that higher-dimensional operators significantly affect N for fixed values of A_s and n_s. This is equivalent to saying that for a fixed N, the values of A_s and n_s are highly sensitive to the operators.

[4] Note that $N_* \leq 60$ yields a conservative constraint, as the actual upper limit is smaller; see discussions at the end of Section 7.1.

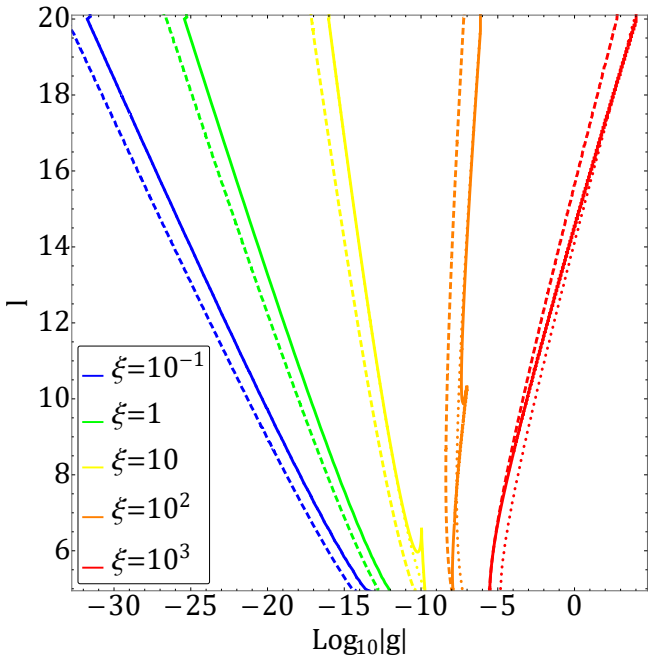

FIGURE 7.2: Constraints on the coupling constant $|g|$ and dimension l of higher-dimensional operators in PQ inflation, from the requirement that the scalar power spectrum amplitude and spectral index match with observations, and the Planck pivot scale exits the horizon 50 to 60 e-folds before inflation ends. The allowed regions are on the left of the curves. The colors denote different values for the non-minimal coupling ξ. The other parameters are taken as $n = 1$ and $\theta_i + \delta = \pi - 0.5$ (solid), $n = 0$ and $\delta = \pi - 0.5$ (dotted), $n = 1$ and $\theta_i + \delta = 0.5$ (dashed), $n = 0$ and $\delta = 0.5$ (dashed); the last two cases overlap and thus are shown by the same dashed lines. The dotted lines overlap with the solid in most part of the plot. The requirement of very small values for $|g|$ manifests the extreme sensitivity of PQ inflation to Planck-suppressed higher-dimensional operators.

lines since they overlap in the plot. Moreover, the dotted lines overlap with the solid in most part of the plot.

As one increases $|g|$, the number of e-folds basically increases (decreases) from the base value $N_* \approx 56.5$ for positive (negative) values of $\cos(n\theta_i + \delta)$, which can be understood from the potential (7.26) being flattened (steepened) by the higher-dimensional operator. In the plot, the dashed lines for cases with $n\theta_i + \delta = 0.5$ show where $N_* = 60$; on the left of these lines are the regions where $56.5 \leq N_* < 60$. The dotted lines for $n = 0$ and $\delta = \pi - 0.5$ show where $N_* = 50$, with the regions on the left giving $50 < N_* \leq 56.5$. On the other hand, the solid lines for $n = 1$ and $\theta_i + \delta = \pi - 0.5$ consist of multiple constraints; we look into this case in detail in the following subsection. (However the reader interested primarily in the general behavior of the constraints may go straight to Section 7.3 upon first reading.)

In our computations we only included one higher-dimensional operator

as shown in (7.23). In the presence of a tower of operators, a consistent PQ inflation can be achieved if all operators satisfy the constraints of Fig. 7.2; here it should be noted that even if operators with different dimensions cancel each other at some particular value of φ, as the field rolls the operators will become non-negligible. The constraints thus indicate that even operators with very high dimensions need to be strongly suppressed. We remark that there is the possibility that multiple higher-dimensional operators conspire to realize a completely different but flat potential at large field values. However we do not pursue such directions since in this paper we are interested in providing discussions that do not rely on the details of the ultraviolet completion.

7.2.3 Constraints around the hilltop

If the higher-dimensional operator breaks $\mathrm{U}(1)_{\mathrm{PQ}}$ and gives a sufficiently large axion mass, then even if the axion is initially placed near a potential hilltop (i.e. $\cos(n\theta_i + \delta) < 0$), it would roll down to the vicinity of a minimum by the time the pivot scale exits the horizon (i.e. $\cos(n\theta_* + \delta) > 0$). This is the reason why in Fig. 7.2 some of the solid lines ($n = 1$ and $\theta_i + \delta = \pi - 0.5$) connect the dotted lines ($n = 0$ and $\delta = \pi - 0.5$, thus $\cos\delta < 0$) to the dashed lines ($n\theta_i + \delta = 0.5$, thus $\cos(n\theta_* + \delta) > 0$).

On the solid lines with $\xi \lesssim 1$ (blue and green) the axion mass is sufficiently small such that the axion barely rolls,[5] hence the lines overlap with the dotted and show where $N_* = 50$. On the solid lines with $\xi \gtrsim 10$ (yellow, orange, and red), the axion can roll away from the hilltop region, and as a consequence the lines exhibit kinks. (The red line has a kink at $l \approx 22$, which is not seen in the displayed area.) For these lines, the segments above the kinks are set by $N_* = 50$, while the segments right below the kinks arise from not being able to produce the observed values for A_s and n_s, and further below the kinks are set by $N_* = 60$.

In Fig. 7.3 we zoom into the regions where the various constraints meet, for cases with $n = 1$. The combined constraints are shown with the same color scheme and line patterns as in Fig. 7.2: $\xi = 10$ (yellow), 10^2 (orange), with $\theta_i + \delta = 0.5$ (dashed), $\pi - 0.5$ (solid). Here we further show the contour lines for the values of N_* (black dashed) and $m_{\theta*}^2/H_*^2$ (brown dotted). On the right of the black solid lines are the regions where there is no combination of (λ, φ_*) that simultaneously yield $A_s = 2.1 \times 10^{-9}$ and $n_s = 0.965$. (The black solid lines are not smooth because of the limited numerical resolution.) In Figs. 7.3(a) and 7.3(c) where $\theta_i + \delta = 0.5$, as $|g|$ increases the e-folding number simply increases from its base value $N_* = 56.5$. On the other hand in Figs. 7.3(b) and 7.3(d) where $\theta_i + \delta = \pi - 0.5$, the e-folding number decreases when $m_{\theta*}^2/H_*^2 \lesssim 0.1$, while it instead increases when $m_{\theta*}^2/H_*^2 \gtrsim 0.1$ due to the axion rolling down to the vicinity of a minimum. Moreover, the contour lines of N_* hit the region where the higher-dimensional operator prevents A_s and n_s from simultaneously taking the observed values. One sees that the

[5] We later explicitly show in (7.46) that the maximum allowed value of m_θ^2/H^2 increases with ξ.

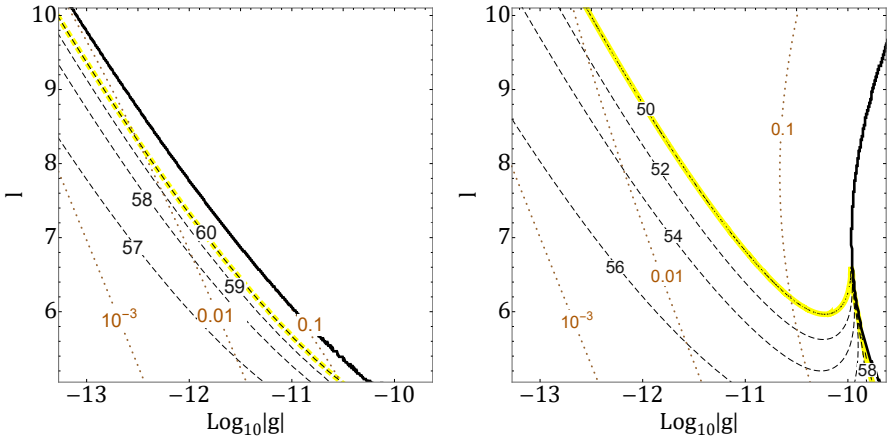

(a) $\xi = 10, \theta_i + \delta = 0.5$ (b) $\xi = 10, \theta_i + \delta = \pi - 0.5$

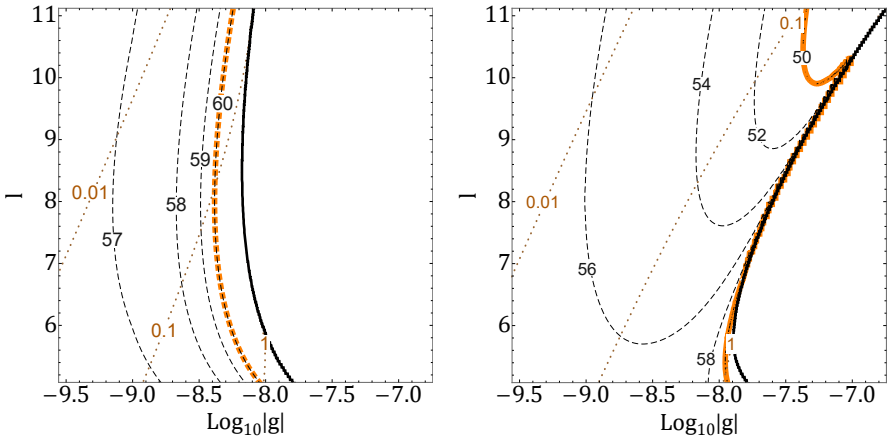

(c) $\xi = 10^2, \theta_i + \delta = 0.5$ (d) $\xi = 10^2, \theta_i + \delta = \pi - 0.5$

FIGURE 7.3: Detailed view of Fig. 7.2, zooming in on regions where different constraints meet. The black dashed contours show values of N_*, and the brown dotted show $m_{\theta*}^2/H_*^2$. All the results are for $n = 1$, while ξ and $\theta_i + \delta$ are varied in each panel. The combined constraints are shown with the same color scheme (yellow/orange) and line patterns (solid/dashed) as in Fig. 7.2. On the right of the black solid lines, A_s and n_s cannot simultaneously take the observed values.

kink in the combined constraint corresponds to where the $N_* = 50$ contour hits this no-go region. The constraint for $\xi = 10^3$ has a similar structure, except for that the kink appears beyond the parameter range displayed in Fig. 7.2.

In order to see the emergence of the no-go regions, in Fig. 7.4 we show the combinations of φ_* and λ that are solutions to $A_s = U_*/24\pi^2 M_{\rm Pl}^4 \epsilon_*$ (shown as dashed lines) and $n_s - 1 = 2\eta_* - 6\epsilon_*$ (solid lines). The observed values of A_s and n_s are simultaneously realized at the intersection of the dashed and solid lines, whose position is indicated by a dot. Lines and dots with different colors correspond to different values of $|g|$. Moreover, n and $n\theta_i + \delta$ are varied in the four panels, while the rest of the parameters are fixed to

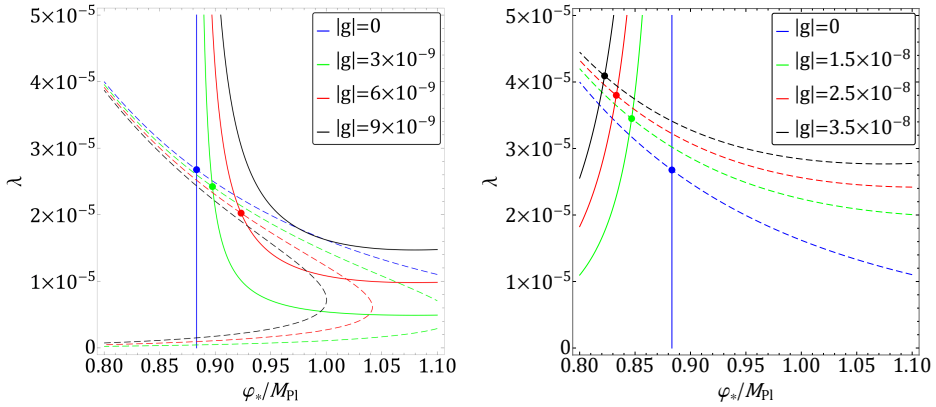

(a) $n = 0, \delta = 0.5$ (b) $n = 0, \delta = \pi - 0.5$

(c) $n = 1, \theta_i + \delta = 0.5$ (d) $n = 1, \theta_i + \delta = \pi - 0.5$

FIGURE 7.4: Combinations of φ_* and λ that satisfy $A_s = U_*/24\pi^2 M_{\rm Pl}^4 \epsilon_*$ (dashed lines) and $n_s - 1 = 2\eta_* - 6\epsilon_*$ (solid lines). The observed values $A_s = 2.1 \times 10^{-9}$ and $n_s = 0.965$ are simultaneously realized at the intersections of the dashed and solid lines, which are indicated by the dots. Different colors correspond to different values of $|g|$. Values of n and $n\theta_i + \delta$ are varied in the four panels. The other parameters are fixed to $l = 8$ and $\xi = 10^2$.

$l = 8$ and $\xi = 10^2$. Looking at Fig. 7.4(d) in which $n = 1$ and $\theta_i + \delta = \pi - 0.5$, as $|g|$ increases the intersection eventually disappears at around $|g| = 2.5 \times 10^{-8}$ and one enters the no-go region; this is also seen directly in Fig. 7.3(d). The disappearance of the intersection is also seen in Fig. 7.4(c) in which $n = 1$ and $\theta_i + \delta = 0.5$, however this happens for values of $|g|$ that give $N_* > 60$; hence the no-go region appears in Fig. 7.3(c) on the right side of the orange line.[6]

One sees in Fig. 7.4(d) that as $|g|$ increases from zero, the value of φ_* at the intersection point first decreases (as is the case in Fig. 7.4(b) for $\delta = \pi - 0.5$), and then turns to increase (as in Figs. 7.4(a) and 7.4(c) for $n\theta_i + \delta = 0.5$). This non-monotonic behavior is due to $m_{\theta*}^2/H_*^2$ approaching unity and

[6] Values of φ_* and λ are derived in (7.41) and (7.42) up to linear order in g, however we note that the no-go region emerges where the g-expansion breaks down.

forcing the axion to roll down to the vicinity of a minimum, as was shown in Fig. 7.3(d). Finally, we should comment on the second branch of intersections seen in Figs. 7.4(a), 7.4(c), and 7.4(d). As $|g|$ increases the solutions in the two branches approach each other, and merge right before one enters the no-go region. We have ignored this second branch, since it appears at values of φ_* larger than those in the first branch, and hence tends to yield N_* that is too large.

7.3 Analytic arguments

We now analytically derive an approximate expression for the constraints in Fig. 7.2, by evaluating the modulation of the number of e-folds by higher-dimensional operators. For this purpose we can ignore the time evolution of the axion and fix it to a constant value at $\theta = \theta_*$, as we will later verify. For the equation of motion of the radial field (7.27) and the Friedmann equation (7.29), we assume them to be approximated respectively by the slow-roll expressions (7.19) and (7.20). The necessary conditions for this can be obtained by comparing the approximations and their derivatives with the full equations, which gives

$$\frac{M_{\rm Pl}^2}{\xi\varphi^2}, \frac{m_\theta^2\varphi^2}{n^2H^2M_{\rm Pl}^2}, \frac{\xi f^2}{M_{\rm Pl}^2}, \frac{\xi|\Lambda|}{\lambda\varphi^2M_{\rm Pl}^2} \ll 1. \tag{7.33}$$

Upon deriving these conditions, we assumed l to be larger than four but at most of order ten, and cosine factors to be of order unity. The smallness of the first term corresponds to the large-field condition (7.16), and the third term is equivalent to the condition (7.4). Given that Λ is chosen as (7.24), then the forth term being small follows from the smallness of the other quantities. The smallness of the second term is imposed by the requirement that the second line of (7.27) is negligible; let us name this parameter as,

$$\kappa = \frac{m_\theta^2\varphi^2}{n^2H^2M_{\rm Pl}^2} \simeq \frac{72|g|\xi}{\lambda}\left(\frac{\varphi}{\sqrt{2}M_{\rm Pl}}\right)^{l-2}. \tag{7.34}$$

Here upon moving to the far right-hand side, we used (7.20) and the definition of the axion mass (7.30).

In order to evaluate the effect of the higher-dimensional operator on the number of e-folds, let us go beyond the leading-order approximations (7.19) and (7.20) by including terms that explicitly depend on g. Under the slow-roll conditions (7.33), one can check that the most relevant g-dependent term in the full equations (7.27) and (7.29) is the second line of (7.27). Hence instead of (7.19), let us use

$$3H\dot{\varphi} \simeq -\frac{\lambda}{6\xi^2(1+6\xi)}\frac{M_{\rm Pl}^4}{\varphi}\left\{1 - \frac{6(l-4)\xi|g|}{\lambda}\left(\frac{\varphi}{\sqrt{2}M_{\rm Pl}}\right)^{l-2}\cos(n\theta_* + \delta)\right\}, \tag{7.35}$$

which combined with (7.20) gives

$$dN = \frac{H}{\dot{\varphi}} d\varphi \simeq -\frac{1+6\xi}{4M_{\rm Pl}^2}\varphi\, d\varphi \left\{1 + \frac{6(l-4)\xi|g|}{\lambda}\left(\frac{\varphi}{\sqrt{2}M_{\rm Pl}}\right)^{l-2}\cos(n\theta_* + \delta)\right\}. \tag{7.36}$$

Here we note that the time evolution of θ affects (7.27) and (7.29) through terms proportional to either $\dot{\theta}^2$ or $m_\theta^2\dot{\theta}\sin(n\theta+\delta)$. Given that the axion velocity is sourced by the higher-dimensional operator, we expect $\dot{\theta} \propto m_\theta^2 \propto g$. Hence the evolution of θ affects the e-folding number at quadratic order in g, and this justifies setting θ to a constant.

Supposing the condition (7.33) to hold throughout inflation and integrating (7.36) gives

$$N_* \simeq (1+6\xi)\left\{\frac{\varphi_*^2}{8M_{\rm Pl}^2} + \frac{3(l-4)}{l}\frac{\xi|g|}{\lambda}\left(\frac{\varphi_*}{\sqrt{2}M_{\rm Pl}}\right)^{l}\cos\left(n\theta_* + \delta\right)\right\}, \tag{7.37}$$

where we have neglected terms that depend on the field value at the end of inflation. The first term in curly brackets is the leading contribution which was derived in (7.21). The second term represents the correction from the higher-dimensional operator; this can either increase or decrease N_* depending on the sign of $\cos(n\theta_* + \delta)$, as discussed in Section 7.2.2.

We further fix φ_* and λ in terms of the scalar power spectrum amplitude and spectral index, as was done in the numerical study in the previous section. Expanding the slow-roll results for the observables (7.13) up to linear order in g gives

$$A_s \simeq \frac{\lambda\,(1+6\xi)\,\varphi_*^4}{4608\pi^2\xi M_{\rm Pl}^4} + \frac{(l-4)\,(1+6\xi)\,|g|}{96\pi^2}\left(\frac{\varphi_*}{\sqrt{2}M_{\rm Pl}}\right)^{l+2}\cos\left(n\theta_* + \delta\right), \tag{7.38}$$

$$n_s - 1 \simeq -\frac{16M_{\rm Pl}^2}{(1+6\xi)\varphi_*^2} - \frac{24\,(l-4)^2\,\xi|g|}{(1+6\xi)\lambda}\left(\frac{\varphi_*}{\sqrt{2}M_{\rm Pl}}\right)^{l-4}\cos\left(n\theta_* + \delta\right). \tag{7.39}$$

Here we obtained each term in the right-hand sides at leading order in $M_{\rm Pl}^2/\xi\varphi_*^2$, and neglected terms containing f and Λ. These equations can be solved for φ_* and λ. Let us expand the quantities in powers of g,

$$\varphi_* = \varphi_{*0} + \varphi_{*1} + \cdots, \quad \lambda = \lambda_0 + \lambda_1 + \cdots, \tag{7.40}$$

where the numbers in the subscript represent orders of g. Then at the zeroth order we get

$$\varphi_{*0} \simeq \frac{4M_{\rm Pl}}{\sqrt{(1-n_s)(1+6\xi)}}, \quad \lambda_0 \simeq 18\pi^2 A_s(1-n_s)^2\xi(1+6\xi), \tag{7.41}$$

as also shown in Fig. 7.1 for $\xi \gtrsim 10^{-2}$. At linear order,

$$\varphi_{*1} \simeq \frac{(l-4)^2}{48}\varphi_{*0}\kappa_{*0}\cos(n\theta_* + \delta), \quad \lambda_1 \simeq -\frac{(l-2)(l-4)}{12}\lambda_0\kappa_{*0}\cos(n\theta_* + \delta), \tag{7.42}$$

where κ_{*0} is as shown in the far right-hand side of (7.34), but with the replacements $\varphi \to \varphi_{*0}$ and $\lambda \to \lambda_0$.

Substituting (7.41) and (7.42) into (7.37), we obtain up to linear order in g,

$$N_* \simeq \frac{2}{1-n_s}\left\{1 + \frac{(l-2)^2(l-4)}{24l}\kappa_{*0}\cos(n\theta_* + \delta)\right\}. \tag{7.43}$$

In the absence of higher-dimensional operators, the e-folding number is given by[7] $N_* \simeq 2/(1-n_s) \approx 57$ for $n_s = 0.965$. The leading correction by the higher-dimensional operator is controlled by the parameter κ; this arises from both the first term of (7.37) through the correction to φ_*, as well as the second term. For the e-folding number to lie within the range $50 < N_* < 60$, the higher-dimensional correction should be at most $\sim 10\%$. This imposes

$$\frac{(l-2)^2(l-4)}{24l}\kappa_{*0} \lesssim 10^{-1}, \tag{7.44}$$

where we assumed the cosine factor to be of order unity. Rewriting κ_{*0} in terms of observables using (7.41), one obtains an upper bound on $|g|$ as

$$\begin{aligned} |g| &\lesssim 10^{-1}\frac{48\pi^2 l A_s(1-n_s)}{(l-2)^2(l-4)}\left\{\frac{(1+6\xi)(1-n_s)}{8}\right\}^{l/2}, \\ &\sim 10^{-9}\frac{l}{(l-2)^2(l-4)}\left(\frac{1+6\xi}{230}\right)^{l/2}. \end{aligned} \tag{7.45}$$

Here, upon moving to the second line we used $A_s = 2.1 \times 10^{-9}$ and $n_s = 0.965$.

In Fig. 7.5, the analytic upper bound (7.45) is shown as black solid lines for different values of ξ, overlaid with the numerical bounds from Fig. 7.2. The analytic estimate is seen to reproduce well the numerical results. The tilt of the bound in the l - $\log|g|$ plane is predominantly set by the sign of $\log[(1+6\xi)/230]$; this factor derives from the ratio $\varphi_*/\sqrt{2}M_{\rm Pl}$ in (7.34). For $\xi \lesssim 40$, the bound on $|g|$ becomes stronger with increasing l. This reflects the fact that such values of ξ require field excursions of $\varphi_* > M_{\rm Pl}$ (see also Fig. 7.1), rendering the system particularly sensitive to higher-dimensional operators.

Using the analytic bound on $|g|$, we can also derive an upper bound for the axion mass during inflation. Rewriting its ratio to the Hubble rate as

[7] The actual e-folding number is shifted to $N_* \approx 56.5$ as reported in Section 7.1, mainly due to deviations from slow-roll towards the end of inflation.

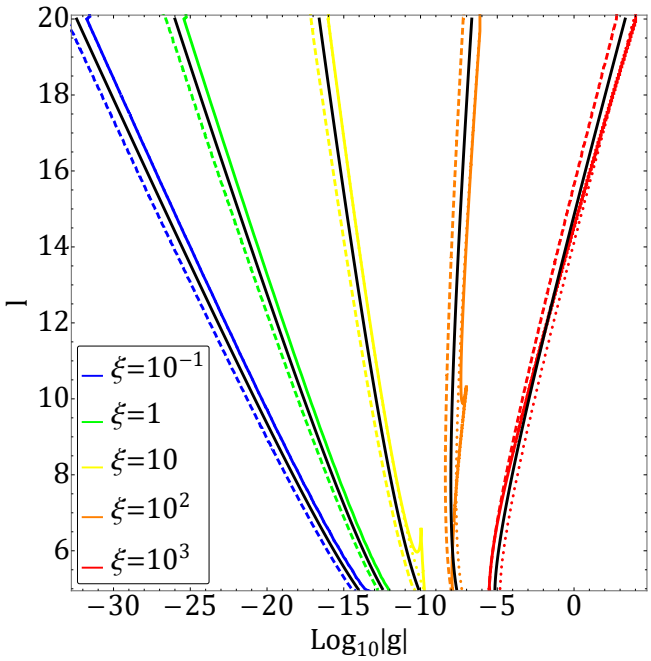

FIGURE 7.5: Analytic bound (7.45) on higher-dimensional operators shown in black solid lines, compared with the numerical bounds from Fig. 7.2.

$m_{\theta*}^2/H_*^2 = n^2\kappa_* M_{\rm Pl}^2/\varphi_*^2$, approximating φ_* and κ_* by their zeroth order values, and using (7.41), (7.44), and $n_s = 0.965$, one obtains

$$\frac{m_{\theta*}^2}{H_*^2} \lesssim 10^{-2}\frac{n^2 l(1+6\xi)}{(l-2)^2(l-4)}. \tag{7.46}$$

This expression explicitly shows that the maximum mass-Hubble ratio allowed within a consistent PQ inflation increases with ξ, as was seen in Fig. 7.3.

7.4 Validity of single-field approximation

In the previous sections we have treated PQ inflation as effectively a single-field model and computed the scalar perturbation, which was then compared to observational results to fix the model parameters. We now verify the validity of the single-field approximation by estimating the contribution of the axion field to the perturbation.

Let us evaluate scalar perturbations, relation (4.148), in the spatially flat gauge [22],

$$\zeta = \frac{H}{\dot\rho}\delta\rho \simeq \frac{H}{\dot\rho}\Big(U_\varphi\delta\varphi + U_\theta\delta\theta\Big), \tag{7.47}$$

where ρ is the background energy density and $\delta\rho$ is the density perturbation. In the far right-hand side we ignored terms containing spacetime derivatives of the fields and expanded the potential energy at linear order in the field

fluctuations, with $U_\varphi = \partial U/\partial\varphi$ and $U_\theta = \partial U/\partial\theta$. We can then go to Fourier space and write the scalar power spectrum as

$$P_\zeta(k) \simeq \left(\frac{H}{\dot\rho}\right)^2 \left(U_\varphi^2 P_{\delta\varphi}(k) + U_\theta^2 P_{\delta\theta}(k)\right), \tag{7.48}$$

where $P_{\delta\varphi}$ and $P_{\delta\theta}$ are the power spectra of the field fluctuations, and we ignored cross-correlations between $\delta\varphi$ and $\delta\theta$.[8]

The time derivative of the background density is evaluated using the continuity equation as,

$$\frac{\dot\rho}{H} = -3\left(I^2\dot\varphi^2 + \frac{\varphi^2}{\Omega^2}\dot\theta^2\right) \simeq -\frac{1}{3H^2}\left(\frac{U_\varphi^2}{I^2} + \frac{\Omega^2 U_\theta^2}{\varphi^2}\right). \tag{7.49}$$

The factors I^2 and φ^2/Ω^2 are respectively the coefficients of the kinetic terms of φ and θ in the Einstein frame action (7.9). Upon moving to the far right-hand side we assumed both fields to slow-roll, namely, to follow $3H\dot\varphi \simeq -U_\varphi/I^2$ and $3H\dot\theta \simeq -U_\theta(\Omega^2/\varphi^2)$. We also evaluate the power spectra of the field fluctuations at the wave mode k_*, when the mode exits the horizon, as

$$P_{\delta\varphi *}(k_*) \simeq \frac{1}{I^2}\left(\frac{H}{2\pi}\right)^2\Bigg|_*, \quad P_{\delta\theta *}(k_*) \simeq \frac{\Omega^2}{\varphi^2}\left(\frac{H}{2\pi}\right)^2\Bigg|_*. \tag{7.50}$$

Combining (7.48), (7.49), and (7.50) with the slow-roll approximation for the Friedmann equation $3M_{\rm Pl}^2H^2 \simeq U$, we obtain the scalar power spectrum at the horizon exit of the wave mode k_* as

$$P_{\zeta *}(k_*) \simeq \frac{I^2U^3}{12\pi^2M_{\rm Pl}^6U_\varphi^2}\left(1 + \frac{I^2\Omega^2}{\varphi^2}\frac{U_\theta^2}{U_\varphi^2}\right)^{-1}\Bigg|_*. \tag{7.51}$$

The expression in front of the parentheses is equivalent to the single-field result of (7.13). The contribution from the axion kinetic term $\dot\theta^2$ through $\dot\rho$ (cf. (7.49)), and the axion fluctuation $P_{\delta\theta}$ (cf. (7.50)), both yield corrections to the scalar power spectrum of order:

$$\alpha = \frac{I^2\Omega^2}{\varphi^2}\frac{U_\theta^2}{U_\varphi^2}\Bigg|_*. \tag{7.52}$$

Focusing on the large-field regime $\xi\varphi_*^2 \gg M_{\rm Pl}^2$, and ignoring g corrections in U_φ, the quantity α is approximated by

$$\alpha \simeq \frac{n^2(1+6\xi)}{144}\kappa_*^2\sin^2(n\theta_* + \delta), \tag{7.53}$$

[8] The interaction between θ and the almost canonical χ through the axion's kinetic term is suppressed at $\xi\varphi^2 \gg M_{\rm Pl}^2$ (cf. (7.9)), while that through the higher-dimensional operator is suppressed by the coupling g.

where κ_* is as shown in the far right-hand side of (7.34) but with the replacement $\varphi \to \varphi_*$. This shows that for instance with $n = 1$, $\kappa_* \lesssim 0.1$, and $\xi \lesssim 0.1$, the contribution by the axion to the scalar power is of $\alpha \lesssim 10^{-4}$. One may expect from (7.53) that the axion contribution increases with ξ, however a large ξ also enhances $m_{\theta*}^2/H_*^2$ and reduces the system to an effective single-field, as we see below.

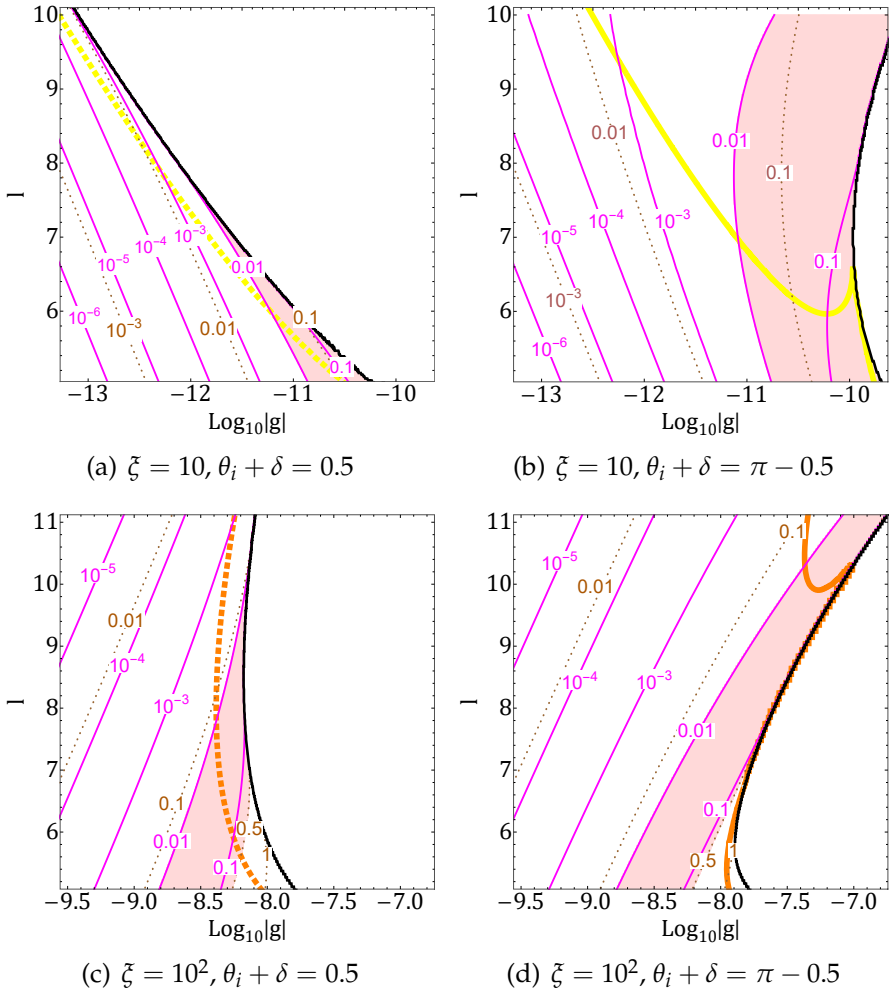

(a) $\xi = 10$, $\theta_i + \delta = 0.5$ (b) $\xi = 10$, $\theta_i + \delta = \pi - 0.5$

(c) $\xi = 10^2$, $\theta_i + \delta = 0.5$ (d) $\xi = 10^2$, $\theta_i + \delta = \pi - 0.5$

FIGURE 7.6: (Un)importance of multi-field effects in PQ inflation. The pink shaded regions show where the axion field affects the scalar power spectrum by more than 1%. The magenta solid contours show the axion's contribution to the scalar power, and the brown dotted show values of $m_{\theta*}^2/H_*^2$. All the results are for $n = 1$, while ξ and $\theta_i + \delta$ are varied in each panel. Overlaid are constraints on higher-dimensional operators as shown in Fig. 7.2. On the right of the black solid lines, A_s and n_s cannot simultaneously take the observed values.

In Fig. 7.6 we show the values of α as defined in (7.52) by magenta contours in the $|g|$ - l plane. All the results are for $n = 1$, while the values of ξ and $\theta_i + \delta$ are varied in each panel. (Note that in the $U(1)_{PQ}$-symmetric

case, i.e. $n = 0$, the axion field fluctuations do not source curvature perturbations.) Upon plotting α, we replaced θ_* in the definition (7.52) with θ_i, which amounts to ignoring the axion rolling before the horizon exit of the pivot scale. This is because if $m_{\theta*}^2 \ll H_*^2$, as assumed in the above discussions, then it follows from (7.32) that $\theta_* \simeq \theta_i$. On the other hand if $m_{\theta*}^2 \gtrsim H_*^2$, the analyses above break down; however in such cases the axion does not obtain super-horizon field fluctuations, and thus it cannot source cosmological perturbations in the first place. To also examine such cases, we show in the plots the values of $m_{\theta*}^2/H_*^2$ as brown dotted contours. Both α and $m_{\theta*}^2/H_*^2$ increase with $|g|$. We assess the contribution from the axion to the scalar power spectrum to exceed $\sim 1\%$ when both $\alpha \gtrsim 0.01$ and $m_{\theta*}^2/H_*^2 < 0.5$ are satisfied; these regions are shown in pink.

Overlaid in the plots are the bounds on higher-dimensional operators from Fig. 7.2, for $\xi = 10$ (yellow), 10^2 (orange), with dashed lines for $\theta_i + \delta = 0.5$ and solid lines for $\theta_i + \delta = \pi - 0.5$. The black solid line denotes the left edge of the no-go region where the observed values of A_s and n_s cannot be simultaneously realized (cf. Section 7.2.3). Some parts of the bounds on higher-dimensional operators, which we have derived using the single-field approximation, are seen to run through the pink regions. Here the exact position of the bounds are subject to corrections from multi-field effects. However we remark that these correspond to very small parts in the displayed area of Fig. 7.2, and in particular that the ranges of $|g|$ over which the bounds pass through the pink regions are less than about one order of magnitude. Other parts of the bounds for $\xi = 10$ and 10^2 in Fig. 7.2 do not cross the pink regions. For $\xi = 10^3$, the range of $|g|$ over which the bounds cross the pink regions are even smaller than the cases shown in Fig. 7.6. The bounds for $\xi = 10^{-1}$ and 1 do not enter the pink regions at all, as one expects from (7.53). Hence we conclude that PQ inflation is well approximated as single-field in most of the parameter space, and moreover, that multi-field effects alter our bounds on higher-dimensional operators by no more than an order of magnitude.

We should remark that in the above discussions we evaluated the curvature perturbation at the time when the mode k_* exits the horizon. However the curvature perturbation can evolve outside the horizon in the presence of isocurvature modes. This effect is analyzed in Appendix B using the δN formalism, where it is shown that the final contribution from the axion to the curvature spectrum is comparable to or smaller than α given in (7.52). Hence the regions in parameter space where the axion's contribution exceeds 1% is actually even smaller than shown in Fig. 7.6.

Let us also comment that, when we consider the axion to slowly roll, we are implicitly assuming the quantum fluctuation (7.50) to be smaller than the classical rolling over a Hubble time, i.e. $P_{\delta\theta*}^{1/2} \ll |\dot{\theta}_*|_{\rm slow-roll}/H_*$. We have checked that this condition actually holds within the displayed regions of Fig. 7.6. On the other hand, the quantum fluctuation can dominate as one moves to even smaller $|g|$, larger l, or $n = 0$. However by combining (7.50)

with (7.16), (7.20), and (7.41), the quantum fluctuation is estimated to be of

$$P_{\delta\theta*}^{1/2} \sim 10^{-7}\sqrt{1+6\xi}, \tag{7.54}$$

which is much smaller than unity, unless ξ is extremely large. Hence we expect that our main conclusion that the axion sources negligible curvature perturbation remains valid even when the axion dynamics is governed by the quantum fluctuation. Likewise, we expect the main conclusions of the other sections that invoke axion slow-roll not to be altered by the domination of the quantum fluctuation.

7.5 Parametric resonance

After inflation, the PQ field begins to oscillate around the vacuum. The oscillatory background can give rise to resonant amplifications of the field fluctuation, which would impact the post-inflation cosmology including reheating and axion dark matter production. One may expect that $\mathrm{U}(1)_{\mathrm{PQ}}$-breaking higher-dimensional operators can source an angular momentum to the PQ field and suppress resonant effects. However we now show that a resonant amplification is actually inevitably triggered after PQ inflation.

Let us focus on the first oscillation of the radial field after the end of inflation. With the oscillation time scale being comparable to or shorter than the Hubble time, and the radial field bounded by $\varphi \leq \varphi_{\mathrm{end}}$, we ignore the expansion of the Universe as well as higher dimensional operators.[9] Hence the $\mathrm{U}(1)_{\mathrm{PQ}}$ symmetry is unbroken and the PQ field's angular momentum is conserved, which we write as $L = \varphi^2\dot{\theta}$. The equation of motion of the radial direction can be written as

$$\ddot{\varphi} = -V'_{\mathrm{eff}}(\varphi), \tag{7.55}$$

where the effective potential is

$$V_{\mathrm{eff}}(\varphi) = V(\varphi) + \frac{L^2}{2\varphi^2}, \tag{7.56}$$

with V given in (7.7). This system has another conserved quantity, which is the energy density: $\rho = \dot{\varphi}^2/2 + V_{\mathrm{eff}}(\varphi)$. It is convenient to introduce dimensionless parameters as

$$u = \frac{\varphi^2}{f^2}, \quad Q = \sqrt{\frac{6}{\lambda}}\frac{|L|}{f^3}, \quad E = \frac{4!\,\rho}{\lambda f^4}. \tag{7.57}$$

[9] It was claimed in [60] that a non-minimal gravitational coupling enhances a non-perturbative decay of the inflaton. Here we show that resonant effects are triggered even without the non-minimal coupling.

Then the field value that minimizes the effective potential is obtained by solving $V'_{\rm eff} \propto u^3 - u^2 - Q^2 = 0$ as

$$u_{\rm min} = \frac{1}{3}\left\{1 + F(Q)^{1/3} + F(Q)^{-1/3}\right\}, \quad F(Q) = \frac{2 + 27Q^2 + 3Q\sqrt{12 + 81Q^2}}{2}. \tag{7.58}$$

When the effective mass of the radial field, $m_\varphi^2 = V''(\varphi) = (\lambda/6)(3\varphi^2 - f^2)$, varies with a time scale shorter than $1/m_\varphi$, then adiabaticity is violated and the PQ field fluctuations are amplified (on wave modes typically of $\sim m_\varphi$) [104, 103, 167, 105]. In fact, the frequency w_φ of the φ field is roughly given by $w_\varphi^2 \sim k^2 + m_\varphi^2$ and on the k we are interested in the adiabaticity condition (5.31) becomes $\dot{m}_\varphi/m_\varphi^2$. From Chapter 5 we know that when (5.31) is violated we have particle creations. According to this, as a measure of adiabaticity, let us evaluate the quantity $\dot{m}_\varphi/m_\varphi^2$, the square of which is written as

$$\left(\frac{\dot{m}_\varphi}{m_\varphi^2}\right)^2 = \frac{Eu - u(u-1)^2 - 2Q^2}{6(u - \frac{1}{3})^3}. \tag{7.59}$$

From (5.31), the PQ mode functions evolve adiabatically if (7.59) is smaller than unity at the minimum (7.58) of the effective potential. If $Q \ll 1$, the adiabaticity parameter at $u = u_{\rm min}$ can be expanded in Q as

$$\left(\frac{\dot{m}_\varphi}{m_\varphi^2}\right)^2_{\rm min} = \left\{\frac{9}{16} + \mathcal{O}(Q^2)\right\} E - \frac{9}{8}Q^2 + \mathcal{O}(Q^4). \tag{7.60}$$

This is smaller than unity for $E \lesssim 16/9$. On the other hand if $Q \gg 1$, then expanding in $1/Q$ yields

$$\left(\frac{\dot{m}_\varphi}{m_\varphi^2}\right)^2_{\rm min} = \left\{\frac{1}{6}Q^{-4/3} + \mathcal{O}(Q^{-2})\right\} E - \frac{1}{2} + \mathcal{O}(Q^{-2/3}), \tag{7.61}$$

which is smaller than unity for

$$Q \gtrsim \left(\frac{E}{9}\right)^{3/4}. \tag{7.62}$$

The special case of $Q = (E/3)^{3/4}$ leads to $(\dot{m}_\varphi/m_\varphi^2)^2_{\rm min} = \mathcal{O}(Q^{-2/3}) \ll 1$; here the PQ field rotates in the complex plane with an almost circular orbit at $\varphi \simeq \varphi_{\rm min}$.

The potential and kinetic energies at the end of inflation are related by

$$V(\varphi_{\rm end}) = (\dot{\varphi}^2 + \varphi^2\dot{\theta}^2)_{\rm end}. \tag{7.63}$$

This yields $\rho = (3/2)V(\varphi_{\rm end})$, and by also using $\varphi_{\rm end}^2 \gg f^2$ we find

$$E \simeq \frac{3}{2}\left(\frac{\varphi_{\rm end}}{f}\right)^4 \gg 1. \tag{7.64}$$

Hence from the discussions around (7.61), the adiabaticity condition $|\dot{m}_\varphi/m_\varphi^2|_{\min} < 1$ is satisfied only if Q is as large as (7.62). From (7.63) it also follows that the ratio between the kinetic energy of the angular direction and the potential energy at the end of inflation is bounded as

$$R = \left.\frac{\varphi^2\dot{\theta}^2}{2V(\varphi)}\right|_{\rm end} \leq 0.5. \tag{7.65}$$

From (7.64), one finds that this energy ratio R is related to the dimensionless angular momentum as

$$Q \simeq \left(\frac{2}{27}\right)^{1/4} E^{3/4} R^{1/2} \tag{7.66}$$

The condition (7.62) thus requires R to lie within the range:

$$0.1 \lesssim R \leq 0.5. \tag{7.67}$$

We stress that this is a necessary but not a sufficient condition for adiabaticity during the oscillations.

Let us now estimate the size of R by supposing that the angular field slow-rolls during inflation along the potential sourced by higher-dimensional operators as (7.31). Then the angular velocity at the end of inflation is estimated, using also $\Omega_{\rm end}^2 \sim 1$, as

$$3H_{\rm end}\dot{\theta}_{\rm end} \sim -n|g|M_{\rm Pl}^2\left(\frac{\varphi_{\rm end}}{\sqrt{2}M_{\rm Pl}}\right)^{l-2}\sin(n\theta_{\rm end}+\delta), \tag{7.68}$$

with the Hubble rate obtained using (7.63) as

$$H_{\rm end} \simeq \sqrt{\frac{\lambda}{48}}\frac{\varphi_{\rm end}^2}{M_{\rm Pl}}. \tag{7.69}$$

Further plugging (7.15) and (7.41) respectively into $\varphi_{\rm end}$ and λ, as well as using the upper bound (7.45) on $|g|$ and $|\sin(n\theta_{\rm end}+\delta)| \leq 1$, one arrives at

$$R \lesssim \begin{cases} \dfrac{10^{-3}}{\xi^2}\dfrac{n^2l^2}{(l-2)^4(l-4)^2}\left(\dfrac{1-n_s}{2}\right)^{l-2} \lesssim 10^{-9}\dfrac{n^2}{\xi^2} & \text{for } \xi \ll 10^{-1}, \\ 10^{-1}\xi\dfrac{n^2l^2}{(l-2)^4(l-4)^2}\left(\dfrac{\sqrt{3}(1-n_s)}{4}\right)^{l-2} \lesssim 10^{-7}n^2\xi & \text{for } \xi \gg 10^{-1}. \end{cases} \tag{7.70}$$

Upon going to the far right-hand sides, we used $n_s = 0.965$, and also that the expressions are maximized at $l = 5$. The upper limit in the first line increases with decreasing ξ, however $\xi \gtrsim 10^{-2}$ is required for the model not to reduce to a φ^4 inflation (cf. Fig. 7.1); this constrains R to be much smaller than 10^{-1}. From the second line one may except R to increase with ξ, however this upper limit cannot always be saturated for large ξ, as we will

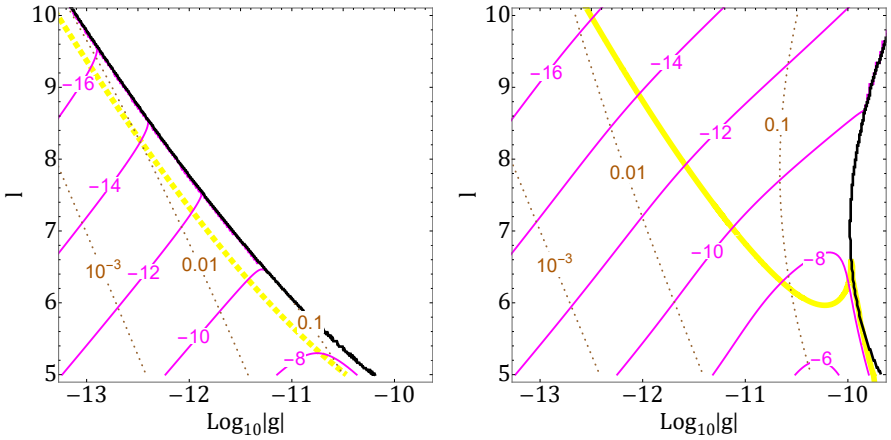

(a) $\xi = 10, \theta_i + \delta = 0.5$

(b) $\xi = 10, \theta_i + \delta = \pi - 0.5$

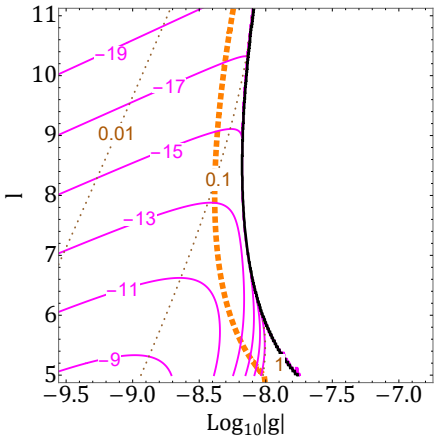

(c) $\xi = 10^2, \theta_i + \delta = 0.5$

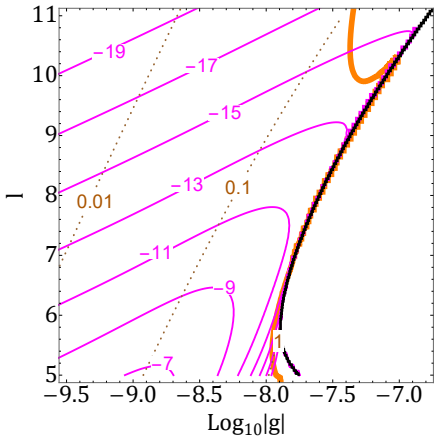

(d) $\xi = 10^2, \theta_i + \delta = \pi - 0.5$

FIGURE 7.7: Ratio R between the angular kinetic energy and potential energy at the end of PQ inflation. The magenta contours show values of $\log_{10} R$, and the brown dotted contours show $m_{\theta*}^2/H_*^2$. All the results are for $n = 1$, while ξ and $\theta_i + \delta$ are varied in each panel. Overlaid are constraints on higher-dimensional operators as shown in Fig. 7.2. On the right of the black solid lines, A_s and n_s cannot simultaneously take the observed values.

soon see.

We also numerically computed R as defined in (7.65), whose values are shown in the $|g|$ - l plane in Fig. 7.7. All the results are for $n = 1$, while ξ and $\theta_i + \delta$ are varied in each panel. The magenta contours show values of $\log_{10} R$. Also shown are brown dashed contours for the values of $m_{\theta*}^2/H_*^2$, constraints on higher-dimensional operators from Fig. 7.2, and black lines denoting the left edge of the no-go region where A_s and n_s cannot simultaneously take the observed values. For $\xi = 10$, the maximum value of R is of 10^{-8} in Fig. 7.7(a) and 10^{-6} in Fig. 7.7(b), realized close to the lower right corner where the yellow line hits the lower edge of $l = 5$. These maximum values roughly match with that given in the second line of (7.70). On the other hand for $\xi = 10^2$,

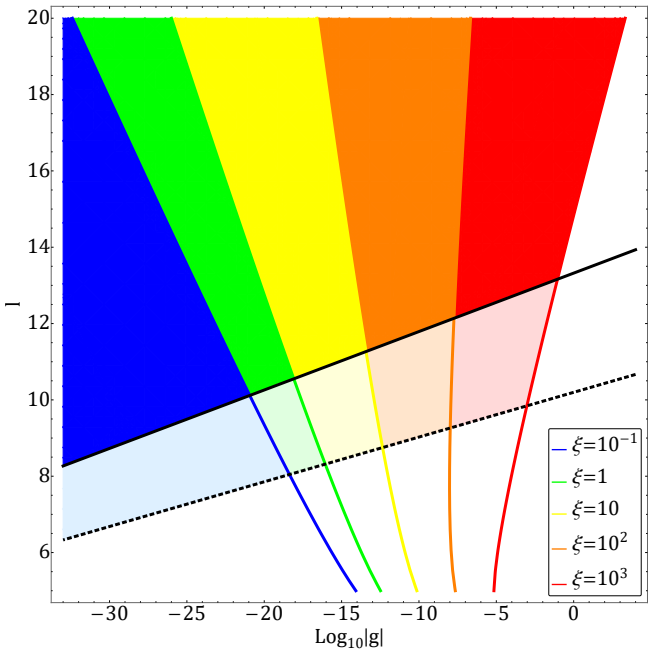

FIGURE 7.8: Combined constraints on the coupling constant $|g|$ and dimension l of higher-dimensional operators for the PQ field to drive inflation and solve the strong CP problem. The black lines show the axion quality constraint on $\mathrm{U}(1)_{\mathrm{PQ}}$-breaking operators, for $f = 10^{12}\,\mathrm{GeV}$ (solid) and $f = 10^{10}\,\mathrm{GeV}$ (dashed). The other lines show constraints on generic operators from the consistency of PQ inflation, with the colors denoting different values of the non-minimal coupling ξ. The colored regions show where both constraints are satisfied; for $\xi = 10^{-1}$ this happens only in the blue region, for $\xi = 1$ the region expands to include green, for $\xi = 10$ it further expands to yellow, etc. The light-colored regions indicate the shift of the axion quality constraint as f decreases from $10^{12}\,\mathrm{GeV}$ to $10^{10}\,\mathrm{GeV}$.

the maximum R is of 10^{-9} in Fig. 7.7(c) and 10^{-7} in Fig. 7.7(d), which are significantly smaller than the upper limit of (7.70). This is because in the lower right corners of these plots, $m_{\theta*}^2/H_*^2$ becomes of order unity and thus the axion rolls down to its potential minimum, suppressing the axion velocity $|\dot{\theta}|$ compared to the value $m_\theta^2/3nH$ which was used for deriving (7.70).

We have thus seen that that, independently of ξ, the energy ratio R is generally much smaller than the minimum value of 10^{-1} required in (7.67) for adiabaticity. We therefore conclude that a non-adiabatic evolution of the field fluctuation is inevitably triggered after PQ inflation.

7.6 Comparison with the Axion quality problem

In line with what we discussed in Section 6.6, it is natural to compare the necessary suppression of higher-dimensional operators from the axion quality, with the constraints derived in the previous sections.

In Fig. 7.8 the axion quality constraint (6.38) is shown in the $|g|$ - l plane as the black lines, for the parameter choice of $N_{\rm DW} = n$ with $f = 10^{12}\,\text{GeV}$ (solid) and $f = 10^{10}\,\text{GeV}$ (dashed). The constraint (7.45) from the consistency of PQ inflation is overlaid, with the same color scheme based on the value of ξ as in Fig. 7.2. The axion quality constraint becomes weaker for smaller f, while the inflationary constraint becomes weaker for larger ξ (although a larger ξ on the other hand lowers the cutoff of the effective field theory). The PQ field can drive inflation and solve the strong CP problem in the colored regions where both constraints are satisfied: With $\xi = 10^{-1}$ this happens only in the blue region, for $\xi = 1$ the region expands to include green, for $\xi = 10$ it further expands to yellow, etc. The light-colored regions indicate the shift of the axion quality constraint as f is varied between $10^{12}\,\text{GeV}$ and $10^{10}\,\text{GeV}$.

In the plane of $\log|g|$ and l, the tilt of the axion quality bound is given by $\log(\sqrt{2}M_{\rm Pl}/f)$, while that of the inflationary bound is predominantly given by $\log(\sqrt{2}M_{\rm Pl}/\varphi_*)$ (see discussions below (7.45)). The latter is smaller since $\varphi_* \gg f$. As a consequence, the axion quality bound is more sensitive to l, while the inflationary bound is more sensitive to $|g|$. The two bounds are thus complementary to each other, and exclude a large parameter region of higher-dimension operators when combined. It should also be noted that, while the axion quality bound only constrains $\mathrm{U}(1)_{\rm PQ}$-breaking operators ($n \neq 0$), the inflationary bound applies to general higher-dimensional operators independently of whether they break the $\mathrm{U}(1)_{\rm PQ}$.

Chapter 8

KM sourced from higher-dimensional operators

In Section 6.4.3, we mentioned that the kinetic misalignment (KM) mechanism relies on a significant value of $\dot{\theta}$. To obtain this term, we will use the potential described in equation (7.23). The purpose of this chapter is to explore whether it is possible to achieve a relic abundance of dark matter using the KM mechanism. We will do this by investigating a specific area in the parameter space where parametric resonances can be avoided. To achieve this, we will need to let go of the assumption that the radial field is the inflaton.

Let us assume radiation domination and instantaneous reheating, for the Hubble parameter we have

$$H(t) = \frac{H_I}{2H_I t + 1}, H(N) = H_I e^{-2N}, \tag{8.1}$$

where H_I is the unknown Hubble scale during inflation and we assumed $a(0) = 1$. We consider a minimally coupled complex scalar field $\Phi = \varphi/\sqrt{2}e^{\imath\theta}$ with potential given by (7.23). The complex scalar field is displaced from the minimum of the potential and we will use $\varphi_0 = \varphi_{\text{in}}$, $\theta_0 = \theta_{\text{in}}$, $\dot{\varphi}_0 = \dot{\theta}_0 = 0$ as initial conditions. The complex field is stuck to the initial values until the Hubble parameter is large. When H_{osc} reaches $m_{\varphi,\text{osc}}$, at the time of oscillation t_{osc}, the radial field starts to oscillate around the minimum. If φ_{in} is sufficiently large then the higher-dimensional operators may become important. They will give rise to angular motion or velocity for θ. Hence, the complex field describes an inspiral motion with an angular momentum that becomes conserved after a sufficiently long time when we recover the $U(1)_{\text{PQ}}$.

Let us call N_{fin} the number of e-folds at which we can neglect the higher-dimensional operators and we recover the scaling $\varphi^2\dot{\theta} \sim a^{-3}$. The condition $2m_{\text{QCD}}(T_*)/|\dot{\theta}(T_*)| < 1$ becomes

$$\frac{2m_{\text{QCD}}}{|\dot{\theta}(T_*)|} = \frac{6H(T_*)f^2a_*^3}{|\dot{\theta}_{\text{fin}}|\varphi_{\text{fin}}^2 a_{\text{fin}}^3}, \tag{8.2}$$

where we used $m_{\text{QCD}}(T_*) = 3H_*$ and the angular momentum conservation from N_{fin} until T_*. Using radiation domination and $\dot{\theta} = Hd\theta/dN = H\theta'$ in

(8.2) we obtain

$$\frac{6f^2}{|\theta'_{\rm fin}|\varphi^2_{\rm fin}}\sqrt{\frac{H_{\rm fin}}{H_*}} < 1. \tag{8.3}$$

In order to evaluate the last expression we numerically compute $\dot{\theta}_{\rm fin}, \varphi_{\rm fin}, H_{\rm fin}$ from the equations of motion for φ and θ with the above initial conditions. We solved the following system

$$H^2\varphi'' + H^2\varphi' + V_{,\varphi} = \varphi\theta'^2, \tag{8.4}$$

$$\varphi^2 H^2\theta'' + H^2\varphi^2\theta' + 2H^2\varphi'\varphi\theta' + V_{,\theta} = 0, \tag{8.5}$$

from 0 to a number of e-folds given by $N_{\rm fin}$. In the numerical simulation, we used $N_{\rm fin} \sim 3-4$ which is a sufficiently "long" time to recover the scaling $\varphi^2\dot{\theta} \sim a^{-3}$. The initial conditions for the fields φ and θ are fixed to be

$$\varphi_{\rm in} = 10^{14}{\rm GeV}, \;\; \theta_{\rm in} \sim \mathcal{O}(1). \tag{8.6}$$

Moreover, from the numerical simulation, we check that the adiabaticity condition

$$|\dot{m}_\varphi|/m^2_\varphi < 1, \tag{8.7}$$

is satisfied near the maximum of $\dot{\varphi}$, where

$$m^2_\varphi = \frac{\lambda}{6}\left(3\varphi^2 - f^2\right) - |g|(l-1)lM^2_{\rm Pl}\left(\frac{\varphi}{\sqrt{2}M_{\rm Pl}}\right)^{l-2}\cos\left(n\theta\right). \tag{8.8}$$

Our main goal is to generate a sizeable $\dot{\theta}$. To achieve this, we must ensure that $m^2_\theta(\varphi_{\rm osc}) \lesssim H^2_{\rm osc}$. Otherwise, the axion will quickly stabilize in the minimum along the angular direction before the radial field oscillations, resulting in zero velocity for θ. This is similar to what we discussed in Section 7.2.2. We have to impose

$$\frac{m^2_\theta(\varphi_{\rm osc})}{H^2_{\rm osc}} = \frac{n^2|g|M^2_{\rm Pl}}{H^2_{\rm osc}}\left(\frac{\varphi_{\rm osc}}{\sqrt{2}M_{\rm Pl}}\right)^{l-2} < 1, \tag{8.9}$$

where we evaluate φ at the oscillation time, namely $m_{\varphi,{\rm osc}} \sim 3H_{\rm osc}$. Similarly, we impose that the motion along the radial direction is dominated by the $\lambda\varphi^4$ term in (7.23). Hence, we require

$$\mathcal{S} = \frac{\left|\sqrt{2}|g|lM^3_{\rm Pl}\left(\frac{\varphi_{\rm in}}{\sqrt{2}M_{\rm Pl}}\right)^{l-1}\cos\left(n\theta_{\rm in}\right)\right|}{\frac{\lambda\varphi_{\rm in}\left(\varphi^2_{\rm in}-f^2\right)}{6}} < 1, \tag{8.10}$$

a condition that if it is initially satisfied, it will remain perpetually. This parameter measures the ratio between the masses of the angular and radial fields. We can write m_θ as

$$m^2_\theta \sim m^2_\varphi\frac{\mathcal{S}}{3l\cos n\theta}, \tag{8.11}$$

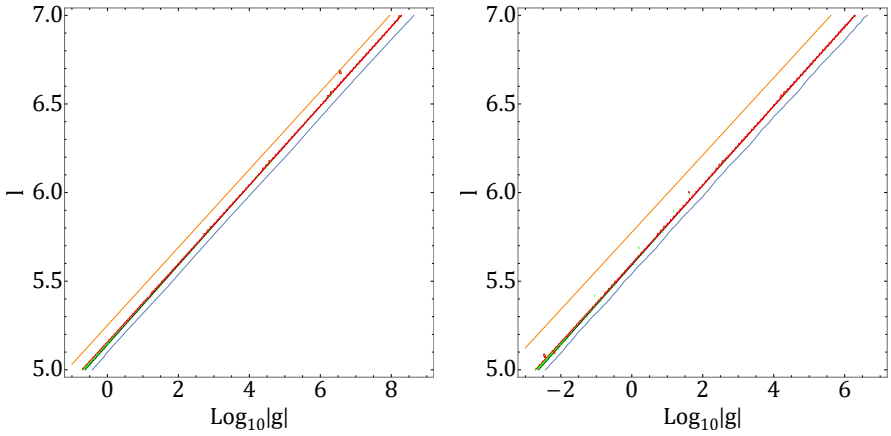

(a) $\lambda = 10^{-4}$ (b) $\lambda = 10^{-6}$

FIGURE 8.1: It is possible to have simultaneously kinetic misalignment and prevent parametric resonances while having a "light" axion. The allowed region is shown in green with overlaid the constraints (8.3) in orange, (8.7) in red, (8.9) in blue, and (8.10) in black. Here we fixed the following parameters $H_I = 10^{13}\text{Gev}, \text{f} = 10^{6}\text{GeV}, \text{n} = 1$ and λ as specified below each panel.

and relation (8.9) becomes $\mathcal{S}_{\text{osc}} \lesssim l/3$. Since $\varphi_{\text{in}} \sim \varphi_{\text{osc}}$, the inequality $\mathcal{S} < 1$ prevents the angular field from relaxing into the minimum before radial oscillations.

For now, we will ignore the axion quality constraint (6.38), even though the potential (7.23) breaks the $U(1)_{\text{PQ}}$ symmetry and has the potential to spoil the solution of the strong-CP problem.

In two panels of Figure 8.1, we have shown that it is possible to have an allowed region that satisfies the combination of the relations (8.3) in orange, (8.7) in red, (8.9) in blue and (8.10) in black. The allowed regions for (8.3) and (8.7) are on the right of the corresponding lines, while for (8.9) and (8.10), the allowed regions are on the left of the blue and black lines. As a result of the combination of these regions, a small green region arises, which enables the creation of a permitted region that satisfies all bounds simultaneously.

It is worth noting that in order to avoid parametric resonances, the value of the $\mathcal{S}$ parameter should be close to one. This was also observed in [48]. By looking at panels 8.1(a) and 8.1(b), we can see how the green region shifts towards smaller values of $|g|$ when we change λ. This is because, according to formula (8.10), if λ decreases, $|g|$ must also change in a similar way to keep $\mathcal{S}$ around 1 while keeping all other parameters fixed. In Figure 8.1, we can see that the blue and black lines mostly overlap, as expected based on the discussion after Equation (8.10).

We also note how the bound (8.3), orange lines in Fig. 8.1, improves going from panel 8.1(a) to 8.1(b). The reason is because the conserved charge $\phi^2\dot{\theta}a^3$ scales like $1/\lambda^{1/4}$. Let's start with the equation (8.5) which can be rewritten

as

$$\frac{d}{da}\left(a^3\varphi^2\dot{\theta}\right) = -\frac{a^2}{H}\frac{\partial V}{\partial\theta}, \tag{8.12}$$

where V is the potential given by (7.23) and we can integrate to obtain

$$a^3\varphi^2\dot{\theta} = 2|g|nM_{\rm Pl}^4\int_{a_{\rm in}}^{a} da\frac{a^2}{H}\left(\frac{\varphi}{\sqrt{2}M_{\rm Pl}}\right)^l \sin n\theta, \tag{8.13}$$

where we used $a^3\varphi_{\rm in}^2\dot{\theta}_{\rm in} = 0$ from the assumed initial conditions. In [73], it is shown that the last expression is maximized at the oscillation time ($m_\varphi \sim 3H_{\rm osc}$), after which the generation of n_θ for $l \geq 4$ and radiation domination is stopped. We assume, for simplicity, that $\varphi_{\rm osc}, \theta_{\rm osc} \approx \varphi_{\rm in}, \theta_{\rm in}$ such that (8.13) becomes

$$\varphi_{\rm in}^2\theta'_{\rm osc} \approx \frac{2}{5}|g|nM_{\rm Pl}^4\left(\frac{\varphi_{\rm in}}{\sqrt{2}M_{\rm Pl}}\right)^l \frac{\sin n\theta_{\rm in}}{H_{\rm osc}^2}, \tag{8.14}$$

where we neglected the initial contribution on the right of (8.13). Relation (8.14) can be recast as

$$\varphi_{\rm in}^2\theta'_{\rm osc} \approx \frac{n\lambda\tan n\theta_{\rm in}}{30l}\frac{\varphi_{\rm in}^4\mathcal{S}}{H_{\rm osc}^2}, \tag{8.15}$$

where we used (8.10) and we assumed $\varphi_{\rm in} \gg f$. From the last expression we see that $a_{\rm osc}^3\varphi_{\rm in}^2\dot{\theta}_{\rm osc} \sim \lambda\varphi_{\rm in}^4\mathcal{S}/H_{\rm osc}^{5/2} \sim 1/\lambda^{1/4}$, where $H_{\rm osc} \sim \sqrt{\lambda/2}\varphi_{\rm in}$.

Using (8.15) in (8.3) we obtain

$$\frac{lf^2H_{\rm osc}^2}{\lambda\varphi_{\rm in}^4\mathcal{S}\tan\theta_{\rm in}}\sqrt{\frac{H_{\rm osc}}{H_*}} \sim \frac{lf^2\lambda^{1/4}}{\varphi_{\rm in}^{3/2}\mathcal{S}\sqrt{H_*}\tan\theta_{\rm in}} < 1, \tag{8.16}$$

where we dropped the numerical factors and we used $H_{\rm osc} \sim \sqrt{\lambda/2}\varphi_{\rm in}$. Relation (8.16) is informative because it shows how the bound caused by kinetic misalignment can be expressed as a bound for the circularity parameter $\mathcal{S}$. Moreover, we observe that decreasing the value of λ results in a decrease in the required value of $\mathcal{S}$, as can be seen in panels 8.1(a) and 8.1(b). We can rewrite (8.16) as

$$\mathcal{S} \gtrsim \frac{lf^2\lambda^{1/4}}{\varphi_{\rm in}^{3/2}\sqrt{H_*}\tan\theta_{\rm in}} \gtrsim 0.4l\lambda^{1/4}. \tag{8.17}$$

where we substituted the values for $f, \varphi_{\rm in}, \theta_{\rm in}, H_*$. Upon analyzing the last relation, we can conclude that if λ is small enough, avoiding parametric resonances becomes the most stringent condition for the model.

In Figure 8.2, we present the numerical estimate given by relation (8.3) in solid orange and the analytical approximation (8.17) in dashed. We observe a good agreement between the two expressions at the order of magnitude level.

Let's explore why avoiding parametric resonances requires a $\mathcal{S}$ value of around one. Initially, the adiabaticity condition is satisfied without any issues up until the moment when the radial field starts to oscillate. From here,

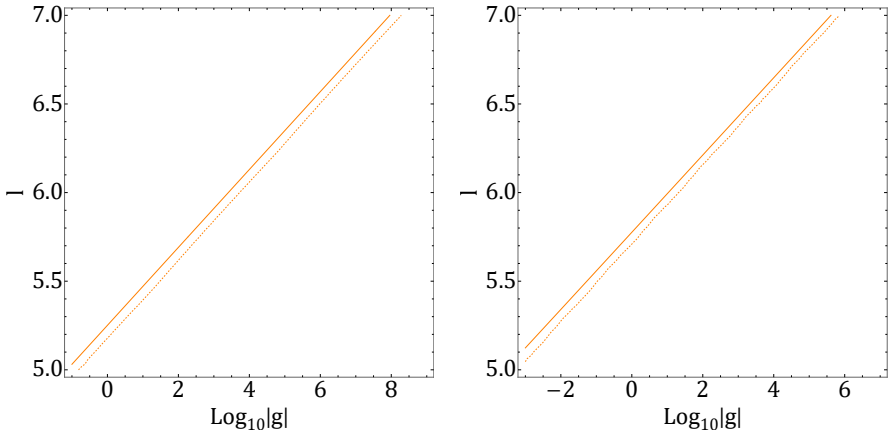

(a) $\lambda = 10^{-4}$ (b) $\lambda = 10^{-6}$

FIGURE 8.2: There is good agreement between the numerical and analytical estimation for the kinetic misalignment mechanism to be the dominant DM production mechanism. The KM constraints (8.3) in solid orange and (8.17) in dashed orange. Here we fixed the following parameters $H_I = 10^{13}$Gev, f $= 10^6$GeV, n $= 1$ and λ as specified below each panel.

the radial field moves towards the potential minimum with an initial kick generated by the oscillation. As the φ field decreases, the contribution from the higher-dimensional operator can be neglected. This means that the system being studied is equivalent to the one in section 7.5, with an angular momentum given by (8.15).

At the order of magnitude level, the adiabaticity condition (8.7) is equivalent to the relation (7.59). Since $\varphi_{\text{in}} \gg f$, the energy constant E is much larger than one, i.e., $E \gg 1$. As a result, the adiabaticity condition becomes similar to (7.62).

Similar to section 7.5, the condition (7.62) can be translated into a condition for R. To avoid parametric resonances R should satisfy

$$R = \left.\frac{\varphi^2\dot{\theta}^2}{2V}\right|_{\text{osc}} \gtrsim 0.1, \tag{8.18}$$

where we evaluate R at the time of oscillation, the upper bound does not apply since φ is no longer the inflaton and $\dot{\theta}$ is generated.

Approximating $\varphi_{\text{osc}} \approx \varphi_{\text{in}}$ and from (8.15) we obtain

$$\varphi_{\text{osc}}^2\dot{\theta}_{\text{osc}}^2 \approx \frac{n^2\lambda\varphi_{\text{in}}^4\mathcal{S}^2\tan n\theta_{\text{in}}{}^2}{50l^2}. \tag{8.19}$$

Using (7.23) and (8.10) we obtain

$$V(\varphi_{\text{osc}}) \approx \frac{\lambda\varphi_{\text{in}}^4}{4!}\left(1 - \frac{4\mathcal{S}}{l}\right). \tag{8.20}$$

Putting (8.20) and (8.19) in (8.18) we obtain

$$R \approx \frac{6 \tan {\theta_{in}}^2 \mathcal{S}^2}{25 l^2 \left(1 - \frac{4\mathcal{S}}{l}\right)} \gtrsim 0.1, \tag{8.21}$$

where we fixed $n = 1$. We choose the initial value of θ (θ_{in}) such that the tangent of θ_{in} is approximately equal to 0. From the last equation, the circularity parameter $\mathcal{S}$ should be approximately equal to $l/4$, which is of the order of 1, to avoid parametric resonances.

Chapter 9

Conclusions

The PQ inflation scenario is a very appealing and economical model that can explain many mysteries of the early Universe. Additionally, it predicts a value of r that falls within the range of future experiments like LiteBIRD [10], making the model falsifiable in the future. Apart from its testability, this thesis explores the UV properties of the PQ model and examines the robustness of its inflationary dynamics against the corrections induced by higher-dimensional operators.

As we showed extensively in Chapter 7, the PQ inflation scenario is sensitive to the ultraviolet completion of the theory for a wide range of values for the non-minimal gravitational coupling ξ, since a large ξ entails a low cutoff of the effective field theory, while a small ξ requires a large inflaton field excursion. We studied the latter effect and demonstrated that the predictions of the scenario are very sensitive to Planck-suppressed higher-dimensional operators. We showed in particular that for PQ inflation to produce the appropriate number of e-folds and curvature perturbations that match with observations, the coupling constant of an operator of dimension l suppressed by $M_{\rm Pl}$ in the Jordan frame is bounded as

$$|g| \lesssim 10^{-9} \frac{l}{(l-4)(l-2)^2} \left(\frac{1+6\xi}{230}\right)^{l/2}. \tag{9.1}$$

For instance, with $\xi = 1$, a dimension-five Planck-suppressed operator needs to be further suppressed by coupling as small as $|g| \lesssim 10^{-13}$, with the constraint becoming more severe with increasing dimension. In this sense, this work intends to underline how the PQ model, which is proposed as a solution to multiple puzzles, is subject to a fine-tuning problem.

Our constraint based on the consistency of PQ inflation is similar in spirit to the axion quality argument which constrains $\mathrm{U}(1)_{\rm PQ}$-breaking higher-dimensional operators by requiring the axion to be able to solve the strong CP problem. However, the resulting constraints are quite different, since the former is a high-energy/large-field effect, while the latter is low-energy/small-field. Moreover, the constraint from PQ inflation applies to generic higher-dimensional operators, independently of whether they break the $\mathrm{U}(1)_{\rm PQ}$ symmetry. In other words, even if the $\mathrm{U}(1)_{\rm PQ}$ symmetry is protected for some reason, PQ inflation is vulnerable to higher-dimensional corrections. The inflationary and axion quality constraints are complementary to each other, and when combined exclude a large parameter space of higher-dimensional

operators, as depicted in Fig. 7.8.

The treatment of the reheating and preheating phase requires complicated numerical simulations to follow not only the time evolution of perturbations but also their spatial distribution. (See [167, 96, 95, 166, 79, 100, 48, 16] for related works).

In light of these facts, we wanted to maintain a more simplified treatment which in any case does not limit us in stating that the parametric resonances process plays a crucial role in the PQ model. This statement is not trivial at all because it implies that the view taken so far on this model, i.e. of a homogeneous evolution of the axion after inflation, is not entirely justified. Based on the constraint on higher-dimensional operators, we showed that the oscillation of the PQ field after inflation inevitably triggers resonant amplifications of the field fluctuations, Fig. 7.7. This raises serious doubts about the validity of the homogeneous evolution after inflation. For a stronger statement, i.e. the invalidity of this scenario, more in-depth studies on symmetry restoration are necessary which would entail, as explained in Chapter 6, a more complex production process.

Here we note that to fully understand the cosmology after PQ inflation including the reheating process, possible formation of axion strings and domain walls, as well as the production of axion dark matter, it is crucial to ascertain the impact of parametric resonance. Our analyses can also be extended to other axion scenarios that make use of higher-dimensional operators, such as [46, 49, 73]. Our results are compatible with those present in the literature [48, 17]; a result not obvious a priori given the different dynamics present in the second reference.

We should remark that most of the analyses in Chapter 7 neglect interactions between the PQ field and other matter fields, whose inclusion will be necessary for understanding the reheating process. Matter couplings may also modify the PQ field dynamics during/after inflation, and alter our results. Another important direction for further study is to seek for ultraviolet completions that control higher-dimensional operators. See e.g. [160, 92] for attempts for realizing high-scale inflation. It would be interesting to study if such constructions exist also for the PQ inflation scenario.

In Chapter 8, we explored the possibility of preventing parametric resonances and obtaining a relic abundance of DM through the kinetic misalignment mechanism by abandoning the assumption that the radial field is the inflaton. We found that it is possible to obtain a small green region in Fig. 8.1 which ensures the avoidance of parametric resonances if the circularity parameter $\mathcal{S}$ is of the order of unity, as shown in [48]. We also put bounds on the size of these operators. In the allowed regions, the relic abundance of the DM is given by the kinetic misalignment mechanism. Moreover, if we reduce the coupling λ, we can obtain a greater final angular momentum, as stated in relation (8.17). Thus, avoiding parametric resonances becomes the most stringent condition for the model if λ is small enough.

However, the treatment performed in Chapter 8 is preliminary, and we cannot exclude the possibility of permitted regions for different parameter

values. Therefore, a more thorough analysis is needed to explore a wider region of the parameters l and $\log_{10}|g|$ with different choices for H_1, f, λ. This study is fundamental not only for the PQ model but also for all those models such as "kination" and "kinetic misalignment" [46, 73, 47] in which the homogeneous evolution of the axion is assumed but not verified.

This thesis encompassed a comprehensive analysis spanning a wide range of topics in cosmology. Noteworthy novel aspects of this thesis are the proven UV sensitivity of the PQ model and the unavoidable presence of parametric resonances within this scenario. We conclude by underlining how the field of axion studies presents itself as a cornerstone for a greater comprehension of the various puzzles that are present in the Universe. The work presented in this thesis is suitable for further extensions as we discussed above.

Appendix A

Effective-Planck-suppressed operators

In the main text we focus on higher-dimensional operators that are suppressed by the present-day Planck scale, however, in Appendix A we study operators suppressed by the effective Planck scale during inflation.

In this appendix we suppose that quantum gravity corrections give rise to higher-dimensional operators suppressed by the effective Planck scale in the Jordan frame, namely, operators of the form (7.23) but with $M_{\rm Pl}$ replaced by $(M_{\rm Pl}^2 + \xi\varphi^2)^{1/2}$. This scale at large fields becomes linear in the field as $\simeq \sqrt{\xi}\varphi$, and thus the operators reduce to the form

$$-\frac{|g|}{2(2\xi)^{\frac{l}{2}-2}}\varphi^4\cos(n\theta+\delta). \tag{A.1}$$

This merely has the effect of shifting the PQ self-coupling by

$$\Delta\lambda = -\frac{12|g|}{(2\xi)^{\frac{l}{2}-2}}\cos(n\theta+\delta). \tag{A.2}$$

PQ inflation would hence match with observations in the presence of such operators, given that the effective coupling $\lambda_{\rm eff} = \lambda + \Delta\lambda$ takes an appropriate value.

On the other hand, if one wishes to make reliable predictions of PQ inflation without detailed knowledge of quantum gravity, then $\Delta\lambda$ needs to be small enough such that it has little effect on the cosmological observables. When fixing the other parameters, the self-coupling is related to the spectral index as $\lambda \propto (n_s - 1)^2$, cf. (7.41). Hence a shift in λ affects n_s by

$$\frac{\Delta n_s}{n_s - 1} \simeq \frac{\Delta\lambda}{2\lambda}. \tag{A.3}$$

Combining with (A.2), approximating the cosine to unity, and substituting (7.41) into λ, we obtain

$$\begin{aligned} |g| &\sim \frac{3\pi^2}{2}A_s(1-n_s)|\Delta n_s|(1+6\xi)(2\xi)^{\frac{l}{2}-1} \\ &\lesssim 10^{-12}(1+6\xi)(2\xi)^{\frac{l}{2}-1}. \end{aligned} \tag{A.4}$$

Upon moving to the second line we substituted $A_s = 2.1 \times 10^{-9}$, $n_s = 0.9649$, and also required the shift in n_s to be smaller than the Planck 1σ uncertainty [9], i.e., $|\Delta n_s| < 0.0042$. For $\xi \lesssim 0.1$, this bound indicates that effective-Planck-suppressed operators should be further suppressed by couplings as small as $|g| \lesssim 10^{-12}$. On the other hand at $\xi \gtrsim 10^4$, the second line is of order unity or larger for $l \geq 5$ and hence the suppression by the effective Planck scale alone renders the operators negligible.

Appendix B

Detailed computation of multi-field effects

We compute the contribution from the axion field to the curvature perturbation by using the δN formalism [163, 154, 173, 125] to take into account the evolution of the perturbation outside the horizon. The analysis in this appendix is close to that presented in [99].

Given relation (4.203), the power spectrum of the curvature perturbation can be written in terms of field derivatives of the e-folding number as

$$P_\zeta(k_*) \simeq \left(\frac{\partial N_*}{\partial \varphi_*}\right)^2 P_{\delta\varphi *}(k_*) + \left(\frac{\partial N_*}{\partial \theta_*}\right)^2 P_{\delta\theta *}(k_*), \tag{B.1}$$

where we expanded the perturbation in terms of field fluctuations up to linear order, and ignored cross-correlations between the radial and angular fluctuations. $P_{\delta\varphi *}$ and $P_{\delta\theta *}$ denote the power spectra of the field fluctuations on the initial flat slice when the wave mode k_* exits the horizon.

Let us focus on PQ inflation in the large-field regime. In particular, we assume the conditions laid out in (7.33), plus $m_\theta^2 \ll H^2$ to hold throughout inflation. Then the equations of motion (7.27), (7.28), and the Friedmann equation (7.29) are approximated by the slow-roll expressions (7.19), (7.31), and (7.20), respectively. Moreover, the power of the field fluctuations at horizon exit are (cf. (7.50)),

$$P_{\delta\varphi *}(k_*) \simeq \frac{\xi}{1+6\xi}\left(\frac{\varphi_*}{M_{\rm Pl}}\right)^2 \left(\frac{H_*}{2\pi}\right)^2, \quad P_{\delta\theta *}(k_*) \simeq \frac{\xi}{M_{\rm Pl}^2}\left(\frac{H_*}{2\pi}\right)^2. \tag{B.2}$$

The infinitesimal variation of the e-folding number is written using (7.19) and (7.20) as

$$dN \simeq -\frac{1+6\xi}{4}\frac{\varphi\, d\varphi}{M_{\rm Pl}^2}, \tag{B.3}$$

hence the radial contribution to the curvature power spectrum is obtained as

$$\left(\frac{\partial N_*}{\partial \varphi_*}\right)^2 P_{\delta\varphi *} \simeq \frac{\xi(1+6\xi)}{16}\frac{\varphi_*^4}{M_{\rm Pl}^6}\left(\frac{H_*}{2\pi}\right)^2. \tag{B.4}$$

Rewriting H_* using (7.20), this reproduces the expression for A_s in (7.18).

Considering inflation to end when the radial field approaches some field value $\varphi_{\rm end}$ which is independent of θ_*, then it is convenient to express the evolution of the angular field in terms of the radial field. Combining (7.19) and (7.31) gives

$$\frac{d\theta}{d\varphi} \simeq \frac{6\xi^2(1+6\xi)}{n\lambda}\frac{\varphi\, m_\theta^2}{M_{\rm Pl}^4}\sin(n\theta+\delta), \tag{B.5}$$

which can be integrated to yield,

$$\tan\left(\frac{n\theta+\delta}{2}\right) \simeq \tan\left(\frac{n\theta_*+\delta}{2}\right)\exp\left[\frac{\mathcal{G}}{2}(x^{l-2}-x_*^{l-2})\right]. \tag{B.6}$$

Here we have introduced

$$x=\frac{\varphi}{\sqrt{2}M_{\rm Pl}}, \quad \mathcal{G}=\frac{12n^2}{l-2}\frac{\xi(1+6\xi)|g|}{\lambda}. \tag{B.7}$$

Following similar prescriptions as in Section 7.3, one finds that under the conditions (7.33) and $m_\theta^2 \ll H^2$, the leading correction to the expression (B.3) for dN from terms that explicitly[1] depend on θ yields (7.36), but with the replacement $\theta_* \to \theta$. (Unlike in Section 7.3, here we are not limiting ourselves to corrections linear in g, and hence the axion is allowed to roll.) Then N_* can be obtained by integrating this expression over $\varphi_* \geq \varphi \geq \varphi_{\rm end}$, noting that θ is a function of φ as given in (B.6). In particular, its θ_*-derivative is written as

$$\frac{\partial N_*}{\partial\theta_*} \simeq \frac{(l-2)(l-4)}{2n}\mathcal{G}\int_{x_*}^{x_{\rm end}} dx\, x^{l-1}\frac{\tan\left(\frac{n\theta_*+\delta}{2}\right)\left\{1+\tan^2\left(\frac{n\theta_*+\delta}{2}\right)\right\}e^{\mathcal{G}(x^{l-2}-x_*^{l-2})}}{\left\{1+\tan^2\left(\frac{n\theta_*+\delta}{2}\right)e^{\mathcal{G}(x^{l-2}-x_*^{l-2})}\right\}^2}. \tag{B.8}$$

In terms of this quantity, the ratio of the contributions to the curvature power spectrum from the angular and radial fields is written as

$$\beta=\frac{(\partial\mathcal{N}_*/\partial\theta_*)^2 P_{\delta\theta*}}{(\partial\mathcal{N}_*/\partial\varphi_*)^2 P_{\delta\varphi*}} \simeq \frac{16}{1+6\xi}\left(\frac{M_{\rm Pl}}{\varphi_*}\right)^4\left(\frac{\partial N_*}{\partial\theta_*}\right)^2. \tag{B.9}$$

Here, upon moving to the far right-hand side we used (B.2) and (B.4).

In order to analytically compute the integral in (B.8), let us for the moment focus on the case of

$$|n\theta_*+\delta| \ll 1. \tag{B.10}$$

Then by expanding the integrand up to linear order in $(n\theta_*+\delta)$, one can perform the integral and obtain

$$\frac{\partial N_*}{\partial\theta_*} \simeq \frac{l-4}{4n}\mathcal{G}e^{-\mathcal{G}x_*^{l-2}}\left[x^l E_{-\frac{2}{l-2}}(-\mathcal{G}x^{l-2})\right]_{x_{\rm end}}^{x_*}(n\theta_*+\delta), \tag{B.11}$$

[1] In principle the axion can also affect N through terms that only depend on φ by modulating the radial field dynamics; however we consider such effects to be negligible.

where

$$E_p(z) = z^{p-1}\int_z^\infty \frac{e^{-y}}{y^p}dy \tag{B.12}$$

is the generalized exponential integral. The argument $\mathcal{G}x^{l-2}$ in (B.11) is, under the conditions (7.33), approximated by

$$\mathcal{G}x^{l-2} \simeq \frac{1+6\xi}{6(l-2)}\frac{m_\theta^2}{H^2}\frac{\varphi^2}{M_{\rm Pl}^2} = \frac{n^2(1+6\xi)}{6(l-2)}\kappa, \tag{B.13}$$

where κ is defined in (7.34). Let us further assume this to be sufficiently small such that $\mathcal{G}x^{l-2} \ll 1$, and expand the generalized exponential integral using [136]

$$E_p(z) = z^{p-1}\Gamma(1-p) - \sum_{s=0}^{\infty}\frac{(-z)^s}{s!(1-p+s)}, \tag{B.14}$$

which is valid for $|\mathrm{ph}\,z| \leq$ ß. Keeping terms up to $s=0$ order, and further using $e^{-\mathcal{G}x_*^{l-2}} \simeq 1$ and $x_*^l \gg x_{\rm end}^l$, we arrive at

$$\frac{\partial N_*}{\partial\theta_*} \simeq -\frac{(l-2)(l-4)}{4nl}\mathcal{G}x_*^l(n\theta_*+\delta). \tag{B.15}$$

This approximate expression starts at linear order in g, and ignores the axion rolling; the same result can also be obtained by taking a θ_*-derivative of the e-folding number derived in (7.37). We thus obtain

$$\beta \simeq \frac{n^2(l-4)^2(1+6\xi)}{144\,l^2}\kappa_*^2(n\theta_*+\delta)^2 \simeq \frac{(l-4)^2}{l^2}\alpha. \tag{B.16}$$

Here α is the relative contribution to the curvature perturbation from the angular field which was derived in (7.53) by ignoring the evolution of the perturbations outside the horizon.

We show in Fig. B.1 the values of β as given in (B.9), by numerically computing the integral (B.8) to evaluate $\partial N_*/\partial\theta_*$. However, here we have replaced θ_* with θ_i, for the same reason as described below (7.53). The contours for β are shown in green. The other lines are the same as in Fig. 7.6: contours of α in magenta, contours of $m_{\theta*}^2/H_*^2$ in brown dotted, the edge of the no-go region in black, and the constraints on higher-dimensional operators with the same color scheme in Fig. 7.2. All the results are for $n=1$, while ξ and $\theta_i+\delta$ are varied in each panel. One sees that $\beta < \alpha$ generically holds in regions where $m_{\theta*}^2/H_*^2 \ll 1$. In particular, as expected from the relation (B.16), β is smaller than α by about two orders of magnitude at $l=5$, while their difference shrinks towards larger l. On the other hand in regions where $m_{\theta*}^2/H_*^2 \sim 1$, the angular field's super-horizon fluctuations get suppressed and their actual contribution to the curvature perturbation becomes smaller than α or β. Hence we conclude that the regions in parameter space where the angular contribution exceeds 1%, namely, where both $\beta \geq 10^{-2}$ and $m_{\theta*}^2/H_*^2 \ll 1$ are satisfied, are actually even smaller than shown in Fig. 7.6.

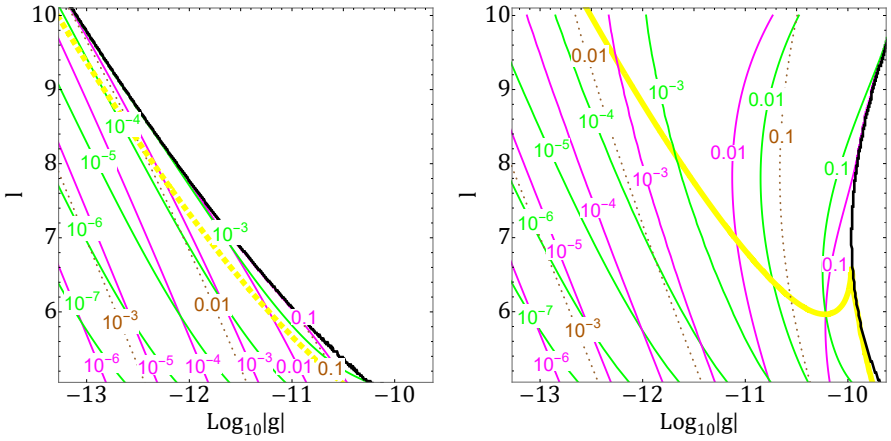

(a) $\xi = 10, \theta_i + \delta = 0.5$ (b) $\xi = 10, \theta_i + \delta = \pi - 0.5$

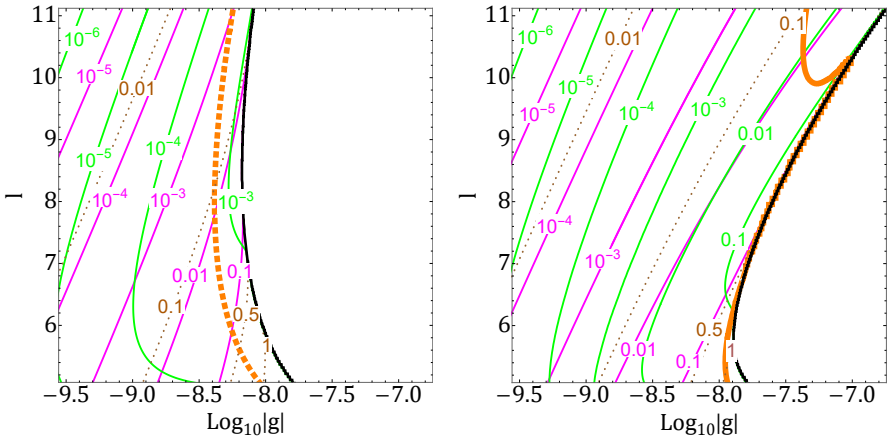

(c) $\xi = 10^2, \theta_i + \delta = 0.5$ (d) $\xi = 10^2, \theta_i + \delta = \pi - 0.5$

FIGURE B.1: Contribution of the axion to the curvature perturbation amplitude evaluated from β (green contours) which takes into account the evolution of the perturbation outside the horizon, and α (magenta contours) which ignores the evolution. The brown dotted contours show values of $m_{\theta*}^2/H_*^2$. Constraints on higher-dimensional operators are taken from Fig. 7.2. On the right of the black solid lines, A_s and n_s cannot simultaneously take the observed values. All the results are for $n = 1$.

Before ending this appendix, we remark that upon using the δN formalism, one should consider the e-folding number up to a final uniform-density slice when the curvature perturbation has approached a constant. In the above discussions we have simply computed the e-folding until the end of inflation, and also assumed the radial field value $\varphi_{\rm end}$ when inflation ends to be independent of the initial conditions φ_* and θ_*. If the end of inflation and/or the post-inflation expansion history are also affected by φ_* and θ_*, then the curvature perturbation would continue to evolve after inflation [123, 153].

Appendix C

Axion isocurvature in a non-vanilla scenario

We showed in Section 7.5 that a resonant amplification of the PQ field fluctuation is triggered after inflation, which is likely to render the axion field highly inhomogeneous. However, in this appendix, we assume that somehow the amplification is suppressed, and moreover that the PQ symmetry is not restored after inflation, such that axion dark matter is produced through the conventional vacuum misalignment scenario. We compute the axion isocurvature perturbation in this hypothetical situation and derive constraints on the model parameters. The calculation we will perform in this section differs from that in Section 6.5 because the radial field is not stabilized in the minimum of the potential $\varphi = f$.

The relic abundance of axions produced via vacuum misalignment is given by (6.16) (see also [170])

$$\Omega_\theta h^2 \approx 0.1 (N_{\rm DW}\theta_*)^2 \left(\frac{f/N_{\rm DW}}{10^{12}{\rm GeV}}\right)^{7/6}, \tag{C.1}$$

where the CP-conserving vacuum is taken as $\theta = 0$, and we inserted again $N_{\rm DW}$ that is the domain wall number. We have assumed $m_\theta^2 \ll H^2$ to hold throughout inflation, and also that the initial misalignment angle satisfies $|N_{\rm DW}\theta_*| < 1$ such that the QCD potential in (6.35) is approximated by a quadratic.[1] We suppose that the axions make up the entire dark matter, i.e. $\Omega_\theta h^2 \approx 0.1$. This sets a direct relation between θ_* and f through the above equation.

Since the angle θ_* acquires super-horizon fluctuations during inflation, axions obtain isocurvature perturbations as $\delta\Omega_\theta/\Omega_\theta \simeq 2\delta\theta_*/\theta_*$, up to linear order in the angular fluctuations. The isocurvature power spectrum is thus written, using (7.50), as

$$P_{\rm iso}(k_*) \simeq \frac{1}{\theta_*^2}\frac{\Omega_*^2}{\varphi_*^2}\frac{H_*^2}{\pi^2}. \tag{C.2}$$

Here Ω_*^2 is the conformal factor at $\varphi = \varphi_*$ and should not be confused with the axion relic abundance Ω_θ. Notice that the inflaton φ is displaced from the minimum, causing the isocurvature power spectrum to differ from the

[1] It is also assumed that the axion begins to oscillate during radiation domination, at temperatures above the QCD scale. This amounts to requiring $f/N_{\rm DW} \lesssim 10^{15}$ GeV, see (6.18).

relation (6.30). Using (C.1) to rewrite θ_* in terms of f, one obtains

$$P_{\rm iso}(k_*) \approx N_{\rm DW}^2 \left(\frac{f/N_{\rm DW}}{10^{12}{\rm GeV}}\right)^{7/6} \frac{\Omega_*^2}{\varphi_*^2}\frac{H_*^2}{\pi^2}. \tag{C.3}$$

The last factor is determined by the inflationary observables. In particular for large fields, $\xi\varphi_*^2 \gg M_{\rm Pl}^2$, one can plug (7.20) and (7.41) respectively into H_* and λ to obtain

$$\frac{\Omega_*^2}{\varphi_*^2}\frac{H_*^2}{\pi^2} \simeq \frac{P_\zeta(k_*)(1-n_s)^2(1+6\xi)}{4}. \tag{C.4}$$

Considering the k_* dependence of (C.2) to be small and also ignoring cross-correlations between $\delta\theta$ and $\delta\varphi$, the axion isocurvature is almost scale-invariant and uncorrelated with curvature perturbations. Parametrizing the power spectrum as $P_{\rm iso}(k)/P_\zeta(k) = \beta_{\rm iso}(k)/\{1-\beta_{\rm iso}(k)\}$, this kind of cold dark matter isocurvature is constrained by Planck [9] as $\beta_{\rm iso}(k_*) < 0.038$ (95% C.L.) at $k_* = 0.05\,{\rm Mpc}^{-1}$. Imposing this constraint on (C.3), and substituting (C.4) and $n_s = 0.965$, we obtain an upper bound on the axion decay constant,

$$f \lesssim \frac{10^{14}\,{\rm GeV}}{N_{\rm DW}^{5/7}(1+6\xi)^{6/7}}. \tag{C.5}$$

We derived this result assuming $\xi\varphi_*^2 \gg M_{\rm Pl}^2$; however can check that the small ξ limit of this expression matches with the bound in the minimal φ^4-inflation regime at small ξ, at the order-of-magnitude level. The upper bound originates from the fact that a larger f requires a smaller θ_* for a fixed relic abundance, which in turn leads to a larger isocurvature. If the PQ field is not the inflaton and its radial component is fixed to f, the axion isocurvature is given by (6.30). The isocurvature then comes with a negative power of f, and the isocurvature constraint yields a *lower* limit on f in terms of an undetermined inflation scale, see relation (6.32). We also remark that for arbitrary ξ, the bound (C.5) is stronger than the condition (7.4) we have been assuming throughout this paper. In Fig. C.1 we show the upper bound on f as a function of ξ by the red line. Here the factor $\Omega_*^2 H_*^2/\varphi_*^2$ is numerically computed as was done for Fig. 7.1. In addition to using the aforementioned values for the observables, in the plot we further set $N_{\rm DW} = 1$.

It should be noted that the above discussions break down at $f/N_{\rm DW} < 10^{12}\,{\rm GeV}$, for which $|N_{\rm DW}\theta_*| > 1$ is required for the axions to make up the entire dark matter. In this regime the full axion potential needs to be taken into account, and its departure from a quadratic increases the relic abundance compared to (C.1) [170, 14], and moreover significantly enhances the axion isocurvature compared to (C.2) [121, 165, 101]. Each of these effects makes the upper bound on f more stringent than (C.5). The isocurvature hence becomes large at both large f in a quadratic axion potential, as well as at small f in an anharmonic potential.[2] Since the anharmonic enhancement

[2]The work [61] also evaluated axion isocurvature assuming vacuum misalignment after PQ inflation. However the conformal factor Ω_*^2 in (C.2) was overlooked, and moreover the

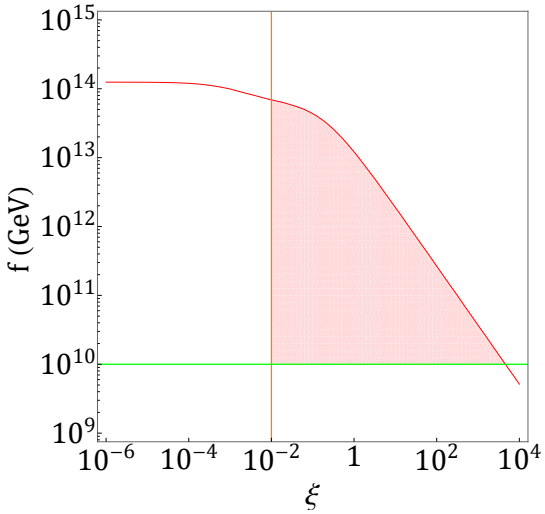

FIGURE C.1: Constraints on the decay constant and gravitational coupling for the hypothetical scenario where axions are produced by vacuum misalignment after PQ inflation. The region where axions can make up dark matter is shown in red. Axion isocurvature exceeds the observational limit in regions above the red line (in a quadratic axion potential), as well as below the green line (anharmonic potential). The tensor-to-scalar ratio exceeds the observational limit on the left of the orange line. Here we have set $N_{\rm DW} = 1$.

of the isocurvature becomes particularly strong at $f/N_{\rm DW} \lesssim 10^{10}\,$GeV [101], in Fig. C.1 we show $f = 10^{10}\,$GeV by the green line as a rough lower bound below which anharmonic effects produce isocurvature beyond the observational limit. Note that the upper bound (C.5) with $N_{\rm DW} = 1$ becomes of $10^{10}\,$GeV at $\xi \sim 10^3$; this sets an absolute upper limit for ξ.

In the plot we also show in orange the lower limit $\xi \gtrsim 10^{-2}$, which derives from the observational limit on the tensor-to-scalar ratio, cf. Fig. 7.1(d). This, together with the upper and lower limits for f, leave us with the red region as the allowed parameter space for the scenario where PQ inflation is followed by a vacuum misalignment.

isocurvature power was underestimated by 8π. It also did not take into account anharmonic effects, and consequently obtained a much larger parameter window than in this appendix.

Bibliography

[1] L. F. Abbott and P. Sikivie. "A Cosmological Bound on the Invisible Axion". In: *Phys. Lett. B* 120 (1983), pp. 133–136.

[2] L. F. Abbott and Mark B. Wise. "Constraints on Generalized Inflationary Cosmologies". In: *Nucl. Phys. B* 244 (1984), pp. 541–548. DOI: 10.1016/0550-3213(84)90329-8.

[3] Larry F. Abbott and Mark B. Wise. "Wormholes and global symmetries." In: *Nuclear Physics B* 325.3 (1989), pp. 687–704.

[4] T. M. C. Abbott et al. "Dark Energy Survey year 1 results: Constraints on extended cosmological models from galaxy clustering and weak lensing". In: *Phys. Rev. D* 99 (12 2019), p. 123505. DOI: 10.1103/PhysRevD.99.123505. URL: https://link.aps.org/doi/10.1103/PhysRevD.99.123505.

[5] C. Abel et al. "Measurement of the Permanent Electric Dipole Moment of the Neutron". In: *Phys. Rev. Lett.* 124.8 (2020), p. 081803. DOI: 10.1103/PhysRevLett.124.081803. arXiv: 2001.11966 [hep-ex].

[6] P. A. R. Ade et al. "BICEP2 / Keck Array x: Constraints on Primordial Gravitational Waves using Planck, WMAP, and New BICEP2/Keck Observations through the 2015 Season". In: *Phys. Rev. Lett.* 121 (2018), p. 221301. DOI: 10.1103/PhysRevLett.121.221301. arXiv: 1810.05216 [astro-ph.CO].

[7] P. A. R. Ade et al. "Improved Constraints on Primordial Gravitational Waves using Planck, WMAP, and BICEP/Keck Observations through the 2018 Observing Season". In: *Phys. Rev. Lett.* 127.15 (2021), p. 151301. DOI: 10.1103/PhysRevLett.127.151301. arXiv: 2110.00483 [astro-ph.CO].

[8] Ian Affleck and Michael Dine. "A new mechanism for baryogenesis". In: *Nuclear Physics B* 249.2 (1985), pp. 361–380. ISSN: 0550-3213. DOI: https://doi.org/10.1016/0550-3213(85)90021-5. URL: https://www.sciencedirect.com/science/article/pii/0550321385900215.

[9] Y. Akrami et al. "Planck 2018 results. X. Constraints on inflation". In: *Astron. Astrophys.* 641 (2020), A10. DOI: 10.1051/0004-6361/201833887. arXiv: 1807.06211 [astro-ph.CO].

[10] E. Allys et al. "Probing Cosmic Inflation with the LiteBIRD Cosmic Microwave Background Polarization Survey". In: *PTEP* 2023.4 (2023), 042F01. DOI: 10.1093/ptep/ptac150. arXiv: 2202.02773 [astro-ph.IM].

[11] Nima Arkani-Hamed et al. "Extra natural inflation". In: *Phys. Rev. Lett.* 90 (2003), p. 221302. DOI: 10.1103/PhysRevLett.90.221302. arXiv: hep-th/0301218.

[12] Nima Arkani-Hamed et al. "Ghost inflation". In: *Journal of Cosmology and Astroparticle Physics* 2004.04 (2004), pp. 001–001. DOI: 10.1088/1475-7516/2004/04/001. URL: https://doi.org/10.1088%2F1475-7516%2F2004%2F04%2F001.

[13] Asimina Arvanitaki et al. "String Axiverse". In: *Phys. Rev. D* 81 (2010), p. 123530. DOI: 10.1103/PhysRevD.81.123530. arXiv: 0905.4720 [hep-th].

[14] Kyu Jung Bae, Ji-Haeng Huh, and Jihn E. Kim. "Update of axion CDM energy". In: *JCAP* 09 (2008), p. 005. DOI: 10.1088/1475-7516/2008/09/005. arXiv: 0806.0497 [hep-ph].

[15] C. A. Baker et al. "et al". In: *"An Improved experimental limit on the electric dipole moment of the neutron," Phys. Rev. Lett.* 97 (2006). arXiv: hep-ex/0602020.

[16] G. Ballesteros et al. "Revisiting isocurvature bounds in models unifying the axion with the inflaton". In: *JCAP* 09 (2021). arXiv: 2104.13847.

[17] Guillermo Ballesteros et al. "Standard Model—axion—seesaw—Higgs portal inflation. Five problems of particle physics and cosmology solved in one stroke". In: *JCAP* 08 (2017), p. 001. DOI: 10.1088/1475-7516/2017/08/001. arXiv: 1610.01639 [hep-ph].

[18] T. Banks and N. Seiberg. "Symmetries and Strings in Field Theory and Gravity". In: *Phys. Rev. D* 83 (2011). arXiv: 1011.5120.

[19] Tom Banks and Willy Fischler. "A Model for high-energy scattering in quantum gravity". In: (1999). arXiv: hep-th/9906038.

[20] J. L. F. Barbon and J. R. Espinosa. "On the Naturalness of Higgs Inflation". In: *Phys. Rev. D* 79 (2009). arXiv: 0903.0355.

[21] James M. Bardeen. "Gauge-invariant cosmological perturbations". In: *Phys. Rev. D* 22 (8 1980), pp. 1882–1905. DOI: 10.1103/PhysRevD.22.1882. URL: https://link.aps.org/doi/10.1103/PhysRevD.22.1882.

[22] N. Bartolo et al. "Non-Gaussianity from inflation: Theory and observations". In: *Phys. Rept.* 402 (2004), pp. 103–266. arXiv: astro-ph/0406398.

[23] Bruce A. Bassett, Shinji Tsujikawa, and David Wands. "Inflation dynamics and reheating". In: *Rev. Mod. Phys.* 78 (2006), pp. 537–589. DOI: 10.1103/RevModPhys.78.537. arXiv: astro-ph/0507632.

[24] R. A. Battye and E. P. S. Shellard. "Axion String Constraints [Phys. Rev. Lett. 73, 2954 (1994)]". In: *Phys. Rev. Lett.* 76 (12 1996), pp. 2203–2204. DOI: 10.1103/PhysRevLett.76.2203. URL: https://link.aps.org/doi/10.1103/PhysRevLett.76.2203.

[25] Daniel Baumann. *Cosmology*. Cambridge University Press, 2022. ISBN: 978-1-108-93709-2, 978-1-108-83807-8. DOI: 10.1017/9781108937092.

[26] Daniel Baumann. "Inflation". In: *Theoretical Advanced Study Institute in Elementary Particle Physics: Physics of the Large and the Small*. 2011, pp. 523–686. DOI: 10.1142/9789814327183_0010. arXiv: 0907.5424 [hep-th].

[27] Daniel Baumann. "Primordial Cosmology". In: *PoS* TASI2017 (2018), p. 009. DOI: 10.22323/1.305.0009. arXiv: 1807.03098 [hep-th].

[28] F. Bezrukov et al. "Higgs inflation: consistency and generalisations". In: *JHEP* 01 (2011). arXiv: 1008.5157.

[29] F. L. Bezrukov and M. Shaposhnikov. "The Standard Model Higgs boson as the inflaton". In: *Phys. Lett. B* 659 (2008), pp. 703–706. arXiv: 0710.3755.

[30] P. Binetruy and G. R. Dvali. "D term inflation". In: *Phys. Lett. B* 388 (1996), pp. 241–246. DOI: 10.1016/S0370-2693(96)01083-0. arXiv: hep-ph/9606342.

[31] J. J. Blanco-Pillado et al. "Racetrack inflation". In: *JHEP* 11 (2004), p. 063. DOI: 10.1088/1126-6708/2004/11/063. arXiv: hep-th/0406230.

[32] Laura Book, Marc Kamionkowski, and Fabian Schmidt. "Lensing of 21-cm Fluctuations by Primordial Gravitational Waves". In: *Phys. Rev. Lett.* 108 (21 2012), p. 211301. DOI: 10.1103/PhysRevLett.108.211301. URL: https://link.aps.org/doi/10.1103/PhysRevLett.108.211301.

[33] S. Borsanyi et al. "Axion cosmology, lattice QCD and the dilute instanton gas". In: *Phys. Lett. B* 752 (2016), pp. 175–181. DOI: 10.1016/j.physletb.2015.11.020. arXiv: 1508.06917 [hep-lat].

[34] S. Borsanyi et al. "et al". In: *"Calculation of the axion mass based on high-temperature lattice quantum chromodynamics," Nature* 539 (2016), pp. 69–71. arXiv: 1606.07494.

[35] S. M. Boucenna and Q. Shafi. "Axion inflation, proton decay, and leptogenesis in $SU(5) \times U(1)_{PQ}$". In: *Phys. Rev. D* 97 (2018). arXiv: 1712.06526.

[36] A. Boyarsky et al. "Sterile neutrino Dark Matter". In: *Prog. Part. Nucl. Phys.* 104 (2019), pp. 1–45. DOI: 10.1016/j.ppnp.2018.07.004. arXiv: 1807.07938 [hep-ph].

[37] Torsten Bringmann, Pat Scott, and Yashar Akrami. "Improved constraints on the primordial power spectrum at small scales from ultra-compact minihalos". In: *Phys. Rev. D* 85 (2012), p. 125027. DOI: 10.1103/PhysRevD.85.125027. arXiv: 1110.2484 [astro-ph.CO].

[38] Wilfried Buchmuller, Laura Covi, and David Delepine. "Inflation and supersymmetry breaking". In: *Phys. Lett. B* 491 (2000), pp. 183–189. DOI: 10.1016/S0370-2693(00)01005-4. arXiv: hep-ph/0006168.

[39] C. P. Burgess, H. M. Lee, and M. Trott. "Power-counting and the Validity of the Classical Approximation During Inflation". In: *JHEP* 09 (2009). arXiv: 0902.4465.

[40] C. P. Burgess, S. P. Patil, and M. Trott. "On the Predictiveness of Single-Field Inflationary Models". In: *JHEP* 06 (2014). arXiv: 1402.1476.

[41] C. P. Burgess et al. "Inflation in realistic D-brane models". In: *JHEP* 09 (2004), p. 033. DOI: 10.1088/1126-6708/2004/09/033. arXiv: hep-th/0403119.

[42] Malte Buschmann, Joshua W. Foster, and Benjamin R. Safdi. "Early-Universe Simulations of the Cosmological Axion". In: *Phys. Rev. Lett.* 124.16 (2020), p. 161103. DOI: 10.1103/PhysRevLett.124.161103. arXiv: 1906.00967 [astro-ph.CO].

[43] B. J. Carr and S. W. Hawking. "Black Holes in the Early Universe". In: *Monthly Notices of the Royal Astronomical Society* 168.2 (1974), pp. 399–415. ISSN: 0035-8711. DOI: 10.1093/mnras/168.2.399. eprint: https://academic.oup.com/mnras/article-pdf/168/2/399/8079885/mnras168-0399.pdf. URL: https://doi.org/10.1093/mnras/168.2.399.

[44] J.A Casas, G.B Gelmini, and A Riotto. "F-term inflation in superstring theories". In: *Physics Letters B* 459.1 (1999), pp. 91–96. ISSN: 0370-2693. DOI: https://doi.org/10.1016/S0370-2693(99)00683-8. URL: https://www.sciencedirect.com/science/article/pii/S0370269399006838.

[45] Jens Chluba. "Science with CMB spectral distortions". In: *49th Rencontres de Moriond on Cosmology*. 2014, pp. 327–334. arXiv: 1405.6938 [astro-ph.CO].

[46] R. T. Co, L. J. Hall, and K. Harigaya. "Axion Kinetic Misalignment Mechanism". In: *Phys. Rev. Lett.* 124 (2020). arXiv: 1910.14152.

[47] R. T. Co, K. Harigaya, and A. Pierce. "Gravitational waves and dark photon dark matter from axion rotations". In: *JHEP* 12 (2021). arXiv: 2104.02077.

[48] R. T. Co et al. "Axion Kinetic Misalignment and Parametric Resonance from Inflation". In: *JCAP* 08 (2020). arXiv: 2004.00629.

[49] R. T. Co et al. "Gravitational wave and CMB probes of axion kination". In: *JHEP* 09 (2022). arXiv: 2108.09299.

[50] Sidney Coleman. "Q-balls". In: *Nuclear Physics B* 262.2 (1985), pp. 263–283. ISSN: 0550-3213. DOI: https://doi.org/10.1016/0550-3213(85)90286-X. URL: https://www.sciencedirect.com/science/article/pii/055032138590286X.

[51] Sidney Coleman. "Why there is nothing rather than something: A theory of the cosmological constant". In: *Nuclear Physics B* 310.3 (1988), pp. 643–668. ISSN: 0550-3213. DOI: https://doi.org/10.1016/0550-3213(88)90097-1. URL: https://www.sciencedirect.com/science/article/pii/0550321388900971.

[52] Peter Coles and Francesco Lucchin. *Cosmology: The Origin and Evolution of Cosmic Structure, Second Edition*. 2002.

[53] G. Grilli di Cortona et al. "The QCD axion, precisely". In: *JHEP* 01 (2016). arXiv: 1511.02867.

[54] Davide Dal Cin and Takeshi Kobayashi. "Ultraviolet sensitivity of Peccei-Quinn inflation". In: *Phys. Rev. D* 108 (6 2023), p. 063530. DOI: 10.1103/PhysRevD.108.063530. URL: https://link.aps.org/doi/10.1103/PhysRevD.108.063530.

[55] Richard Lynn Davis. "Goldstone bosons in string models of galaxy formation". In: *Phys. Rev. D* 32 (12 1985), pp. 3172–3177. DOI: 10.1103/PhysRevD.32.3172. URL: https://link.aps.org/doi/10.1103/PhysRevD.32.3172.

[56] M. Dine and W. Fischler. "The Not So Harmless Axion". In: *Phys. Lett. B* 120 (1983), pp. 137–141.

[57] M. Dine, W. Fischler, and M. Srednicki. "A Simple Solution to the Strong CP Problem with a Harmless Axion". In: *Phys. Lett. B* 104 (1981), pp. 199–202.

[58] Valerie Domcke and Kai Schmitz. "Inflation from High-Scale Supersymmetry Breaking". In: *Phys. Rev. D* 97.11 (2018), p. 115025. DOI: 10.1103/PhysRevD.97.115025. arXiv: 1712.08121 [hep-ph].

[59] G. R. Dvali and S. H. Henry Tye. "Brane inflation". In: *Phys. Lett. B* 450 (1999), pp. 72–82. DOI: 10.1016/S0370-2693(99)00132-X. arXiv: hep-ph/9812483.

[60] Y. Ema et al. "Violent Preheating in Inflation with Nonminimal Coupling". In: *JCAP* 02 (2017). arXiv: 1609.05209.

[61] M. Fairbairn, R. Hogan, and D. J. E. Marsh. "Unifying inflation and dark matter with the Peccei-Quinn field: observable axions and observable tensors". In: *Phys. Rev. D* 91 (2015). arXiv: 1410.1752.

[62] Sergio Ferrara and A. Sagnotti. "Supersymmetry and Inflation". In: *Int. J. Mod. Phys.* 1 (2017). Ed. by Massimo Bianchi, Robert T. Jantzen, and Remo Ruffini, pp. 29–50. DOI: 10.1142/9789813226609_0003. arXiv: 1509.01500 [hep-th].

[63] Elisa G. M. Ferreira. "Ultra-light dark matter". In: *Astron. Astrophys. Rev.* 29.1 (2021), p. 7. DOI: 10.1007/s00159-021-00135-6. arXiv: 2005.03254 [astro-ph.CO].

[64] Wendy L. Freedman et al. "The Carnegie-Chicago Hubble Program. VIII. An Independent Determination of the Hubble Constant Based on the Tip of the Red Giant Branch". In: *The Astrophysical Journal* 882.1 (2019), p. 34. DOI: 10.3847/1538-4357/ab2f73. URL: https://doi.org/10.3847%2F1538-4357%2Fab2f73.

[65] Katherine Freese. "Review of Observational Evidence for Dark Matter in the Universe and in upcoming searches for Dark Stars". In: *EAS Publ. Ser.* 36 (2009). Ed. by E. Pécontal et al., pp. 113–126. DOI: 10.1051/eas/0936016. arXiv: 0812.4005 [astro-ph].

[66] Katherine Freese, Joshua A. Frieman, and Angela V. Olinto. "Natural inflation with pseudo Nambu-Goldstone bosons". In: *Phys. Rev. Lett.* 65 (26 1990), pp. 3233–3236. DOI: 10.1103/PhysRevLett.65.3233. URL: https://link.aps.org/doi/10.1103/PhysRevLett.65.3233.

[67] K. Fujikawa and H. Suzuki. *Path integrals and quantum anomalies*. 2004. DOI: 10.1093/acprof:oso/9780198529132.001.0001.

[68] Steven B. Giddings and Andrew Strominger. "String wormholes". In: *Physics Letters B* 230.1 (1989), pp. 46–51. ISSN: 0370-2693. DOI: https://doi.org/10.1016/0370-2693(89)91651-1. URL: https://www.sciencedirect.com/science/article/pii/0370269389916511.

[69] Steven B. Giddings and Scott D. Thomas. "High-energy colliders as black hole factories: The End of short distance physics". In: *Phys. Rev. D* 65 (2002), p. 056010. DOI: 10.1103/PhysRevD.65.056010. arXiv: hep-ph/0106219.

[70] Gerald Gilbert. "Wormhole-induced proton decay". In: *Nuclear Physics B* 328.1 (1989), pp. 159–170. ISSN: 0550-3213. DOI: https://doi.org/10.1016/0550-3213(89)90097-7. URL: https://www.sciencedirect.com/science/article/pii/0550321389900977.

[71] G. F. Giudice and H. M. Lee. "Unitarizing Higgs Inflation". In: *Phys. Lett. B* 694 (2011), pp. 294–300. arXiv: 1010.1417.

[72] M. Gorghetto, E. Hardy, and G. Villadoro. "More axions from strings". In: *SciPost Phys.* 10 (2021). arXiv: 2007.04990.

[73] Yann Gouttenoire, Geraldine Servant, and Peera Simakachorn. "Kination cosmology from scalar fields and gravitational-wave signatures". In: (2021). arXiv: 2111.01150 [hep-ph].

[74] Kim Griest and Marc Kamionkowski. "Unitarity limits on the mass and radius of dark-matter particles". In: *Phys. Rev. Lett.* 64 (6 1990), pp. 615–618. DOI: 10.1103/PhysRevLett.64.615. URL: https://link.aps.org/doi/10.1103/PhysRevLett.64.615.

[75] A. H. Guth. "The Inflationary Universe: A Possible Solution to the Horizon and Flatness Problems". In: *Phys. Rev. D* 23 (1981), pp. 347–356.

[76] Alan H. Guth. "Eternal inflation and its implications". In: *J. Phys. A* 40 (2007). Ed. by Joan Sola, pp. 6811–6826. DOI: 10.1088/1751-8113/40/25/S25. arXiv: hep-th/0702178.

[77] K. Hamaguchi, Y. Kanazawa, and N. Nagata. "Axion quality problem alleviated by nonminimal coupling to gravity". In: *Phys. Rev. D* 105 (2022). arXiv: 2108.13245.

[78] Diego Harari and Pierre Sikivie. "Effects of a Nambu-Goldstone boson on the polarization of radio galaxies and the cosmic microwave background". In: *Physics Letters B* 289.1 (1992), pp. 67–72. ISSN: 0370-2693. DOI: https://doi.org/10.1016/0370-2693(92)91363-E. URL: https://www.sciencedirect.com/science/article/pii/037026939291363E.

[79] K. Harigaya et al. "Dynamics of Peccei-Quinn Breaking Field after Inflation and Axion Isocurvature Perturbations". In: *JCAP* 11 (2015). arXiv: 1507.00119.

[80] D. Harlow and H. Ooguri. "Symmetries in quantum field theory and quantum gravity". In: *Commun. Math* 383 (2021), pp. 1669–1804. arXiv: 1810.05338.

[81] S. W. Hawking. "Particle Creation by Black Holes". In: *Commun. Math. Phys.* 43 (1975). Ed. by G. W. Gibbons and S. W. Hawking. [Erratum: Commun.Math.Phys. 46, 206 (1976)], pp. 199–220. DOI: 10.1007/BF02345020.

[82] S. W. Hawking and W. Israel. *General Relativity: An Einstein Centenary Survey*. Cambridge, UK: Univ. Pr., 1979. ISBN: 978-0-521-29928-2.

[83] Stephen Hawking. "Gravitationally collapsed objects of very low mass". In: *Mon. Not. Roy. Astron. Soc.* 152 (1971), p. 75. DOI: 10.1093/mnras/152.1.75.

[84] M. P. Hertzberg. "On Inflation with Non-minimal Coupling". In: *JHEP* 11 (2010). arXiv: 1002.2995.

[85] H Hildebrandt et al. "KiDS-450: cosmological parameter constraints from tomographic weak gravitational lensing". In: *Monthly Notices of the Royal Astronomical Society* 465.2 (2016), pp. 1454–1498. ISSN: 0035-8711. DOI: 10.1093/mnras/stw2805. eprint: https://academic.oup.com/mnras/article-pdf/465/2/1454/24243465/stw2805.pdf. URL: https://doi.org/10.1093/mnras/stw2805.

[86] Takashi Hiramatsu et al. "Production of dark matter axions from collapse of string-wall systems". In: *Phys. Rev. D* 85 (10 2012), p. 105020. DOI: 10.1103/PhysRevD.85.105020. URL: https://link.aps.org/doi/10.1103/PhysRevD.85.105020.

[87] R. Holman et al. "Solutions to the strong CP problem in a world with gravity". In: *Phys. Lett. B* 282 (1992), pp. 132–136. arXiv: hep-ph/9203206.

[88] Lam Hui. "Wave Dark Matter". In: *Ann. Rev. Astron. Astrophys.* 59 (2021), pp. 247–289. DOI: 10.1146/annurev-astro-120920-010024. arXiv: 2101.11735 [astro-ph.CO].

[89] Ryusuke Jinno et al. "Higgs inflation in metric and Palatini formalisms: Required suppression of higher dimensional operators". In: *JCAP* 03 (2020), p. 063. DOI: 10.1088/1475-7516/2020/03/063. arXiv: 1904.05699 [hep-ph].

[90] D. I. Kaiser. "Primordial spectral indices from generalized Einstein theories". In: *Phys. Rev. D* 52 (1995), pp. 4295–4306. arXiv: astro-ph/9408044.

[91] R. Kallosh et al. "Gravity and global symmetries". In: *Phys. Rev. D* 52 (1995), pp. 912–935. arXiv: hep-th/9502069.

[92] N. Kaloper and A. Lawrence. "Natural chaotic inflation and ultraviolet sensitivity". In: *Phys. Rev. D* 90 (2014). arXiv: 1404.2912.

[93] M. Kamionkowski and J. March-Russell. "Planck scale physics and the Peccei-Quinn mechanism". In: *Phys. Lett. B* 282 (1992), pp. 137–141. arXiv: hep-th/9202003.

[94] Panagiota Kanti. "Black holes in theories with large extra dimensions: A Review". In: *Int. J. Mod. Phys. A* 19 (2004), pp. 4899–4951. DOI: 10.1142/S0217751X04018324. arXiv: hep-ph/0402168.

[95] S. Kasuya and M. Kawasaki. "Topological defects formation after inflation on lattice simulation". In: *Phys. Rev. D* 58 (1998). arXiv: hep-ph/9804429.

[96] S. Kasuya, M. Kawasaki, and T. Yanagida. "Cosmological axion problem in chaotic inflationary universe". In: *Phys. Lett. B* 409 (1997), pp. 94–100. arXiv: hep-ph/9608405.

[97] T W B Kibble. "Topology of cosmic domains and strings". In: *Journal of Physics A: Mathematical and General* 9.8 (1976), p. 1387. DOI: 10.1088/0305-4470/9/8/029. URL: https://dx.doi.org/10.1088/0305-4470/9/8/029.

[98] Jihn E. Kim. "Weak-Interaction Singlet and Strong CP Invariance". In: *Phys. Rev. Lett.* 43 (2 1979), pp. 103–107. DOI: 10.1103/PhysRevLett.43.103. URL: https://link.aps.org/doi/10.1103/PhysRevLett.43.103.

[99] T. Kobayashi and S. Mukohyama. "Effects of Light Fields During Inflation". In: *Phys. Rev. D* 81 (2010). arXiv: 1003.0076.

[100] T. Kobayashi and F. Takahashi. "Cosmological Perturbations of Axion with a Dynamical Decay Constant". In: *JCAP* 08 (2016). arXiv: 1607.04294.

[101] Takeshi Kobayashi, Ryosuke Kurematsu, and Fuminobu Takahashi. "Isocurvature Constraints and Anharmonic Effects on QCD Axion Dark Matter". In: *JCAP* 09 (2013), p. 032. DOI: 10.1088/1475-7516/2013/09/032. arXiv: 1304.0922 [hep-ph].

[102] Hideo Kodama and Misao Sasaki. "Cosmological Perturbation Theory". In: *Progress of Theoretical Physics Supplement* 78 (1984), pp. 1–166. ISSN: 0375-9687. DOI: 10.1143/PTPS.78.1. eprint: https://academic.oup.com/ptps/article-pdf/doi/10.1143/PTPS.78.1/5321391/78-1.pdf. URL: https://doi.org/10.1143/PTPS.78.1.

[103] L. Kofman, A. D. Linde, and A. A. Starobinsky. "Nonthermal phase transitions after inflation". In: *Phys. Rev. Lett.* 76 (1996), pp. 1011–1014. arXiv: hep-th/9510119.

[104] L. Kofman, A. D. Linde, and A. A. Starobinsky. "Reheating after inflation". In: *Phys. Rev. Lett.* 73 (1994), pp. 3195–3198. arXiv: hep-th/9405187.

[105] L. Kofman, A. D. Linde, and A. A. Starobinsky. "Towards the theory of reheating after inflation". In: *Phys. Rev. D* 56 (1997), pp. 3258–3295. arXiv: hep-ph/9704452.

[106] Edward W Kolb. "First-order inflation". In: *Physica Scripta* 1991.T36 (1991), p. 199. DOI: 10.1088/0031-8949/1991/T36/021. URL: https://dx.doi.org/10.1088/0031-8949/1991/T36/021.

[107] Edward W. Kolb, Daniel J. H. Chung, and Antonio Riotto. "WIMPzillas!" In: *AIP Conf. Proc.* 484.1 (1999). Ed. by H. Falomir, R. E. Gamboa Saravi, and F. A. Schaposnik, pp. 91–105. DOI: 10.1063/1.59655. arXiv: hep-ph/9810361.

[108] Edward W. Kolb and Michael S. Turner. *The Early Universe*. Vol. 69. 1990. ISBN: 978-0-201-62674-2. DOI: 10.1201/9780429492860.

[109] H.A. Kramers. "Wellenmechanik und halbzahlige Quantisierung". In: *Zeitschrift für Physik* 39 (1926), pp. 828–840. DOI: https://doi.org/10.1007/BF01451751.

[110] Daile La and Paul J. Steinhardt. "Extended Inflationary Cosmology". In: *Phys. Rev. Lett.* 62 (4 1989), pp. 376–378. DOI: 10.1103/PhysRevLett.62.376. URL: https://link.aps.org/doi/10.1103/PhysRevLett.62.376.

[111] Andrew R Liddle and Samuel M Leach. "How long before the end of inflation were observable perturbations produced?" In: *Phys. Rev. D* 68 (2003), p. 103503. arXiv: astro-ph/0305263.

[112] Andrew R. Liddle and D. H. Lyth. *Cosmological inflation and large scale structure*. 2000. ISBN: 978-0-521-57598-0, 978-0-521-82849-9. DOI: 10.1017/CBO9781139175180.

[113] A. Linde, M. Noorbala, and A. Westphal. "Observational consequences of chaotic inflation with nonminimal coupling to gravity". In: *JCAP* 03 (2011). arXiv: 1101.2652.

[114] A. D. Linde. "A New Inflationary Universe Scenario: A Possible Solution of the Horizon, Flatness, Homogeneity, Isotropy and Primordial Monopole Problems". In: *Phys. Lett. B* 108 (1982), pp. 389–393.

[115] A. D. Linde. "Axions in inflationary cosmology". In: *Phys. Lett. B* 259 (1991), pp. 38–47.

[116] A. D. Linde and D. H. Lyth. "Axionic domain wall production during inflation". In: *Phys. Lett. B* 246 (1990), pp. 353–358.

[117] A.D. Linde. "A new inflationary universe scenario: A possible solution of the horizon, flatness, homogeneity, isotropy and primordial monopole problems". In: *Physics Letters B* 108.6 (1982), pp. 389–393. ISSN: 0370-2693. DOI: https://doi.org/10.1016/0370-2693(82)91219-9. URL: https://www.sciencedirect.com/science/article/pii/0370269382912199.

[118] A.D. Linde. "Chaotic inflation". In: *Physics Letters B* 129.3 (1983), pp. 177–181. ISSN: 0370-2693. DOI: https://doi.org/10.1016/0370-2693(83)90837-7. URL: https://www.sciencedirect.com/science/article/pii/0370269383908377.

[119] Andrei Linde. "Hybrid inflation". In: *Phys. Rev. D* 49 (2 1994), pp. 748–754. DOI: 10.1103/PhysRevD.49.748. URL: https://link.aps.org/doi/10.1103/PhysRevD.49.748.

[120] F. Lucchin and S. Matarrese. "Power Law Inflation". In: *Phys. Rev. D* 32 (1985), p. 1316. DOI: 10.1103/PhysRevD.32.1316.

[121] D. H. Lyth. "Axions and inflation: Sitting in the vacuum". In: *Phys. Rev. D* 45 (1992), pp. 3394–3404. DOI: 10.1103/PhysRevD.45.3394.

[122] D. H. Lyth. "Axions and inflation: Vacuum fluctuations". In: *Phys. Rev. D* 45 (10 1992), pp. 3394–3404. DOI: 10.1103/PhysRevD.45.3394. URL: https://link.aps.org/doi/10.1103/PhysRevD.45.3394.

[123] D. H. Lyth. "Generating the curvature perturbation at the end of inflation". In: *JCAP* 11 (2005). arXiv: astro-ph/0510443.

[124] D. H. Lyth. "What would we learn by detecting a gravitational wave signal in the cosmic microwave background anisotropy?" In: *Phys. Rev. Lett.* 78 (1997), pp. 1861–1863. arXiv: hep-ph/9606387.

[125] D. H. Lyth, K. A. Malik, and M. Sasaki. "A General proof of the conservation of the curvature perturbation". In: *JCAP* 05 (2005). arXiv: astro-ph/0411220.

[126] David H. Lyth and Antonio Riotto. "Particle physics models of inflation and the cosmological density perturbation". In: *Phys. Rept.* 314 (1999), pp. 1–146. DOI: 10.1016/S0370-1573(98)00128-8. arXiv: hep-ph/9807278.

[127] David H. Lyth and Antonio Riotto. "Particle physics models of inflation and the cosmological density perturbation". In: *Physics Reports* 314.1 (1999), pp. 1–146. ISSN: 0370-1573. DOI: https://doi.org/10.1016/S0370-1573(98)00128-8. URL: https://www.sciencedirect.com/science/article/pii/S0370157398001288.

[128] David H. Lyth and David Wands. "Conserved cosmological perturbations". In: *Phys. Rev. D* 68 (10 2003), p. 103515. DOI: 10.1103/PhysRevD.68.103515. URL: https://link.aps.org/doi/10.1103/PhysRevD.68.103515.

[129] Roy Maartens et al. "Chaotic inflation on the brane". In: *Phys. Rev. D* 62 (2000), p. 041301. DOI: 10.1103/PhysRevD.62.041301. arXiv: hep-ph/9912464.

[130] Fernando Marchesano, Gary Shiu, and Angel M. Uranga. "F-term Axion Monodromy Inflation". In: *JHEP* 09 (2014), p. 184. DOI: 10.1007/JHEP09(2014)184. arXiv: 1404.3040 [hep-th].

[131] David J. E. Marsh. "Axion Cosmology". In: *Phys. Rept.* 643 (2016), pp. 1–79. DOI: 10.1016/j.physrep.2016.06.005. arXiv: 1510.07633 [astro-ph.CO].

[132] Jerome Martin and Christophe Ringeval. "First CMB Constraints on the Inflationary Reheating Temperature". In: *Phys. Rev. D* 82 (2010), p. 023511. DOI: 10.1103/PhysRevD.82.023511. arXiv: 1004.5525 [astro-ph.CO].

[133] Jerome Martin, Christophe Ringeval, and Vincent Vennin. "Encyclopædia Inflationaris". In: *Phys. Dark Univ.* 5-6 (2014), pp. 75–235. DOI: 10.1016/j.dark.2014.01.003. arXiv: 1303.3787 [astro-ph.CO].

[134] V. F. Mukhanov and G. V. Chibisov. "Quantum Fluctuations and a Nonsingular Universe". In: *JETP Lett.* 33 (1981), pp. 532–535.

[135] N. Okada, M. U. Rehman, and Q. Shafi. "Tensor to Scalar Ratio in Non-Minimal ϕ^4 Inflation". In: *Phys. Rev. D* 82 (2010). arXiv: 1005.5161.

[136] F. W. J. Olver et al. *NIST Handbook of Mathematical Functions*. Cambridge University Press, 2010.

[137] Leonard E. Parker and D. Toms. *Quantum Field Theory in Curved Spacetime: Quantized Field and Gravity*. Cambridge Monographs on Mathematical Physics. Cambridge University Press, 2009. ISBN: 978-0-521-87787-9, 978-0-521-87787-9, 978-0-511-60155-2. DOI: 10.1017/CBO9780511813924.

[138] R. D. Peccei and H. R. Quinn. "CP Conservation in the Presence of Instantons". In: *Phys. Rev. Lett.* 38 (1977), pp. 1440–1443.

[139] Will J. Percival et al. "Baryon acoustic oscillations in the Sloan Digital Sky Survey Data Release 7 galaxy sample". In: *Monthly Notices of the Royal Astronomical Society* 401.4 (2010), pp. 2148–2168. ISSN: 0035-8711. DOI: 10.1111/j.1365-2966.2009.15812.x. eprint: https://academic.oup.com/mnras/article-pdf/401/4/2148/3901461/mnras0401-2148.pdf. URL: https://doi.org/10.1111/j.1365-2966.2009.15812.x.

[140] S. Perlmutter et al. "Measurements of Ω and Λ from 42 High-Redshift Supernovae". In: *The Astrophysical Journal* 517.2 (1999), p. 565. DOI: 10.1086/307221. URL: https://dx.doi.org/10.1086/307221.

[141] Kalliopi Petraki and Raymond R. Volkas. "Review of asymmetric dark matter". In: *Int. J. Mod. Phys. A* 28 (2013), p. 1330028. DOI: 10.1142/S0217751X13300287. arXiv: 1305.4939 [hep-ph].

[142] David Polarski and Alexei A Starobinsky. "Semiclassicality and decoherence of cosmological perturbations". In: *Classical and Quantum Gravity* 13.3 (1996), pp. 377–391. DOI: 10.1088/0264-9381/13/3/006. URL: https://doi.org/10.1088%2F0264-9381%2F13%2F3%2F006.

[143] J. Preskill, M. B. Wise, and F. Wilczek. "Cosmology of the Invisible Axion". In: *Phys. Lett. B* 120 (1983), pp. 127–132.

[144] Lisa Randall. "Supersymmetry and inflation". In: *Adv. Ser. Direct. High Energy Phys.* 21 (2010). Ed. by Gordon L. Kane, pp. 545–564. DOI: 10.1142/9789814307505_0016. arXiv: hep-ph/9711471.

[145] Lisa Randall, Marin Soljacic, and Alan H. Guth. "Supernatural inflation: Inflation from supersymmetry with no (very) small parameters". In: *Nucl. Phys. B* 472 (1996), pp. 377–408. DOI: 10.1016/0550-3213(96)00174-5. arXiv: hep-ph/9512439.

[146] Lisa Randall and Raman Sundrum. "An Alternative to Compactification". In: *Phys. Rev. Lett.* 83 (23 1999), pp. 4690–4693. DOI: 10.1103/PhysRevLett.83.4690. URL: https://link.aps.org/doi/10.1103/PhysRevLett.83.4690.

[147] Lisa Randall and Raman Sundrum. "Large Mass Hierarchy from a Small Extra Dimension". In: *Phys. Rev. Lett.* 83 (17 1999), pp. 3370–3373. DOI: 10.1103/PhysRevLett.83.3370. URL: https://link.aps.org/doi/10.1103/PhysRevLett.83.3370.

[148] Adam G. Riess et al. "Large Magellanic Cloud Cepheid Standards Provide a 1% Foundation for the Determination of the Hubble Constant and Stronger Evidence for Physics beyond ΛCDM". In: *The Astrophysical Journal* 876.1 (2019), p. 85. DOI: 10.3847/1538-4357/ab1422. URL: https://dx.doi.org/10.3847/1538-4357/ab1422.

[149] Adam G. Riess et al. "Milky Way Cepheid Standards for Measuring Cosmic Distances and Application to Gaia DR2: Implications for the Hubble Constant". In: *The Astrophysical Journal* 861.2 (2018), p. 126. DOI: 10.3847/1538-4357/aac82e. URL: https://dx.doi.org/10.3847/1538-4357/aac82e.

[150] Adam G. Riess et al. "Observational Evidence from Supernovae for an Accelerating Universe and a Cosmological Constant". In: *The Astronomical Journal* 116.3 (1998), p. 1009. DOI: 10.1086/300499. URL: https://dx.doi.org/10.1086/300499.

[151] Leszek Roszkowski, Enrico Maria Sessolo, and Sebastian Trojanowski. "WIMP dark matter candidates and searches—current status and future prospects". In: *Rept. Prog. Phys.* 81.6 (2018), p. 066201. DOI: 10.1088/1361-6633/aab913. arXiv: 1707.06277 [hep-ph].

[152] D. S. Salopek, J. R. Bond, and J. M. Bardeen. "Designing density fluctuation spectra in inflation". In: *Phys. Rev. D* 40 (6 1989), pp. 1753–1788. DOI: 10.1103/PhysRevD.40.1753. URL: https://link.aps.org/doi/10.1103/PhysRevD.40.1753.

[153] M. Sasaki. "Multi-brid inflation and non-Gaussianity". In: *Prog. Theor. Phys.* 120 (2008), pp. 159–174. arXiv: 0805.0974.

[154] M. Sasaki and E. D. Stewart. "A General analytic formula for the spectral index of the density perturbations produced during inflation". In: *Prog. Theor. Phys.* 95 (1996), pp. 71–78. arXiv: astro-ph/9507001.

[155] Misao Sasaki and Ewan D. Stewart. "A General analytic formula for the spectral index of the density perturbations produced during inflation". In: *Prog. Theor. Phys.* 95 (1996), pp. 71–78. DOI: 10.1143/PTP.95.71. arXiv: astro-ph/9507001.

[156] Katsuhiko Sato. "First-order phase transition of a vacuum and the expansion of the Universe". In: *Monthly Notices of the Royal Astronomical Society* 195.3 (1981), pp. 467–479.

[157] M. A. Shifman, A. I. Vainshtein, and V. I. Zakharov. "Can Confinement Ensure Natural CP Invariance of Strong Interactions?" In: *Nucl. Phys. B* 166 (1980), pp. 493–506.

[158] Kris Sigurdson and Asantha Cooray. "Cosmic 21-cm delensing of microwave background polarization and the minimum detectable energy scale of inflation". In: *Phys. Rev. Lett.* 95 (2005), p. 211303. DOI: 10.1103/PhysRevLett.95.211303. arXiv: astro-ph/0502549.

[159] Pierre Sikivie. "Axion Cosmology". In: *Lect. Notes Phys.* 741 (2008). Ed. by Markus Kuster, Georg Raffelt, and Berta Beltran, pp. 19–50. DOI: 10.1007/978-3-540-73518-2_2. arXiv: astro-ph/0610440.

[160] E. Silverstein and A. Westphal. "Monodromy in the CMB: Gravity Waves and String Inflation". In: *Phys. Rev. D* 78 (2008). arXiv: 0803.3085.

[161] Lee Smolin. "Towards a theory of spacetime structure at very short distances". In: *Nuclear Physics B* 160.2 (1979), pp. 253–268. ISSN: 0550-3213. DOI: https://doi.org/10.1016/0550-3213(79)90059-2. URL: https://www.sciencedirect.com/science/article/pii/0550321379900592.

[162] A. A. Starobinsky. "A New Type of Isotropic Cosmological Models Without Singularity". In: *Phys. Lett. B* 91 (1980), pp. 99–102.

[163] A. A. Starobinsky. "Multicomponent de Sitter (Inflationary) Stages and the Generation of Perturbations". In: *JETP Lett.* 42 (1985), pp. 152–155.

[164] A. A. Starobinsky. "Spectrum of relict gravitational radiation and the early state of the universe". In: *JETP Lett.* 30 (1979), pp. 682–685.

[165] Karl Strobl and Thomas J. Weiler. "Anharmonic evolution of the cosmic axion density spectrum". In: *Phys. Rev. D* 50 (1994), pp. 7690–7702. DOI: 10.1103/PhysRevD.50.7690. arXiv: astro-ph/9405028.

[166] I. Tkachev et al. "Cosmic strings from preheating". In: *Phys. Lett. B* 440 (1998), pp. 262–268. arXiv: hep-ph/9805209.

[167] I. I. Tkachev. "Phase transitions at preheating". In: *Phys. Lett. B* 376 (1996), pp. 35–40. arXiv: hep-th/9510146.

[168] Sean Tulin and Hai-Bo Yu. "Dark Matter Self-interactions and Small Scale Structure". In: *Phys. Rept.* 730 (2018), pp. 1–57. DOI: 10.1016/j.physrep.2017.11.004. arXiv: 1705.02358 [hep-ph].

[169] Michael S. Turner. "Cosmic and local mass density of "invisible" axions". In: *Phys. Rev. D* 33 (4 1986), pp. 889–896. DOI: 10.1103/PhysRevD.33.889. URL: https://link.aps.org/doi/10.1103/PhysRevD.33.889.

[170] Michael S. Turner. "Cosmic and Local Mass Density of Invisible Axions". In: *Phys. Rev. D* 33 (1986), pp. 889–896. DOI: 10.1103/PhysRevD.33.889.

[171] Cumrun Vafa and Edward Witten. "Parity Conservation in Quantum Chromodynamics". In: *Phys. Rev. Lett.* 53 (6 1984), pp. 535–536. DOI: 10.1103/PhysRevLett.53.535. URL: https://link.aps.org/doi/10.1103/PhysRevLett.53.535.

[172] Alexander Vilenkin. "Birth of inflationary universes". In: *Phys. Rev. D* 27 (12 1983), pp. 2848–2855. DOI: 10.1103/PhysRevD.27.2848. URL: https://link.aps.org/doi/10.1103/PhysRevD.27.2848.

[173] D. Wands et al. "A New approach to the evolution of cosmological perturbations on large scales". In: *Phys. Rev. D* 62 (2000). arXiv: astro-ph/0003278.

[174] S. Weinberg. "A New Light Boson?" In: *Phys. Rev. Lett.* 40 (1978), pp. 223–226.

[175] Steven Weinberg. *Cosmology*. 2008. ISBN: 978-0-19-852682-7.

[176] Gregor Wentzel. "Eine Verallgemeinerung der Quantenbedingungen für die Zwecke der Wellenmechanik". In: *Z. Phys.* 38.6 (1926), pp. 518–529. DOI: 10.1007/BF01397171.

[177] F. Wilczek. "Problem of Strong P and T Invariance in the Presence of Instantons". In: *Phys. Rev. Lett.* 40 (1978), pp. 279–282.

[178] Sergei Winitzki. "Cosmological particle production and the precision of the WKB approximation". In: *Phys. Rev. D* 72 (10 2005), p. 104011. DOI: 10.1103/PhysRevD.72.104011. URL: https://link.aps.org/doi/10.1103/PhysRevD.72.104011.

[179] Kenneth C Wong et al. "H0LiCOW – XIII. A 2.4 per cent measurement of $H0$ from lensed quasars: 5.3 σ tension between early- and late-Universe probes". In: *Monthly Notices of the Royal Astronomical Society* 498.1 (2019), pp. 1420–1439. DOI: 10.1093/mnras/stz3094. URL: https://doi.org/10.1093%2Fmnras%2Fstz3094.

[180] Masahide Yamaguchi, M. Kawasaki, and Jun'ichi Yokoyama. "Evolution of axionic strings and spectrum of axions radiated from them". In: *Phys. Rev. Lett.* 82 (1999), pp. 4578–4581. DOI: 10.1103/PhysRevLett.82.4578. arXiv: hep-ph/9811311.

[181] A. Zee. "Broken-Symmetric Theory of Gravity". In: *Phys. Rev. Lett.* 42 (7 1979), pp. 417–421. DOI: 10.1103/PhysRevLett.42.417. URL: https://link.aps.org/doi/10.1103/PhysRevLett.42.417.

[182] A. R. Zhitnitsky. "On Possible Suppression of the Axion Hadron Interactions. (In Russian)". In: *Sov. J. Nucl. Phys.* 31 (1980), p. 260.

[183] Kathryn M. Zurek. "Asymmetric Dark Matter: Theories, Signatures, and Constraints". In: *Phys. Rept.* 537 (2014), pp. 91–121. DOI: 10.1016/j.physrep.2013.12.001. arXiv: 1308.0338 [hep-ph].